การพัฒนาแบบจำลองของเซลล์เชื้อเพลิงสังกะสี-อากาศ และอิเลคโทรไลเซอร์สังกะสีแบบอัลคาไลน์

นายวรนันท์ เล้าอติมาน

วิทยานิพนธ์นี้เป็นส่วนหนึ่งของการศึกษาตามหลักสูตรปริญญาวิศวกรรมศาสตรมหาบัณฑิต
สาขาวิชาวิศวกรรมเคมี ภาควิชาวิศวกรรมเคมี
คณะวิศวกรรมศาสตร์ จุฬาลงกรณ์มหาวิทยาลัย
ปีการศึกษา 2559

Modelling of Zinc-Air Fuel Cell and Alkaline Zinc Electrolyzer

Mr. Woranunt Lao-atiman

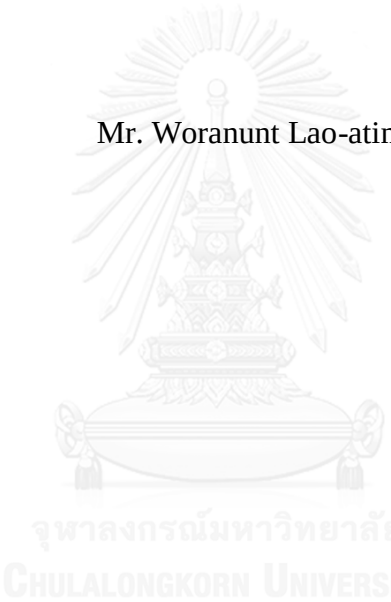

A Thesis Submitted in Partial Fulfillment of the Requirements
for the Degree of Master of Engineering Program in Chemical Engineering
Department of Chemical Engineering
Faculty of Engineering
Chulalongkorn University
Academic Year 2016

Thesis Title	Modelling of Zinc-Air Fuel Cell and Alkaline Zinc Electrolyzer
By	Mr. Woranunt Lao-atiman
Field of Study	Chemical Engineering
Thesis Advisor	Associate Professor Soorathep Kheawhom, Ph.D.

Accepted by the Faculty of Engineering, Chulalongkorn University in Partial Fulfillment of the Requirements for the Master's Degree

.....Dean of the Faculty of Engineering
(Associate Professor Supot Teachavorasinskun, D.Eng.)

THESIS COMMITTEE

.....Chairman
(Professor Paisan Kittisupakorn, Ph.D.)

.....Thesis Advisor
(Associate Professor Soorathep Kheawhom, Ph.D.)

.....Examiner
(Assistant Professor Amornchai Arpornwichanop, D.Eng.)

.....External Examiner
(Assistant Professor Pornchai Bumroongsri, D.Eng.)

วรนันท์ เล้าอติมาน : การพัฒนาแบบจำลองของเซลล์เชื้อเพลิงสังกะสี-อากาศและอิเลคโทรไลเซอร์สังกะสีแบบอัลคาไลน์ (Modelling of Zinc-Air Fuel Cell and Alkaline Zinc Electrolyzer) อ.ที่ปรึกษาวิทยานิพนธ์หลัก: รศ. ดร. สุรเทพ เขียวหอม, 73 หน้า.

เซลล์เชื้อเพลิงสังกะสีอากาศได้รับความสนใจอย่างกว้างขวางในด้านการผลิตไฟฟ้า ยิ่งไปกว่านั้นเมื่อทำงานร่วมกับอิเลคโทรไลเซอร์สังกะสีแบบอัลคาไลน์แล้วจะกลายเป็นระบบกักเก็บพลังงานที่มีศักยภาพ งานวิจัยนี้จึงมุ่งที่จะพัฒนาแบบจำลองทางคณิตศาสตร์แบบพลวัตของเซลล์เชื้อเพลิงสังกะสีอากาศและอิเลคโทรไลเซอร์สังกะสีแบบอัลคาไลน์ รวมไปถึงศึกษาอิทธิพลของพารามิเตอร์ต่างๆที่มีผลต่อประสิทธิภาพของเซลล์เชื้อเพลิงและอิเลคโทรไลเซอร์ โดยในส่วนของการทดลองได้ออกแบบเซลล์เชื้อเพลิงสังกะสีอากาศเป็นเซลล์แบบท่อ ใช้สารละลายโพแทสเซียมไฮดรอกไซด์ผสมรวมกับผงสังกะสี เป็นอิเลคโทรไลท์ไหลผ่านภายในเซลล์ ใช้ตาข่ายเหล็กกล้าไร้สนิมและโฟมนิกเกิลเป็นตัวเก็บกระแสของขั้วแอโนดและแคโทดตามลำดับ นำแมงกานีสไดออกไซด์ผสมกับแกรไฟท์เคลือบลงบนโฟมนิกเกิลเพื่อใช้เป็นตัวเร่งปฏิกิริยาของฝั่งแคโทด สำหรับอิเลคโทรไลเซอร์สังกะสี ออกแบบให้เป็นเซลล์ไฟฟ้าแบบขั้วจุ่มสองขั้ว ใช้สารละลายโพแทสเซียมไฮดรอกไซด์ผสมกับสังกะสีออกไซด์เป็นอิเลคโทรไลท์ ใช้แผ่นทองแดงและโฟทนิกเกิลเป็นตัวเก็บกระแสของชั้วแคโทดและแอโนดตามลำดับ วิเคราะห์เส้นโค้งโพลาร์ไรเซชันโดยใช้เครื่องวิเคราะห์แบตเตอรี แบบจำลองพัฒนาขึ้นโดยใช้โปรแกรม MATLAB และทำการตรวจสอบเทียบกับเส้นโค้งโพลาร์ไรเซชันจากผลการทดลอง พบว่าค่าจากแบบจำลองมีความสอดคล้องกับผลการทดลองในระดับที่ยอมรับได้ จากนั้นจึงนำแบบจำลองที่พัฒนามาศึกษาผลการพารามิเตอร์ 4 ตัว ได้แก่ ความเข้มข้นของโพแทสเซียมไฮดรอกไซด์ อัตราการไหล ความเข้มข้นของซิงค์เคตไอออน และการเติมคาร์บอนนำไฟฟ้า จากผลการจำลองของเซลล์เชื้อเพลิงสังกะสีอากาศพบว่าการเพิ่มความเข้มข้นของโพแทสเซียมไฮดรอกไซด์ช่วยเพิ่มแรงดันไฟฟ้าของเซลล์ แต่หากเพิ่มความเข้มข้นสูงกว่า 7 โมลาร์จะทำให้ค่าแรงดันไฟฟ้าลดลงเนื่องจาก ค่าความนำไอออนของอิเลคโทรไลท์และค่าความหนาแน่นกระแสไฟฟ้าแลกเปลี่ยนของขั้วแอโนดมีค่าลดลงเมื่อเพิ่มความเข้มข้นของโพแทสเซียมไฮดรอกไซด์เกิน 7 โมลาร์ การใช้อัตราการไหลของอิเลคโทรไลท์สูงจะช่วยให้เซลล์สามารถรักษาระดับปริมาณสังกะสีและความเข้มข้นของอิเลคโทรไลต์ให้สูงอยู่ตลอดเวลาได้ ทำให้ประสิทธิภาพในการดำเนินการระยะยาวของเซลล์เชื้อเพลิงเพิ่มมากขึ้นอีกด้วย เมื่อเพิ่มความเข้มข้นซิงค์เคตไอออนจะลดแรงดันไฟฟ้าของเซลล์ลง เมื่อเพิ่มปริมาณสังกะสีออกไซด์มากขึ้นจะทำให้ค่าความนำไอออนและพื้นที่ทำปฏิกิริยาของขั้วสังกะสีลดลง การเพิ่มคาร์บอนนำไฟฟ้าไม่ส่งผลพัฒนาต่อประสิทธิภาพเซลล์อย่างมีนัยสำคัญ สำหรับผลของอิเลคโทรไลเซอร์สังกะสีพบว่าแรงดันไฟฟ้าต่ำสุดอยู่ที่ความเข้มข้นของโพแทสเซียมไฮดรอกไซด์ 7 โมลาร์ ซึ่งมีค่าความนำไอออนสูงสุด ส่วนที่ความเข้มข้นค่าอื่นนั้นให้ค่าแรงดันไฟฟ้าที่สูงกว่า การเพิ่มความเข้มข้นของซิงค์เคตไอออนทำให้แรงดันไฟฟ้าของเซลล์ลดลงในช่วงที่ซิงค์เคตเข้มข้นน้อยกว่าค่าความเข้มข้นอิ่มตัว การเพิ่มค่าความเข้มข้นสูงเกินค่าอิ่มตัวไม่ส่งผลอย่างมีนัยสำคัญ สำหรับค่าประสิทธิภาพกระแสไฟฟ้าของอิเลคโทรไลเซอร์ การเพิ่มความหนาแน่นกระแสไฟฟ้า ความเข้มข้นของโพแทสเซียมไฮดรอกไซด์และซิงค์เคตไอออน ทำให้ประสิทธิภาพกระแสไฟฟ้าเพิ่มขึ้น

ภาควิชา วิศวกรรมเคมี ลายมือชื่อนิสิต .....

สาขาวิชา วิศวกรรมเคมี ลายมือชื่อ อ.ที่ปรึกษาหลัก .....

ปีการศึกษา 2559

5770561221 : MAJOR CHEMICAL ENGINEERING
KEYWORDS: ZINC-AIR FUEL CELL / ZINC ELECTROLYZER / MODELLING

WORANUNT LAO-ATIMAN: Modelling of Zinc-Air Fuel Cell and Alkaline Zinc Electrolyzer. ADVISOR: ASSOC. PROF. SOORATHEP KHEAWHOM, Ph.D., 73 pp.

A zinc-air fuel cell (ZAFC) is attracting widespread interest for electricity generation. Furthermore, ZAFC combining with alkaline zinc electrolyzer is a potential candidate for an energy storage system. This work aims to develop dynamic mathematical models of ZAFC and alkaline zinc electrolyzer and to investigate the effects of operating parameters on the cell performance. The ZAFC was devised as a tubular cell with electrolyte flow inside. Potassium hydroxide (KOH) solution mixed with zinc powder was used as the electrolyte. Stainless steel mesh and nickel foam were used as current collectors of anode and cathode, respectively. Manganese dioxide mixed with graphite used as the catalyst was coated on nickel foam. The electrolyzer cell was devised as electroplating cell with stirred electrolyte. KOH solution mixed with zinc oxide (ZnO) was used as the electrolyte of the electrolyzer. Copper sheet and nickel foam were used as the current collectors of cathode and anode, respectively. The developed models were implemented in MATLAB and validated with experimental data. Good agreement between the predicted data and experimental data was obtained for both ZAFC and electrolyzer. The proposed models were then used to investigate the effects of four parameters: KOH concentration, flow, zincate ion concentration and conductive carbon. By increasing KOH concentration, the cell voltage increased. Nevertheless, at the KOH concentration above 7 M, the cell voltage dropped as the KOH concentration increased because of the adverse effects on ionic conductivity and anodic exchange current density. ZAFC performance improved by using high flow rate. For long-time operation, using higher flow rate could maintain zinc content and electrolyte concentration better than that of lower flow rate. Higher concentration of zincate ion resulted in lower Nernst potential and cell voltage. A Higher amount of ZnO provided lower electrode conductivity and active area of zinc electrode. Adding carbon did not improve cell performance significantly. For the electrolyzer, the highest ionic conductivity was also observed at 7 M. Therefore, this concentration provided lowest cell voltage at high current. KOH concentration lower or greater than 7 M provided higher cell voltage. Below the saturation limit of zincate ion, increasing zincate ion concentration decreased cell voltage. Increasing zincate ion concentration above the saturation limit provided no significant improvement. For current efficiency (C.E.) of zinc electrolyzer, higher current density provided higher C.E. in all conditions. Moreover, increasing concentration of both KOH and zincate ion increased C.E.

Department:	Chemical Engineering	Student's Signature	.....
Field of Study:	Chemical Engineering	Advisor's Signature	.....
Academic Year:	2016		

ACKNOWLEDGEMENTS

First of all, I would like to show my appreciation to my thesis advisor, Assoc. Prof. Soorathep Kheawhom, for his advice and support throughout my graduate course. His suggestion greatly improved my work and research insight. Without his assistance, the completion of this work would have been impossible.

I am gratefully acknowledged Prof. Paisarn Kittisupakorn, Asst. Prof. Amornchai Arpornwichanop and Asst. Prof. Pornchai Bumroongsri, who are the thesis committee member for their comments and recommendations. I would like to thank staffs of department of chemical engineering who provide assistance to my work especially Mr.Kijchai Karnkajanaprapakul. He greatly provided technical assistance to my thesis experiment.

I would like to thank my father and mother for everything they have given to me. Without their support, life would not come this far. Next, I would like to acknowledge my family for their support especially my aunt who support me about fund for master's degree.

I would like to express my thankfulness to my friends who contributed me while I was studying in master's degree. My master's degree friend from process control and life cycle engineering laboratory have played an important role in my graduate pursuit about sharing knowledge and attitude.

Finally, I would like to show my gratefulness to Miss Nutthakarn Phumkokrux for her love, friendship, advice, care and encouragement.

CONTENTS

Page

LIST OF FIGURES

Page

LIST OF TABLES

Page

LIST OF SYMBOLS

	Description	Unit
a_0	initial solid-solution interface area per unit volume	dm^2 / dm^3
a_c	specific surface area of catalyst per unit volume	dm^2 / dm^3
a_s	solid-solution interface area per unit volume	dm^2 / dm^3
A	cross sectional area	dm^2
C^{ref}	reference state concentration	mol / dm^3
C_{DL}^{zinc}	double layer capacitance of zinc electrode	F / dm^2
C_k^j	concentration of specie k at electrode j	mol / cm^3
D_k	diffusivity / diffusion coefficient	dm^2 / s
$E_{0,cell}$	Nernst potential / standard electrode potential	V
E_{cell}	cell voltage	V
F	Faraday constant	C / mol
F_{conv}	convective volume flow	dm^3 / s
$F_{k,in}$	inlet molar flowrate of specie k	mol / s
$F_{k,out}$	outlet molar flowrate of specie k	mol / s
I	electrical current	A
i^{cell}	current density	A/dm^2
i_0	exchange current density	A/dm^2
i_0^{ref}	reference exchange current density	A/dm^2
i_{lim}	limiting current density	A/dm^2
J_k	molar transfer rate between electrodes	mol / s
j_k^{conv}	convective molar flow rate	mol / s
j_k^{diff}	diffusion molar flow rate	mol / s
j_k^{mig}	migration molar flow rate	mol / s
k_s	rate constant of ZnO precipitation reaction	dm^3 / s
N_k^j	moles of specie k at electrode j	mol
P^{ref}	reference pressure	atm
P_{O_2}	partial pressure of oxygen	atm
Q	electrical charge	C

	Description	Unit
r_i	rate of reaction I	mol / s
R	gas constant	J / mol · K
R_{air}	resistance of air electrode	Ω
R_{comp}	resistance of cell component	Ω
$R_{electrolyte}$	resistance of electrolyte	Ω
R_{ohmic}	total ohmic resistance	Ω
R_{zinc}	resistance of solid zinc electrode	Ω
t	time	s
t_k	transference number of ion k	-
T	temperature	K
$V_{electrolyte}^{j}$	volume of electrolyte at electrode j	dm^3
V_{solid}^{zinc}	volume of solid zinc electrode	dm^3
$V_{solid,k}$	volume of solid specie k	dm^3
$\bar{V}_k$	specific molar volume of specie k	dm^3 / mol
X_{zinc}	active surface fraction of zinc in solid phase	-
$z_k^{\pm}$	ion number of specie k	-
Z_e	number of exchange electron involved in the reaction	-

Greek symbol

α	charge transfer coefficient	-
δ_{air}	thickness of air electrode	dm
$\delta_{electrolyte}$	thickness of electrolyte	dm
δ_{zinc}	thickness of zinc electrode	dm
δ_{active}	thickness of active reaction zone	dm
δ_{Sep}	thickness of separator	dm
δ_{GDL}	thickness of gas diffusion layer	dm
$\Delta\Phi$	potential gradient between electrolyte phase	V / dm
ΔE	potential difference between zinc and hydrogen electrode	V
ε	porosity of zinc electrode	-
ε_0	initial porosity of zinc electrode	-
ε^{Sep}	porosity of separator	-

	Description	Unit
ε_{active}	effectiveness of gas transport to triple-phase boundary	-
η_{act}	activation loss / activation overpotential	V
η_{conc}	concentration loss / concentraiton overpotential	V
η_{ionic}^{Sep}	ionic separator loss	V
η_{ohmic}	ohmic loss / ohmic overpotential	V
σ_{anode}	total conductivity of anode	S / dm
$\sigma_{cathode}$	total conductivity of cathode	S / dm
σ_k	conductivity of specie k	S / dm
$\upsilon_{k,i}$	stoichiometric coefficient of specie k in reaction i	-

Subscripts and Superscripts

act	referring to activation loss
active	referring to active side or active surface
air	air electrode
anode	anode electrode
cathode	cathode electrode
cell	indicating the zinc-air fuel cell or electrolyzer
comp	cell component
conv	convective flow
diff	diffusion
elec	electrochemical reaction
electrolyte	referring to electrolyte
H	hydrogen electrode / hydrogen evolution reaction
i	reaction i (1,2,3,4)
in	inlet
j	electrode j (air, zinc)
k	specie k
lim	referring to limiting current density
mig	migration
ohmic	referring to ohmic loss
out	outlet
ref	reference state of concentration or pressure

	Description
sep	separator
solid	solid phase
zinc	zinc electrode
Zn	zinc specie / zinc electrode / reaction of zinc
0	initial point / zero current condition

CHAPTER I
INTRODUCTION

1.1 Background

Renewable energy technologies have been continuously being developed because of pressure on environmental awareness and accessibility limitations of fossil fuel. Renewable energy is promising but has intermittent characteristic. For instance, Solar energy can be convert to electricity by using photovoltaic (PV) system. The performance of PV system depends on solar radiation which is highly intermittent resulting in variation in the electricity generation. An energy storage plays an important role in the effective utilization of the energy.

Electrically rechargeable batteries and fuel cells (mechanically rechargeable battery) are attracting widespread interest. Metal-air fuel cell is a potential candidate for energy storage, particularly Zinc-air fuel cell (ZAFC). Compare with hydrogen fuel cell, ZAFC is safer, more environmentally friendly and more economical. Among other metal-air fuel cell, Zinc is high energy density material which is abundantly available and has appropriately corrosion resistance. Furthermore, zinc reacted in ZAFC to provide zinc oxide (ZnO) as product. ZnO product can be regenerated into zinc. There are many process which can regenerate ZnO. One of them is electrolysis process which is the backward process in ZAFC. Electricity energy can be store in zinc via electrolysis process and can be discharge via ZAFC.

Previously, a model of a ZAFC or a zinc electrolyzer has not been published. However, zinc-air battery (ZAB) models were previously developed. Mao and White (1992) develop mathematical model for study a primary ZAB. Later, rechargeable ZAB model was developed (Deiss, Holzer et al. 2002). Recently, another model was developed to study the effect of air composition on the performance of rechargeable ZAB (Schröder and Krewer 2014). Modeling of ZAFC can be very useful in investigation of operating parameters since the experimental studies of ZAFC is very time consuming.

In this work, the mathematical models of ZAFC and zinc electrolyzer are developed and simulated in MATLAB. The developed models are validated with the experimental data. The models are used to investigate effect of operating parameters on the performance of ZAFC and zinc electrolyzer. The studies parameters are feed flowrate and composition of zinc, potassium hydroxide (KOH) and conductive carbon.

1.2 Objective

1) To develop mathematical dynamic models of ZAFC and zinc electrolyzer
2) To investigate the effect of operating parameters on the performance of ZAFC
3) To investigate the effect of operating parameters on the performance of zinc electrolyzer

1.3 Scope of research

1) Modelling and dynamic simulation is performed in MATLAB
2) The models are validated by experimental data of ZAFC and zinc electrolyzer.
3) The design parameters of ZAFC are based on experimental ZAFC. The designed components and parameters are shown in table 1.1 and 1.2.
4) The design parameters of zinc electrolyzer are based on experimental electrolyzer. The designed components and parameters are shown in table 1.3.
5) The studied parameters are feed flowrate and compositions of zinc, ZnO, KOH and conductive carbon.

Table 1.1 Component of ZAFC

Component	**Material**
Anode Current collector	Stainless steel mesh
Cathode Current collector	Nickel foam
Separator	Nylon membrane
Anode / Cathode electrode	Zinc powder / O_2 in the air
Electrolyte	9 M KOH solution
Gas diffusion and catalytic layer	Graphite / Polytetrafluoroethylene / MnO_2

Table 1.2 Design parameters of ZAFC

Parameter	**Values**
KOH concentration	9 M
Separator thickness	100 μm
Gas diffusion layer thickness	1.6 mm
Active surface area	10 cm^2
Anode volume	10 cm^3

Table 1.3 Component and design parameters of alkaline zinc electrolyzer

Component / Parameter	**Material / Values**
Anode Current collector	Nickel foam
Cathode Current collector	Copper plate
Electrolyte	100g of 9 M KOH solution
Experimental system	100-ml beaker
Electrode distance	10 mm
Reactant	12.75 g of ZnO (1.05 M Zincate ion)
Active surface area	8 cm^2

1.4 Research Framework

Table 1.4 Planning

No.	Activity	Month								
		1	2	3	4	5	6	7	8	9
1	Review an overview of ZAFC and zinc electrolyzer									
2	Develop model of ZAFC									
3	Study the effect of operating parameters on ZAFC									
4	Develop model of zinc electrolyzer									
5	Study the effect of operating parameters on zinc electrolyzer									

CHAPTER II

THEORIES AND LITERATURE REVIEWS

2.1 Theories

2.1.1 Basic Principle of Electrochemistry

Electrochemistry is the study of chemical process that the movement of electrical charges is involved. The electrochemical reaction causes change in chemical and electrical of substances. The chemical reactions with electron transfer between molecules or atom are called oxidation-reduction reaction or redox reaction.

2.1.1.1 Redox Reaction

Redox reaction is a chemical reaction which the oxidation number / states of atoms or molecules are changed. The redox reaction can be divided into two half reactions which are oxidation and reduction. Oxidation reaction is the half reaction that donates electrons and reduction reaction is the half reaction that accepts electrons. These two half reactions must occur at the same time and combine into the redox reaction. For oxidation, the substances that donate electrons have oxidation number increased and are oxidized. For reduction, the substances that accept electrons have oxidation number decreased and are reduced.

2.1.1.2 Electrochemical cell

An electrochemical cell is a device which converts chemical energy into electrical energy or vice versa. The electrochemical cell can be classified into two types which are galvanic cell and electrolysis cell.

Galvanic cell, such as battery, can generate electrical current via a spontaneous electrochemical reaction. This kind of cell consists of two electrodes: anode and cathode. The anode is the electrode where oxidation reaction occurs. The cathode is the electrode where reduction reaction occurs. In between these electrodes, ions contained electrolyte is filled therefore the ions can freely move between the electrodes. The electrons emitted from anode transfer to cathode past external circuit. These processes make the circuit complete and electricity is produced. For galvanic cell, anode is negative electrode and cathode is positive electrode.

The other electrochemical cell is electrolysis cell. The reaction in electrolysis cell is conducted by externally supplied electricity. Electrolysis reaction is non-spontaneous which requires external energy to activate the reaction. This type of cell also consists of two electrodes same as galvanic cell: anode and cathode. For electrolysis cell, anode is positive electrode and cathode is negative electrode unlike in galvanic cell.

2.1.2 Zinc-air fuel cell (ZAFC)

A ZAFC is a type of galvanic cell. The anode is zinc electrode where zinc oxidation reaction occurs. The cathode is air electrode where oxygen reduction reaction occurs. Electrolyte usually contains hydroxide ion such as potassium hydroxide (KOH).

The schematic diagram of ZAFC is shown in figure 2.1. At anode, zinc is oxidized with hydroxide ions then transforms to tetrahydroxo-zincate ion ($Zn(OH)_4^{2-}$ or 'zincate ion' for short) as expressed in equation 2.1. Zincate ion remains in the solution to the saturation limit then transforms to zinc oxide and water as expressed in equation 2.2. At cathode, oxygen is reduced with electrons and water then transforms to hydroxide ions as expressed in equation 2.3. The overall reaction can be expressed as equation 2.4. Theoretically, the standard cell potential of ZAFC is 1.65 volt. However, the actual open circuit voltage (OCV) is less than the that because of various potential losses and practically found to be 1.45 volt (Sapkota and Kim 2009).

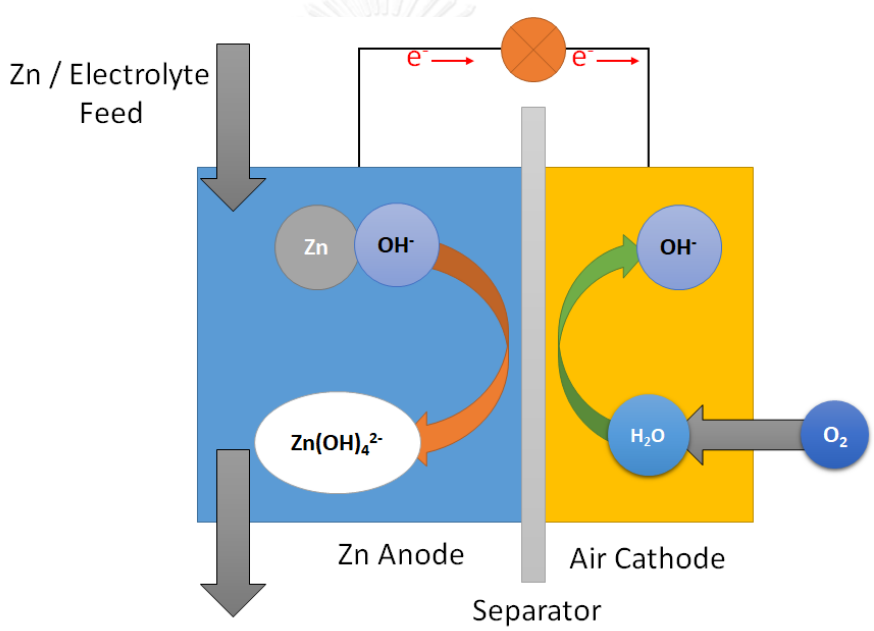

Figure 2.1 Schematic diagram of a zinc-air fuel cell

Anode reaction: $Zn+4\ OH^- \overset{r1}{\leftrightarrow} Zn(OH)_4^{2-}+2e^-$ (2.1)

$Zn(OH)_4^{2-} \overset{r2}{\leftrightarrow} ZnO+2\ OH^-+H_2O$ (2.2)

Cathode reaction: $\frac{1}{2}O_2+H_2O+2\ e^- \overset{r3}{\leftrightarrow} 2\ OH^-$ (2.3)

Overall reaction: $2\ Zn+O_2 \leftrightarrow 2\ ZnO$ (2.4)

Typically, the performance of electrochemical cell is usually expressed in term of polarization curve. As shown in figure 2.2, the polarization curve indicates behavior of cell potential in the function of current or current density. The polarization curve can be generally divided into 3 zones. The first zone is activation loss zone. This zone ranges from OCV to the initial steep of potential decrease. The activation losses are

losses from slowness of the reactions. These losses dominate the first zone of polarization curve. Secondly, ohmic loss zone where the voltage slowly decreases is dominated by losses from electrical resistance of the cell components (electrodes and interconnection parts) and the resistance to the flow of ions in the electrolyte. The last zone is concentration loss zone. This loss occurs at high current density due to mass transport limitation resulting in rapidly decreasing of voltage.

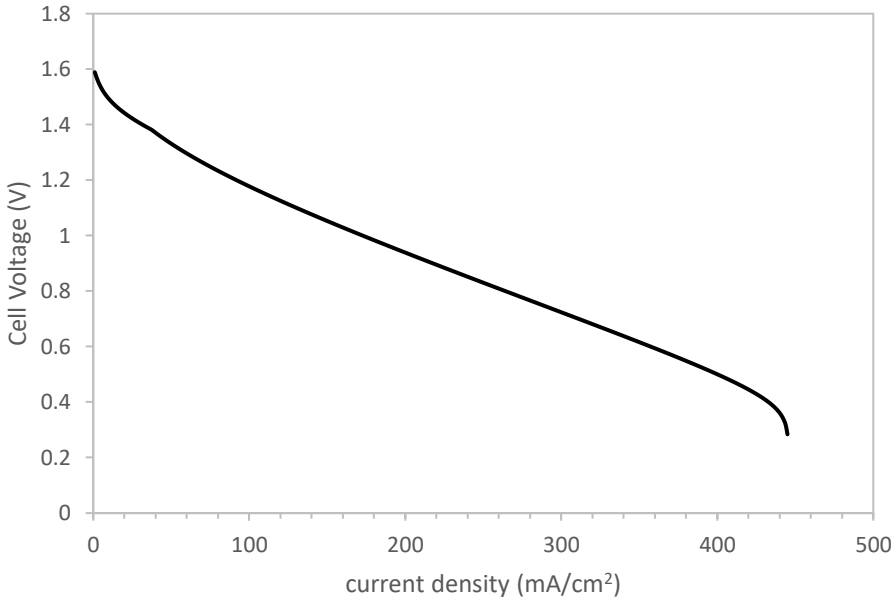

Figure 2.2 Polarization curve of a ZAFC

2.1.3 Zinc regeneration

Zinc is used as fuel of ZAFC. The reacted zinc transforms to zincate ion and ZnO. There are various methods to regenerate zinc from zincate ion and ZnO. This work interests in electrolysis method. Electrolysis is a process which used external electrical energy to induce the non-spontaneous redox reaction. This method is appropriate for ZAFC because anodic product of ZAFC consists of ZnO and hydroxide ions which are same as reactants of electrolysis process. The reactions in this electrolysis cell are the backward reactions of Zinc-air galvanic cell as expressed in equation 2.5 to 2.8. The reactions can begin with ZnO or zincate ion and provide zinc and oxygen as products. The electrolysis of water is side reaction in cathode of the electrolysis cell as expressed in equation 2.9. The other side reaction is corrosion of zinc in alkaline as expressed in equation 2.10 and 2.11. The standard cell potential is 1.65 volt same as galvanic cell except the sign is opposite which means how much potential supply to make reactions theoretically occurred.

Cathode reaction: $ZnO+2OH^-+H_2O \rightarrow Zn(OH)_4^{2-}$ (2.5)

$Zn(OH)_4^{2-}+2e^- \rightarrow Zn+4OH^-$ (2.6)

Anode reaction: $2OH^- \rightarrow \frac{1}{2}O_2+H_2O+2e^-$ (2.7)

Overall reaction: $ZnO \rightarrow Zn + \frac{1}{2}O_2$ (2.8)

Side reaction: $2H_2O + 2e^- \rightarrow H_2 + 2OH^-$ (2.9)

$Zn + 2OH^- + 2H_2O \rightarrow Zn(OH)_4^{2-} + H_2$ (2.10)

$Zn + 2H_2O \rightarrow Zn(OH)_2 + H_2$ (2.11)

The polarization curve of electrolysis cell is different from galvanic cell as shown in figure 2.3. The potential losses stack up over the OCV opposite with the galvanic cell. Cell potential increases along with the current density. For the electrolyzer, there is another performance

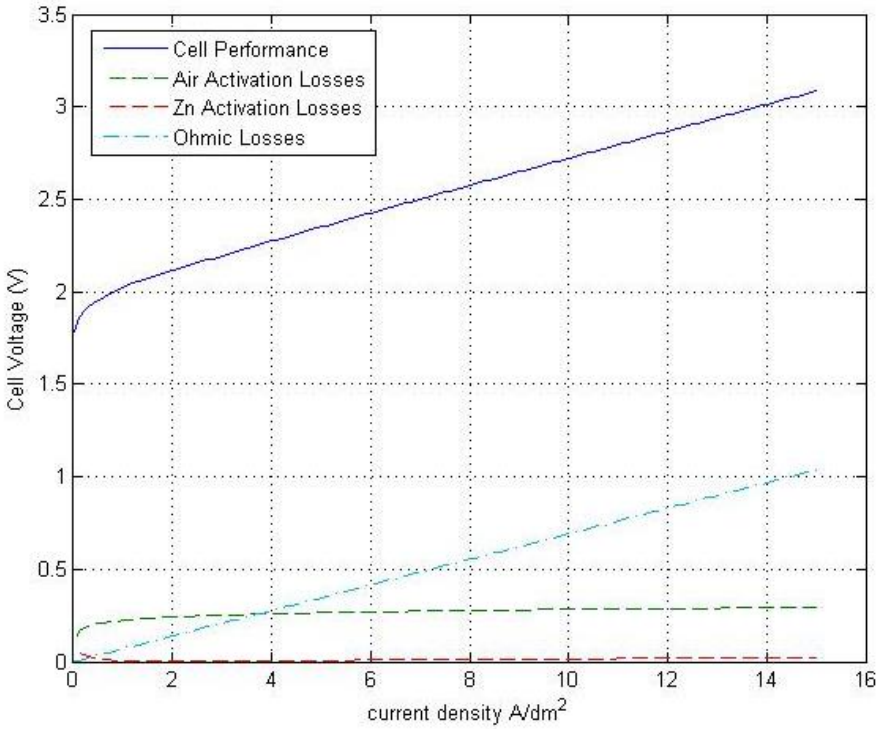

Figure 2.3 Example of electrolysis polarization curve

2.1.4 Cell Potential

For operation of ZAFC, the electrical energy generated from chemical energy ($W_{electrical}$) is mathematically express by the product of cell electromotive force (E_{emf}) and total charge transfer (Q) as express in equation (2.12).

$$W_{electrical} = -Q \times E_{emf} \quad (2.12)$$

$$Q = nF \quad (2.13)$$

Where n is the number of electrons involve in the reaction and F is Faraday constant.

At zero current state without any loss in the system, the maximum E_{emf} is obtained. At this state, the maximum possible electrical energy can be extract from the

system therefore this maximum extracted energy is equivalent to the Gibbs free energy change (ΔG).

$$\Delta G = -nFE_{emf} \quad (2.14)$$

The change of Gibbs free energy can indicate the spontaneity of the electrochemical reaction. From equation (2.14), when cell potential is negative, the change of Gibbs free energy is positive which indicates that the reaction is spontaneous reaction. For electrolyzer, positive cell potential provides negative change in Gibbs free energy. This means the system requires the external energy to drive the reaction. The Gibbs free energy change can also use to calculate equilibrium half-cell voltage or standard electrode potential (E^0).

$$E_{emf} = E^0 = -\frac{\Delta G}{nF} \quad (2.15)$$

From equation (2.15), the standard electrode potential of reaction (2.1), (2.3) and (2.9) can be calculated and equal to -1.25, +0.401 and -0.878 Volt versus standard hydrogen electrode (SHE), respectively. For standard state, the standard electrode potential can be used to calculated the equilibrium cell potential. However, the cell potential deviate from the standard potential at non-standard state. In this case, Nernst equation is used to explain the influence of the activity of reactant. Then, the half-cell potential can be used to calculated the open circuit voltage (OCV) as expressed in equation (2.17).

$$E = E^0 - \frac{RT}{nF} ln \frac{a_{red}}{a_{ox}} \quad (2.16)$$

$$E_{cell} = E_{cathode} - E_{anode} \quad (2.17)$$

Where a_{red} and a_{ox} are the activity of reduced and oxidized form of reactant, respectively. E is electrode potential and superscript 0 stands for standard state.

OCV is the electrical potential difference of the electrochemical cell which measured at disconnected any external circuit or zero current state. Theoretically, OCV of zinc-air cell is about 1.65 volt. However, the actual OCV and the theoretical OCV is different for this case. The theoretical OCV is the equilibrium cell voltage but the actual OCV includes some losses to activation and resistance. Practically, the measured OCV of zinc-air cell is approximately 1.3 - 1.4 volt.

2.1.5 Reaction Kinetics and Mechanisms

2.1.5.1 Zinc Electrode

As mentioned in section 2.1.2 and 2.1.3, the reactions of zinc electrode are described in reaction (2.1) and (2.2) which are simplified reactions.

$$Zn + 4\,OH^- \overset{r1}{\leftrightarrow} Zn(OH)_4^{2-} + 2e^- \quad (2.1)$$

$$Zn(OH)_4^{2-} \overset{r2}{\leftrightarrow} ZnO + 2\,OH^- + H_2O \quad (2.2)$$

However, the real mechanisms are very complicated and remain argued and disputed topic. There are two most acceptable mechanism. One of them was proposed by Hampson and coworker (Farr and Hampson 1967, Hampson, Herdman et al. 1970,

Dirkse and Hampson 1972). The mechanism was derived from galvanostatic and double-impulse methods, and can be expressed by reactions (2.18) – (2.21).

$$Zn+OH^- \leftrightarrow Zn(OH)_{ads}^- \quad (2.18)$$

$$Zn(OH)_{ads}^- \leftrightarrow Zn(OH)_{ads}+e^- \quad (2.19)$$

$$Zn(OH)_{ads}+OH^- \leftrightarrow Zn(OH)_2+e^- \quad (2.20)$$

$$Zn(OH)_2+2OH^- \leftrightarrow Zn(OH)_4^{2-} \quad (2.21)$$

This mechanism includes absorption of Zn species. The charge transfer reactions in this mechanism are reactions (2.19) and (2.20). The rate-determining step for anodic process is reaction (2.18). For cathodic process, reaction (2.19) is considered as the rate-determining step. The other mechanism was proposed by Bockris, Nagy et al. (1972). It was derived by using galvanostatic and potentiostatic transient techniques, and can be described as reaction (2.22) – (2.25).

$$Zn+OH^- \leftrightarrow Zn(OH)+e^- \quad (2.22)$$

$$Zn(OH)+OH^- \leftrightarrow Zn(OH)_2^- \quad (2.23)$$

$$Zn(OH)_2^-+OH^- \leftrightarrow Zn(OH)_3^-+e^- \quad (2.24)$$

$$Zn(OH)_3^-+OH^- \leftrightarrow Zn(OH)_4^{2-} \quad (2.25)$$

In this mechanism, the reaction (2.24) is proposed to be the rate-determining step of both anodic and cathodic processes. The charge transfer reactions are reactions (2.22) and (2.24). The debated topics of these two mechanisms are about the rate-determining step and the presence / absence of $Zn(OH)_3^-$.

2.1.5.2 Air Electrode

For air electrode, the oxygen reduction reaction and oxygen evolution reaction are simply described in reversible reaction (2.3).

$$\frac{1}{2}O_2+H_2O+2\,e^- \overset{r3}{\leftrightarrow} 2\,OH^- \quad (2.3)$$

The real mechanism is also very complicated same as zinc electrode. In alkaline aqueous electrolyte, there are two main paths of oxygen reduction that widely accepted: the direct 4-electron pathway and the 2-electron peroxide pathway (Song and Zhang 2008). For the direct 4-electron pathway, the overall reaction was shown as reaction (2.3). The standard reduction potential of this pathway is 0.401 volt versus SHE. On this pathway, oxygen is directly reduced to hydroxide ion. The other pathway is the 2-electron peroxide pathway. The reactions of this pathway are expressed by reactions (2.26) – (2.28).

$$O_2+H_2O+2\,e^- \leftrightarrow HO_2^- + OH^- \quad (2.26)$$

$$HO_2^- + H_2O+2\,e^- \leftrightarrow 3OH^- \quad (2.27)$$

$$HO_2^- \leftrightarrow OH^- + \frac{1}{2}O_2 \quad (2.28)$$

For reaction (2.26), oxygen is reduced to peroxide ion and this reaction has standard electrode potential of -0.076 volt versus SHE. The peroxide ion can be reacted further

by reduction reaction (2.27) or disproportionation reaction (2.28). The standard electrode potential of reaction (2.27) is 0.878 volt versus SHE. The overall reaction is still reaction (2.3). This pathway is widely agreed and the mechanism dominates for the most carbons and metal oxide catalyst.

Additionally, there are many studies that investigated about the complexity of peroxide pathway. For carbon material, the peroxide pathway could be described by elementary reactions as follows (Appleby and Marie 1979):

$$O_2 + e^- \leftrightarrow O_2^- \quad (2.29)$$

$$O_2^- + H_2O \leftrightarrow HO_2^- + OH \quad (2.30)$$

$$OH + e^- \rightarrow OH^- \text{ (rapid)} \quad (2.31)$$

Reaction (2.30) is proposed to be the rate-determining step. The reaction orders which respect to oxygen and hydroxide ion are first order and zero order, respectively.

2.1.6 Cell performance evaluation and effecting parameters.

Generally, the performance of electrochemical cell is evaluated by open circuit voltage (OCV), power density and polarization curve. In some case, the efficiency of the cell can also be calculated. For electrolyzer case, current efficiency can be evaluated to indicate the utilization of electrical energy supplied to regenerate zinc.

2.1.6.1 Open Circuit Voltage (OCV)

As mentioned in section 2.1.4, OCV is the potential difference measured at zero current state. It represented the equilibrium cell potential which included some activation and resistance loss. The main equation that describe OCV is equation (2.17). The equation (2.17) can be combined with Nernst equation of zinc-air case resulted in equation (3.20).

$$E_{cell} = E_{cathode} - E_{anode} \quad (2.17)$$

$$E_{0,cell} = \left[0.401 + \frac{RT}{Z_e^{air} \cdot F} ln\left(\frac{(P_{O_2}/P^{ref})}{(C_{OH^-}^{air}/C^{ref})^4}\right)\right] - \left[-1.266 + \frac{RT}{Z_e^{zinc} \cdot F} ln\left(\frac{(C_{Zn(OH)_4^{2-}}^{zinc}/C^{ref})}{(C_{OH^-}^{zinc}/C^{ref})^4}\right)\right] \quad (3.20)$$

The parameter that affected OCV is temperature and the activity of reactants and products of the reactions.

2.1.6.2 Polarization Curve and the Overpotential.

Polarization curve explains the relationship of cell voltage and applied current. When external electrically load changes, cell voltage changes along with current. Figure 2.5 depicted the polarization with overpotentials of ZAFC. The curve can be divided in to three regions based on the dominant overpotential.

A) Activation Overpotential

The activation overpotential is the energy loss from the activation of the electrochemical reaction. This loss dominates the early region to the middle region of the polarization curve ranging from OCV to the initial constant slope zone. For zinc-air case, activation overpotentials are caused by reaction (2.1) and (2.3). For zinc activation

loss, concentration of electrolyte and surface area of zinc are the major parameters that provide effect to this loss. The major activation overpotential is the activation loss of air electrode. There are various parameters that affect the air overpotential due to the complexity and sluggishness of the oxygen reduction and evolution reaction. The parameters that involve in mass transfer of oxygen are mainly concerned such as diffusivity of oxygen in gas diffusion layer.

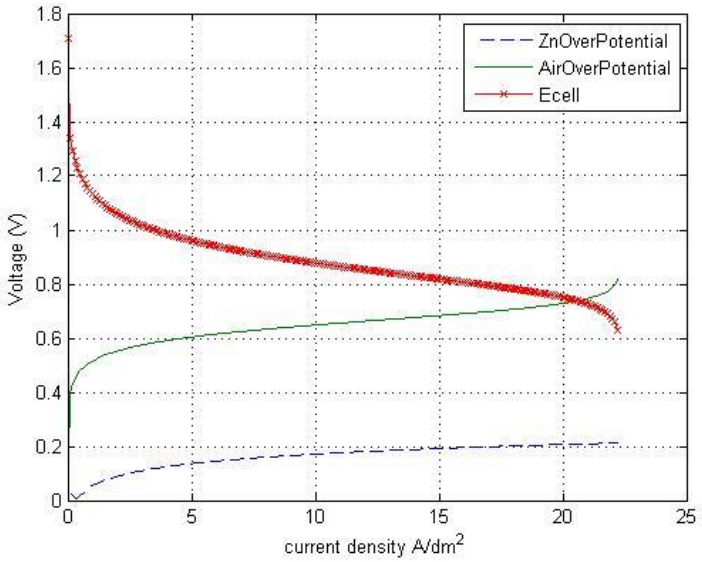

Figure 2.4 polarization curve and overpotentials of a ZAFC

B) Ohmic Overpotential

The ohmic overpotential is the energy loss from the resistance of the electrode, electrolyte and other cell components. This loss dominates the middle region of the curve ranging over the constant slope zone. The parameters that affect the resistance in the cell contributed to ohmic loss. For instance, changing concentration of KOH solution affect the conductivity of electrolyte.

C) Concentration Overpotential

The concentration overpotential is the energy loss from the depletion of reactant due to mass transfer limitation. This loss dominates the high current region of the curve demonstrating in the rapidly drop of discharging cell voltage or the highly surge of charging voltage. For zinc-air discharging case, diffusion limit of oxygen to the air cathode is the predominant contribution to the concentration loss. Mass transfer limit of hydroxide ion is the second dominant. Most of the zinc-air case suffer from the oxygen diffusion limit before the hydroxide ion transfer limit can even occur. For electrolyzer case, mass transfer limit of zincate ion happened and caused the dendrite formation.

2.1.6.3 Power Density

Knowing the overall cell power does not guarantee whether the cell performance is high or low. The power need to be normalized to the active area of the electrode. The normalized specific power is called power density.

$$P_{density} = \frac{Net\ power}{Active\ Area} = I_{density}E_{cell} \quad (2.18)$$

In zinc-air case, active area is usually the air cathode area. This power density can be used to compare among the report literature.

2.1.6.4 Current Efficiency (C.E.)

For alkaline zinc electrolyzer case, the cell performance evaluation other than cell voltage is current efficiency. Current efficiency or coulombic efficiency is the ratio of the electrochemical equivalent current for the specific reaction to the total applied current. In this simulation, C.E. was defined as the ratio of zinc regeneration current density to the total current density applied.

$$C.E. = \frac{i_{Zn}}{i_{Cell}} \quad (2.19)$$

This efficiency indicates whether how much actual current is supplied to the zinc regeneration reaction compared to the total current applied. The low C.E. indicates that a lot of current loss to the other side reaction.

2.2 Literature reviews

2.2.1 Zinc-Air Fuel Cells / Batteries

Zinc-air fuel cells and zinc-air batteries has been developed for many years. Laboratories de Marcoussis (C.G.E.) proposed zinc-air circulating flow battery system for using as vehicle power source (Appleby and Jacquier 1976). The batteries were design as tubular cells. Zinc was mixed with electrolyte and stored in the reservoir. The electrolysis unit also proposed. This system was capable of 110 Wh/kg, 80 W/kg for an urban vehicle and up to 125 Wh/kg for heavy duty application. The energy density of this system was three times higher than that of the lead-acid battery.

Savaskan, Huh et al. (1992) studied a zinc-air cell with packed bed anode. This cell had air electrode area of 76 cm^2. The peak power density of 185 mW/cm^2 was exhibited at temperature of 45 degree Celsius with current density of 200 mA/cm^2. Projected specific energy and projected specific power of the cell were 110 Wh/kg and 97 W/kg under the Simplified Federal Urban Driving Schedule. In optimized capacity mode, the specific energy and specific power increased to 228 Wh/kg and 97 W/kg, respectively. In maximized power mode, the values changed to 101 Wh/kg and 150 W/kg, respectively.

Sapkota and Kim (2010) studied the ZAFC performance with inexpensive manganese oxide (MnO_2) catalyst and organic polymer separator. This cell design as a taper-end cell with anode incline angle of 3 degrees. Air cathode was compared between three types. It was found that MnO_2 mixed with cerium oxide provided the best performance. Separator was compared between 4 types of polymer membrane. The

result showed different separators did not provide remarkably difference on ZAFC performance. However, nylon net filter performed better stability than the others in alkaline solution.

Ma, Wang et al. (2014) developed an Electrically rechargeable ZAB stack. The peak power density of 64 mW/cm^2 was achieved at current density of 80 mA/cm^2. The total peak power was 4500 mW. The estimated average cell resistance was about 12.7 $\Omega \cdot cm^2$ for charging process and 9.7 $\Omega \cdot cm^2$ for discharging process. The average energy efficiency before and after 10 charge-discharge cycles reached 89.28 and 72.19 %, respectively (discharging and charging current of 25 and 15 mA/cm^2). The charging voltage increased 1.56 % after 100 charge-discharge cycles, which performed excellent stability.

Jiratchayamaethasakul, Srijaroenpramong et al. (2014) studied the effect of flow channel design and orientation on performance of ZAFC. The cell was filled with zinc powder and was continuously fed with KOH solution. Different flow rates of 2, 4 and 6 ml/h was investigated. The result revealed that anode-bottom orientation had higher cell performance than anode-top orientation. Anode-top orientation cause the flooding of cathode that induced by gravity force. For the flow channel effects, serpentine flow channel provided total charge per gram of zinc higher than that with parallel channel. For this case, the optimum flowrate that yielded maximum discharge capacity was 4 ml/h. The peak power density of 240 mW/cm^2 at current density of 500 mA/cm^2 was observed.

High performance ZAFC stack was developed (Pei, Ma et al. 2014). This cell used MnO_2 as catalyst for oxygen reduction reaction. The circulation of KOH made the reaction product low and act as coolant. The characteristics of polarization, constant current discharging and dynamic response were investigated by experiment. The maximum power density of 435 mW/cm^2 (0.86 V at 510 mA/cm^2) was observed. Effects of cell location, filled state of zinc, contact resistance and flow state of electrolyte were studied. The result showed that location of cell could affected the temperature of cell and consequently cell performance. Anode chamber of type Y provide better performance in filled state of zinc than type V. Contact resistance needed to be minimize for cell improvement. Flow rate of electrolyte should be sufficient to maintain high concentration of hydroxide and removed ZnO away.

Bockelmann, Kunz et al. (2016) proposed electrically rechargeable zinc-oxygen flow battery with three electrode configurations. A copper foam was used as substrate for zinc electrodeposition. Potassium hydroxide was used as electrolyte. Nickel foam was used as oxygen reduction electrode and silver was used as oxygen evolution electrode. The peak power density of 270 mW/cm^2 was obtained at current density of 460 mA/cm^2. This cell was able to charge and discharge up to 600 mA/cm^2, and was able to operate more than 600 charge-discharge cycles.

Because zinc was stored in the electrolyte in some configuration of ZAFC, the corrosion of zinc should be accounted. Kim, Jo et al. (2015) studied corrosion inhibition in ZAFC. Inhibitors coating on zinc surface was implemented to improve electrochemical performance of zinc anode. Coating material on zinc surface slowed down corrosion but increased charge transfer resistance compared with pure zinc. The

hydrogen overpotentials of coated zinc were negatively higher than pure zinc therefore hydrogen evolution reaction was suppressed.

2.2.2 Zinc-air modelling

Previously, a few mathematical models of zinc-air battery (ZAB) were developed but there is no model that develops for zinc-air fuel cell (ZAFC). The published model was mostly about zinc-air battery. Mathematical modeling of a primary ZAB was studied by Mao and White (1992). This model was used to investigate the behavior of primary ZAB with respect to battery design features. The resulting simulations had good agreement with experimental data. The result concluded that anode material utilization is limited by depletion of hydroxide ions.

Next, ZAB model was developed to include charging process therefore the battery model could simulate in cycle. A rechargeable ZAB model was developed by Deiss, Holzer et al. (2002) to analyze galvanostatic experimental data. The simulation data of this model were in good agreement with the experimental values. The results predicted that hydroxide ion depletion is limiting factor for high-current discharge and unwanted redistribution of Zn per cycle decrease with increasing cycle number.

Schröder and Krewer (2014) developed an isothermal mathematical model of a secondary ZAB to investigate the effect of air composition on the performance of battery. The studied parameters of this work were the relative humidity, carbon dioxide and oxygen. The simulation result showed that air composition strongly impacts ZAB operation. The air humidity can contribute electrode flooding or electrolyte drying out. The carbon dioxide reduces the hydroxide ion concentration and shortens battery life-time. The oxygen affects the limiting current density. The electrode flooding problem was studied further. Schröder, Laue et al. (2016) proposed one-dimensional gas diffusion electrode model with moving gas-liquid interface to investigate the electrode flooding and pulse current operation. This model was calculated by finite volume method and could analyze concentration distribution in the electrode.

Wang, Pei et al. (2015) proposed a model of recharging process in ZAB which included the growth of oxygen bubbles. Oxygen was generated at the air electrode during the charging process. The simulation suggested that oxygen bubble coalescence was inhibited by using flowing electrolyte and partial insulation electrode structure.

Jung, Kim et al. (2016) proposed one dimensional model that used to investigate design parameters of the ZAB and analyze zinc utilization. This model considered the effect of hydroxide ion on the ZnO precipitation in order to obtain realistic prediction. The predicted discharge curves were validated with experiment data at discharging current of 10 mA/cm^2. The proposed model was used to studied the effect of thickness of anode and separator on the utilization of zinc. It was found that the highest zinc utilization of 97% was observed at compact anode with thickness of 0.61 mm and sufficiently thick separator with thickness of 0.11 mm. Using thicker anode and thinner separator than these decreased the zinc utilization.

Recently, modelling was utilized to study ZnO precipitation in ZAB (Stamm, Varzi et al. 2017). Nucleation and growth of ZnO during ZAB discharging was modelled. For validation, the predicted discharge curves were compared with the

experimental discharge curves at various discharge current density. The proposed model expresses the convection of electrolyte and considered the nucleation and growth of ZnO product. Inhomogeneity of zinc dissolution and ZnO deposition was observed in primary ZAB. It was found that adding ZnO to zinc electrode improved the rechargeable capacity although the initial discharge capacity was reduced. Effect of carbon dioxide (CO_2) was also investigated. The result showed that CO_2 limited the lifetime of battery because absorption of CO_2 significantly decreased the hydroxide concentration in the electrolyte.

2.2.3 Electrolytes

Zinc-air system consisted of alkaline electrolytes. Potassium hydroxide (KOH) is the most commonly used alkaline because of its high conductivity, high activity and good low temperature performance (Xu, Ivey et al. 2015). The conductivity of KOH at various concentration was displayed in figure 2.5. At 25 degrees Celsius, a maximum conductivity of 625 mS/cm is observed at 30 wt% KOH (about 7 M). 7 to 9 M KOH was chosen to use in many studies because of its good conductivity and high concentration of hydroxide ion. This suggested that electrolyte conductivity play an important role in ZAFC and improvement of the electrolyte conductivity is the promising solution to enhance the ZAFC performance.

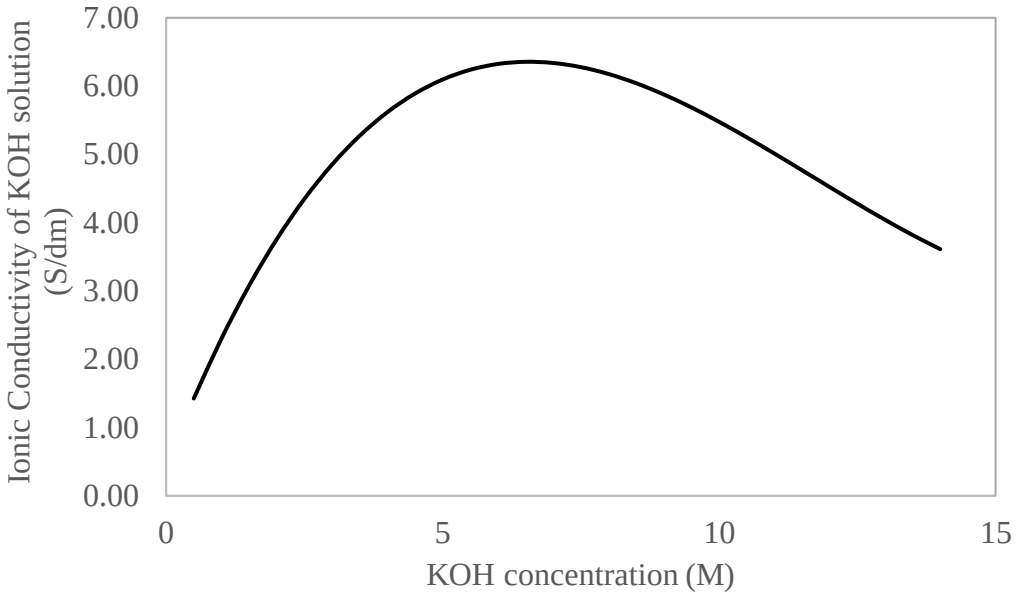

Figure 2.5 ionic conductivity of KOH solution at various concentration from the correlation proposed by See and White (1997)

Sapkota and Kim (2010) studied about electrolyte in ZAFC. The electrolyte was compared between potassium hydroxide (KOH) and sodium hydroxide (NaOH). The result indicated that KOH was provide higher performance of ZAFC than NaOH because K^+ has higher ionic conductivity than Na^+. Then, the effect of concentration on the cell performance was examine by the KOH concentration of 4, 8 and 16 M. The cell performance increased along with the concentration at low current density (figure 2.6). However, once the viscosity become too high, it negatively affects the cell performance

at high current density. Due to the high viscosity of 16 M KOH electrolyte, the cell performance with 8 and 16 M KOH electrolyte were not different at high current density.

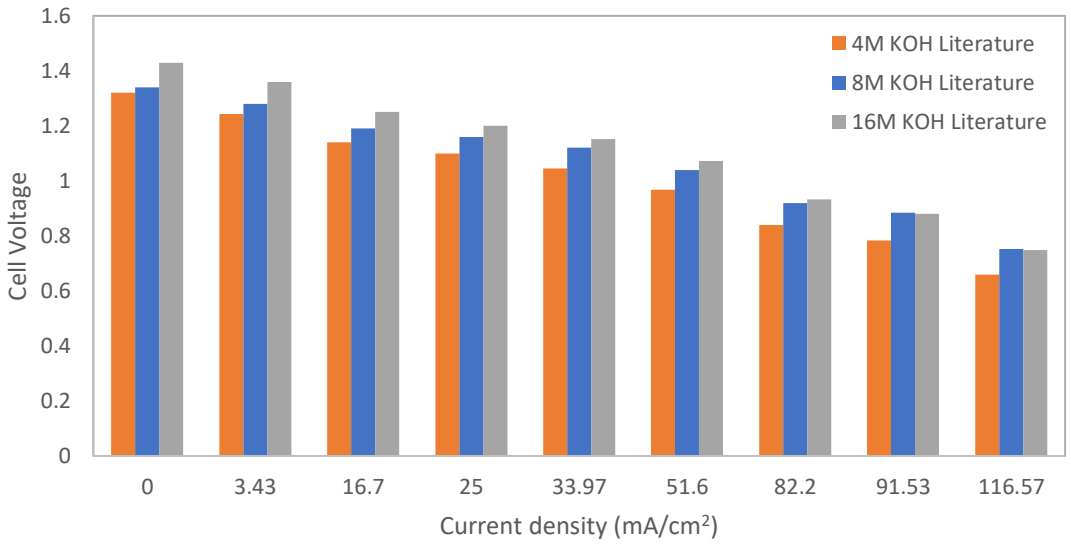

Figure 2.6 comparison of the ZAFC performance between various KOH compositions (Sapkota and Kim 2010)

Effect of electrolyte concentration and depth of discharge on ZAFC was studied by Li, Zhang et al. (2015). ZAFC in this experiment was characterized by voltammetry, discharge profile and electrochemical impedance spectroscopy (EIS) method. The maximum cell performance obtained at 7 M KOH (current density of 102 mA/cm2 at 1 Volt). The cell performance reduced when discharge time increased. Replacing zinc and electrolyte was able to improve cell performance for long-time operation.

The electrolyte flow is an advantage of ZAFC over ZAB. The studied of flow and gelled electrolyte in ZAFC was studied by Puapattanakul, Therdthianwong et al. (2013). Comparison between flowing and non-flowing electrolyte was examined. The result showed that ZAFC with flowing electrolyte provided 27% higher average current than that with non-flowing electrolyte. The gelled electrolyte did not significantly affect the cell performance but it provided lower amount of gas evolution. Furthermore, the patent of Kim, Suh et al. (2013) invented a ZAFC and compared the circulation rate of electrolyte. The compared circulation rate is 0 to 150 ml/min. It was observed that the circulation of electrolyte remarkably enhanced the cell performance comparing to the cell without electrolyte circulation. The higher circulation rate up to 50 ml/min provided higher cell performance. The circulation rate over 50 ml/min did not significantly improve the cell performance.

2.2.4 ZnO formation

ZnO formation has negative effect on zinc-air system performance because of ZnO low electrical conductivity. ZnO precipitates as an electrical insulating paste and coats on the cell components resulting in higher ohmic overpotential. ZnO can be form on the zinc surface which makes the electrode passivated (also known as zinc

passivation). Influence of ZnO precipitation on the cycling stability of rechargeable ZAB was systematically investigated (Kim, Kim et al. 2015). The sample with zinc content higher than the supersaturation solubility limit (SSL) has ZnO formation and has lower cycling stability than the sample with zinc content lower than the SSL. The investigation result suggested that controlling of zincate ion concentration below supersaturated solubility limit could prolong the cycle life of ZAB because ZnO precipitation was prohibited. Design the amount of zinc below the SSL or design the electrolyte with higher SSL was suggested as a procedure to control ZnO formation.

It is well known that electrolyte additives can inhibit ZnO precipitation. Scavenging zincate by calcium hydroxide in ZAFC was investigated (Zhu, Duch et al. 2015). Calcium hydroxide reacts with zincates and forms calcium zincate which can be regenerate to zincate later. It was found that calcium hydroxide was able to remove zincate ion from electrolyte rather than ZnO. By the excess free water, ZnO could dissolve more because of decreasing in zincate ion concentration. The result indicated that scavenging zincate using calcium hydroxide can increase the electrolyte capacity of ZAFC.

Modelling was also used to account the phenomenon of ZnO formation. A two-dimensional mathematical model of porous zinc electrode was developed by Isaacson, McLarnon et al. (1990). This model included potential of electrode and electrolyte, current density distribution, electrolyte concentrations and ZnO distribution. The simulation result showed that active zinc moved from the center of the electrode toward the electrode surface.

The importance of equilibrium zincate ion concentration in modelling was investigated by Kriegsmann and Cheh (1999). The expression of equilibrium zincate ion was revised in a mathematical model of the zinc/manganese oxide alkaline cell. The ZnO data of Kordesch was used to model the new expression. The revised model predicted lower and more uniform zincate ion concentration profiles.

2.2.5 Recharging process / Zinc regeneration

The deposition of electrolytic zinc from alkaline zincate solution was investigate (Sharifi, Mojtahedi et al. 2009). The effect of parameters on current efficiency, morphology and specific area of zinc powders were analyzed. The resulted showed that the current efficiency increases with increasing current density under all condition but the morphology changes from dense and uniaxial to dendritic and loose. The higher zincate concentration provides higher current efficiency. Decreasing KOH concentration from 11 to 9M increases the current efficiency because hydrogen evolution occurs more in higher KOH concentration.

Morphology of zinc deposition was significant issue for zinc regeneration. Simičić, Popov et al. (2000) study the zinc morphology in alkaline electrolyte at low direct and pulsating overpotential. It was found that low nucleation rate with mass transfer limit caused the spongy morphology. In the pulsating square-wave overpotential pattern, the morphology was less agglomerated than in direct overpotential pattern.

Dendritic formation of zinc should be avoided in ZAB and ZAFC. Morphology control of zinc regeneration was investigated by Wang, Pei et al. (2014). This work analyzes the mechanism of shape change and controls the zinc morphology during regeneration. The three-dimensional model was developed and simulated with COMSOL software. It was found that zinc morphology development depends on the rate of ion transfer, charge transfer and atom attachment at different depositing conditions. For morphology control, uniform morphology is obtained at low current, pulsating current and flow electrolyte. Higher zincate and lower KOH concentration are also favored.

Wang, Pei et al. (2015) further investigated dendrite growth in recharging process of ZAB with phase-field model. The model was used to study the effect of dendrite growth on cell potential and zinc ion concentration gradient. The result showed that low charging current can inhibit the dendrite growth. Pulsating current and electrolyte flow could slow down the dendrite growth. It was concluded that the morphology of zinc deposition depended on activation control in early stage. At the late stage, diffusion-limited control of zinc ions was dominated.

Gavrilović-Wohlmuther, Laskos et al. (2015) studied the effect of electrolyte concentration, temperature, flow velocity and current density on zinc deposition morphology. It was found that highly alkaline electrolyte provided mossy and spongy morphology. Mossy zinc deposition was found in higher zincate ion concentration, higher temperature. Increasing current density promoted dendritic growth. The highest coulombic efficiencies of 87 – 93% were observed at the condition of 0.5 M ZnO in 8 M KOH at temperature of 50-70 degree Celsius with current density of 100 mA/cm^2 and linear flow velocity higher than 6.7 cm/s.

The other issue that should be account is hydrogen evolution in zinc electrode. Einerhand, Visscher et al. (1988) studied about hydrogen generation during zinc electrodeposition in alkaline solution. They investigate the effect of current density and KOH and zincate ion concentration. It was found that increasing current density promoted hydrogen generation. Increasing KOH and zincate ion concentration reduced hydrogen evolution. It was concluded that hydrogen was generated from corrosion of zinc rather than from electrochemical formation.

Saleh, Weidner et al. (1995) studied electrowinning of zinc with hydrogen evolution. A mathematical model of electrowinning process was proposed. Reasonable agreement between the model and the experiment was obtained at low current density range. The simulation result showed that When mass transfer control dominated the zinc reaction, coulombic efficiency was improved by increasing electrolyte flowrate and zincate ion concentration.

Electrically recharging process in ZAFC with additives was studied (Lee, Sathiyanarayanan et al. 2006). The electrode additives were cellulose and lead oxide which were employed to address dendrite formation and hydrogen evolution. The additives were able to partially reduce dendrite formation and increase hydrogen overpotential.

Many zinc regeneration processes has been developed. The regeneration method is mainly classified into two processes: electrolysis and carbothermal. Electrolysis is more favored than carbothermal method (Zabaleta 2011). Lawrence

Livermore National Laboratory (LNLL) had developed various zinc regeneration method such as electrolysis at bipolar nickel electrode (Cooper and Krueger 2006). Zinc recovery with electrolysis at bipolar nickel electrode had same reaction as rechargeable ZAB therefore this method is favorable for ZAFC.

Wen, Cheng et al. (2009) studied zinc electrolysis with propanol oxidation as counter electrode. The highest organic-electro-synthesis efficiency of 82% was obtained when the propanol concentration was up to 1M. Huh, Savaskan et al. (1992) studied regeneration of zinc and electrolyte by fluidized bed electrodeposition. The lowest energy consumption of 1.92 kWh/kg of zinc was achieved at 1000 A/m^2 superficial current density. Combining with the previously proposed discharging cell, the roundtrip efficiency of the system for discharging and charging were 50 and 46%, respectively. Jiricny, Siu et al. (2000) proposed zinc electrolysis cell with a spouted-bed electrode. The range of obtained particle was from 0.4 to 1 mm. A larger cell was able to regenerate zinc up to 10 kg per day and performed cell voltages and energy consumption rate approximately to smaller cells.

ZAFC can be integrated with zinc regeneration process. A regenerative ZAFC was proposed (Smedley and Zhang 2007). Discrete particle electrolyzer was used as regenerator. The system was designed to serve as source of backup emergency power. It contained a 12 cell stacks providing 1.8 kW. The schematic diagram of the example integrated system is shown in figure 2.7.

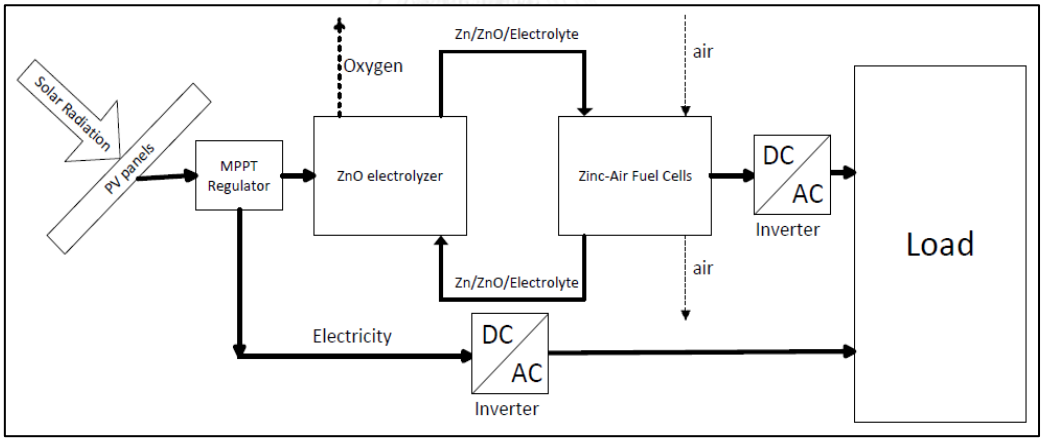

Figure 2.7 Schematic diagram of a ZAFC, zinc regenerator and photovoltaic cells integrated system.

Table 2.1 Literature reviews of ZAFC / ZAB

Description	Performance	Reference
Zinc-air circulation flow battery for using as vehicle power source	Specific energy of 110 Wh/kg Specific power of 80 W/kg	Appleby and Jacquier (1976)
Zinc-air cell with packed bed anode	Peak power density of 185 mW/cm^2 at 20 mA/cm^2 45°C	Savaskan, Huh et al. (1992)
A regenerative ZAFC	12 cell stacks a1.8 kW. Net power output of 1.1 kW for 24h	Smedley and Zhang (2007)
ZAFC with MnO_2 catalyst and polymer separator	Current density of about 70 mA/cm^2 at 1 Volt	Sapkota and Kim (2010)
ZAFC with flowing gelled electrolyte	Current of about 370 mA at 1 Volt	Puapattanakul, Therdthianwong et al. (2013)
ZAFC with circulation electrolyte	Current density of about 70 mA/cm^2 at 1 Volt	Kim, Suh et al. (2013)
Rechargeable ZAB stack	Peak power density of 64 mW/cm^2 at 80mA/cm^2 Total peak power of 4.5 W	Ma, Wang et al. (2014)
ZAFC with serpentine and parallel anode flow channel	Peak power density of 240 mW/cm^2 at 500 mA/cm^2 with 4 ml/h flowrate	Jiratchayamaethasakul, Srijaroenpramong et al. (2014)
High performance ZAFC stack with MnO_2	Peak power density of 435 mW/cm^2 at 510 mA/cm^2 0.86V	Pei, Ma et al. (2014)
ZAFC with inhibitor coated zinc	N/A	Kim, Jo et al. (2015)
ZAFC used to study effect of KOH concentration and depth of discharge	Current density of 102 mA/cm^2 at 1 Volt	Li, Zhang et al. (2015)
ZAFC with calcium hydroxide	N/A	Zhu, Duch et al. (2015)
Rechargeable zinc-oxygen flow battery	Peak power density of 270 mW/cm^2 at 460 mA/cm^2	Bockelmann, Kunz et al. (2016)

Table 2.2 Literature reviews of zinc regeneration

Description	Performance / remarkable conclusion	Reference
Regeneration of zinc and electrolyte fluidized bed electrodeposition	Lowest energy consumption of 1.92 kWh/kg of zinc at 1000 A/m^2	Huh, Savaskan et al. (1992)
Zinc deposition with low direct and pulsating overpotential	Morphology was less agglomerated in pulsating overpotential	Simičić, Popov et al. (2000)
Zinc electrolysis cell with spout bed electrode	Particle range 0.4 to 1 mm regeneration rate of 10 kg per day	Jiricny, Siu et al. (2000)
Electrolysis cell with bipolar nickel electrode	Energy consumption of about 1.8 Wh/kg, cell voltage of 4.2 V, current density < 1 kA/m^2	Cooper and Krueger (2006)
Electrical recharging process in ZAFC with additives	Cellulose and lead oxide partially reduce dendrite growth and hydrogen.	Lee, Sathiyanarayanan et al. (2006)
Discrete particle electrolyzer integrated with regenerative ZAFC	0.5-0.6 mm dense zinc particle.	Smedley and Zhang (2007)
Deposition of electrolytic zinc from alkaline solution	Effect of current density and electrolyte concentration on morphology, surface area and C.E.	Sharifi, Mojtahedi et al. (2009)
Zinc electrolysis with propanol oxidation as counter electrode	The highest Organic-electro-synthesis efficiency of 82% at propanol up to 1 M	Wen, Cheng et al. (2009)
Study effect of current density, temperature, flow velocity and concentration	Highest C.E. of 87 – 93 % at 0.5M ZnO in 8 M KOH, 50-70 °C, 100 mA/cm^2	Gavrilović-Wohlmuther, Laskos et al. (2015)

Table 2.3 Literature reviews of zinc-air modelling

Description	remarkable conclusion	Reference
Two-dimensional porous zinc electrode model	Active zinc moved from center of electrode toward the surface of electrode	Isaacson, McLarnon et al. (1990)
Primary ZAB model investigating the behavior of ZAB with respect to design	Anode material utilization is limited by depletion of hydroxide ions	Mao and White (1992)
A rechargeable ZAB model Galvanostatic experiment data analysis	Hydroxide ion is limiting factor for high-current discharge	Deiss, Holzer et al. (2002)
Isothermal mathematical model of secondary ZAB studying air composition impact	Air humidity contribute electrode flooding or drying. O_2 affects limiting current. CO_2 reduces OH^- and battery life	Schröder and Krewer (2014)
Oxygen bubble growth in recharging process of ZAB	Oxygen bubble coalescene can be inhibited by using flowing electrolyte and partial insulation electrode	Wang, Pei et al. (2015)
ZAB with phase-field model investigating dendrite growth	Pulsating current and electrolyte flow slow down dendrite growth. Morphology of zinc depends on activation control in early stage and diffusion-limit control in late stage	Wang, Pei et al. (2015)
One-dimensional GDL model with moving gas-liquid interface	Concentration distribution in the air electrode can be analyzed	Schröder, Laue et al. (2016)
One-dimensional ZAB model including ZnO precipitate considering effect of thickness of anode and separator on Zn utilization	97 % utilization with compact anode, 0.61 mm anode thickness and 0.11 mm separator thickness	Jung, Kim et al. (2016)
ZAB model with nucleation and growth of ZnO	Adding ZnO to zinc electrode improved rechargeable capacity but reduced initial discharge capacity.	Stamm, Varzi et al. (2017)

CHAPTER III

MATHEMATICAL MODEL

In the following sections, the development of the isothermal dynamic models is proposed. The models are developed and simulation in MATLAB software. The assumptions have been made including:

- The system is operated isothermally at 298.15K. Therefore, energy balance is not concerned.

- Zero-dimension model is applied. There is no concentration gradient.

- Distance between cells is assumed to be very short and can be neglected.

- All physical properties, electrode areas and thickness are constant.

- Reactions (2.1) and (2.2) occur only at zinc electrode. Similarly, reaction (2.3) occurs only at air electrode.

- The involved species are Zn, ZnO, $Zn(OH)_4^{2-}$, OH^-, H_2O, O_2, K^+ and conductive carbon. The other species are neglected.

- Quasi-electroneutrality is assumed. The net value of charge concentration in bulk electrolyte is close to 0.

- Ideal gas behavior is assumed.

- In mass diffusion concern, binary diffusion is assumed.

3.1 Chemical Species Balance

For modelling ZAFC and electrolyzer, basic principle of the model is mass balance as shown in equation (3.1).

$$Accumulation = Input - output + generation - consumption \quad (3.1)$$

The mass balance in ZAFC base on molar concentration in liquid electrolyte. Molar concentration of species k at electrode j is applied as

$$N_k^j = C_k^j V_{electrolyte}^j \quad (3.2)$$

Where N_k is moles of species k, C_k is concentration of species k and $V_{electrolyte}$ is electrolyte volume. Superscript j represents the electrode. Equation (3.2) is differentiated by time. The molar balance of species is expressed as equation (3.3).

$$\frac{dN_k^j}{dt} = C_k^j \frac{dV_{electrolyte}^j}{dt} + V_{electrolyte}^j \frac{dC_k^j}{dt} \quad (3.3)$$

Molar transfer between two electrodes can be expressed as equation (3.4). Molar transfer rate across the electrodes of species k (J_k) can be expressed as the summation of diffusion, migration and convection molar flow rates.

$$J_k = J_k^{diff} + J_k^{mig} + J_k^{conv} \quad (3.4)$$

With: $$J_k^{diff} = D_k \cdot \frac{\left(C_k^{air} - C_k^{zinc}\right)}{\delta_{Sep}} \cdot \varepsilon^{Sep} \cdot A_{Sep} \quad (3.4a)$$

$$J_k^{mig} = \frac{t_k}{z_k^{\pm} F} \cdot i^{cell} \cdot \varepsilon^{Sep} \cdot A_{Sep} \quad (3.4b)$$

$$J_k^{conv} = F_{conv} \cdot C_k^{zinc} \quad (3.4c)$$

Where $z^{\pm}_k$ is ion number of the species. F_{conv} is the convective volume flow mentioned in section 3.3.

Equation 3.3 can be rearranged into concentration terms combining with molar transfer term and reaction term (equation (3.5)). The result equation is the first order ordinary differential equations:

$$\frac{dC_k^j}{dt} = \frac{1}{V_{electrolyte}^j} \cdot \left[F_{k,in} - F_{k,out} + J_k^{diff} + J_k^{mig} + J_k^{conv} + \sum_i v_{k,i} \cdot r_i - C_k^j \frac{dV_{electrolyte}^j}{dt}\right] \quad (3.5)$$

Where F_k is molar flowrate of species k and r_i is rate of reaction i (mol/time). This equation can be used to balance the chemical species involved in ZAFC.

From quasi-electroneutrality assumption, the positive ion can be calculated by ionic species charge balance. In this case, potassium ion can be accounted by the electroneutrality.

$$\sum_k z_k^{\pm} C_k^j = 0 \quad (3.6)$$

$$C_{K^+}^j - C_{OH^-}^j - 2C_{Zn(OH)_4^{2-}}^j = 0 \quad (3.7)$$

For solid species in zinc electrode, the accumulation of ZnO is expressed by molar balance with reaction (2.2). Solid zinc is done in the same way with reaction (2.1).

$$\frac{dN_{ZnO}}{dt} = F_{ZnO,in} - F_{ZnO,out} + v_{ZnO,2} \cdot r_2 \quad (3.8)$$

$$\frac{dN_{Zn}}{dt} = F_{Zn,in} - F_{Zn,out} + v_{Zn,1} \cdot r_1 \quad (3.9)$$

For electrolyzer model, the electrolyzer does not divide into 2 chambers therefore the species concentration of both zinc electrode and air electrode are the same. For same reason, the equation 3.4 is not included because there is no molar transfer between the electrode.

3.2 Reaction Rate

The reaction (2.1) and (2.3) are electrochemical reaction. The rate of electrochemical reaction depends on the rate of electron generation or consumption. Therefore, the electrochemical reaction rate can be directly calculated from measurement of the measured electrical current. From faraday's law, the rate of charge transfer is:

$$I = \frac{dQ}{dt} \tag{3.10}$$

Where I is electrical current, Q is charge and t is time. The electrochemical reaction generates electron resulting in charge transfer per time or electrical current. Reaction rate in the unit of mole per time can be calculated.

$$r_{elec} = \frac{dN}{dt} = \frac{I}{Z_e F} \tag{3.11}$$

Where F is the faraday constant and Z_e is the number of exchanged electrons involved in the reaction.

For ZnO precipitation reaction (2.2), the rate of reaction is expressed by a saturation approach (Sunu and Bennion 1980).

$$r_2 = k_s(C_{Zn(OH)_4^{2-}} - C^{sat}_{Zn(OH)_4^{2-}}) \tag{3.12}$$

Where k_s is the rate constant of this reaction and $C^{sat}_{Zn(OH)_4^{2-}}$ is the saturation concentration of zincate ion.

For electrolyzer, equation 3.11 can be used to calculate the rate of anodic reaction 2.7. For cathode, there are 2 cathodic reaction (2.6 and 2.9) on the same zinc electrode. The equation 3.11 is modified into 3.11a and 3.11b to calculate the rate of the cathodic reaction 2.6 and 2.9, respectively.

$$r_{elec,Zn} = \frac{I_{Zn}}{Z_e F} \tag{3.11a}$$

$$r_{elec,H} = \frac{I_H}{Z_e F} \tag{3.11b}$$

Where I_{Zn} and I_H are the supplied current of reaction 2.6 and 2.9, respectively.

3.3 Volume Change

The volume of electrode is accounted by calculating the volume of each species. The volume of each species can be calculated from partial molar volume of each species. The solid volume of zinc electrode is the summation of the volume of zinc, zinc oxide and carbon which is expressed with equation (3.13) and it is changing with time as shown in equation (3.14). Carbon is an inert species which is not reacted or transferred to cathode therefore it is not appear in equation (3.14).

$$V^{zinc}_{solid} = N_{Zn} \cdot \bar{V}_{Zn} + N_{ZnO} \cdot \bar{V}_{ZnO} + N_{Carbon} \cdot \bar{V}_{Carbon} \tag{3.13}$$

$$\frac{dV^{zinc}_{solid}}{dt} = \frac{dN_{Zn}}{dt} \cdot \bar{V}_{Zn} + \frac{dN_{ZnO}}{dt} \cdot \bar{V}_{ZnO} \tag{3.14}$$

The same approach is done with the electrolyte volume of zinc electrode.

$$V^{zinc}_{electroyte} = \sum_k N^{zinc}_k \cdot \bar{V}_k \tag{3.15}$$

$$\frac{dV^{zinc}_{electrolyte}}{dt} = \sum_k \left(V^{zinc}_{electroyte} \cdot \frac{dC^{zinc}_k}{dt} + C^{zinc}_k \cdot \frac{dV^{zinc}_{electrolyte}}{dt} \right) \cdot \bar{V}_k \tag{3.16}$$

In order to express the electrolyte volume of air electrode, the volume transfer between two electrodes is being involved. The volume transfer between two electrodes is calculated from molar transfer rate (J_k) and the partial molar volume of each species.

$$F_{conv} = \sum_k J_k \cdot \bar{V}_k \quad (3.17)$$

Where F_{conv} is convective volume flow. F_{conv} is defined as the volume of electrolyte flow from air electrode to zinc electrode therefore it is positive sign at zinc electrode and negative sign at air electrode. The volume change of air electrolyte is expressed as:

$$\frac{dV^{air}_{electrolyte}}{dt} = -F_{conv} + r_3 \sum_k v_{k,3} \cdot \bar{V}_k \quad (3.18)$$

For electrolyzer, the electrolyzer does not divide into 2 chambers therefore only zinc electrode volume is used in electrolyzer model. The equation 3.17 and 3.18 are not included in this model.

3.4 Cell Potential

The cell potential (E_{cell}) of ZAFC can from Nernst potential ($E_{0,cell}$) minus with the overpotentials as expressed in equation 3.19. As mentioned, before in polarization curve section, potential losses or overpotentials consisted of three main losses: Activation (η_{act}), Ohmic (η_{ohmic}) and concentration loss (η_{conc}). Nernst potential or standard cell potential is given by Nernst equation and can be calculated from equation 3.20 (Schröder and Krewer 2014).

$$E_{cell} = E_{0,cell} - \eta^{zinc}_{act} - \eta^{air}_{act} - \eta_{ohmic} - \eta_{conc} \quad (3.19)$$

$$E_{0,cell} = \left[0.401 + \frac{RT}{Z^{air}_e \cdot F} ln\left(\frac{(P_{O_2}/P^{ref})}{(C^{air}_{OH}/C^{ref})^4}\right)\right] - \left[-1.266 + \frac{RT}{Z^{zinc}_e \cdot F} ln\left(\frac{(C^{zinc}_{Zn(OH)_4^{2-}}/C^{ref})}{(C^{zinc}_{OH}/C^{ref})^4}\right)\right] \quad (3.20)$$

Where R is gas constant and T is temperature.

3.4.1 Activation Loss

The relationship between the activation loss and the current density is described by the Butler-Volmer equation (Spiegel 2008). It explains how the electrical current on an electrode related with the electrode potential.

$$i^{Cell} = i_0 \cdot \left[\exp\left(\frac{\alpha Z_e F}{RT}\eta\right) - exp\left(-\frac{(1-\alpha) Z_e F}{RT}\eta\right)\right] \quad (3.21)$$

Where i^{Cell} is cell current density, i_0 is the exchange current density which is the rate of current proceeded at reaction equilibrium and α is charge transfer coefficient. Commonly, symmetric electron transfer is assumed and α is equal to 0.5. Then, the equation (3.21) can be simplified to activation potential equation in the term of inverse hyperbolic sine.

$$\eta_{act} = \frac{2RT}{Z_e F} sinh^{-1}\left(\frac{i^{cell}}{2i_0}\right) \quad (3.22)$$

The exchange current density of any reaction can be determined by experiment. It is a function of temperature, active surface area and some species concentration. However, the temperature influence is neglect because of isothermal condition. For the anode, the effective exchange current density is given by equation (3.23)

$$i^{zinc}_0 = i^{ref,zinc}_0 a_s \delta_{zinc} X_{zinc} \quad (3.23)$$

Where $i_0^{ref,zinc}$ is the reference exchange current density, a_s is the solid-solution interface area per unit volume, δ_{zinc} is the thickness of zinc electrode and X_{zinc} is the active surface fraction of zinc in solid phase. a_s and X_{zinc} can be estimated from equation (3.24) and (3.25), respectively (Sunu and Bennion 1980).

$$a_s = a_0 \left(\frac{1-\varepsilon}{1-\varepsilon_0}\right)^{2/3} \tag{3.24}$$

$$X_{zinc} = \frac{{V_{solid,Zn}}^{2/3}}{{V_{solid,Zn}}^{2/3}+{V_{solid,ZnO}}^{2/3}+{V_{solid,C}}^{2/3}} \tag{3.25}$$

The reference exchange current density can be calculated from an expression fitted with experimental data by Dirkse and Hampson (1972). Equation (3.26) is the correlation the exchange current density and concentration hydroxide ion.

$$i_0^{Zn,ref} = 0.0281 + 0.0613C_{OH^-} - 0.0041{C_{OH^-}}^2 \tag{3.26}$$

For cathode, the effective exchange current density is calculated differently from anode. Equation (3.27) expresses the exchange current density in a function of active surface area, active thickness and oxygen concentration at catalyst surface. The effectiveness specific surface area of catalyst can be calculated from equation (3.28).

$$i_0^{Air} = i_0^{ref,Air} a_c^{eff} \delta_{active} \left(\frac{P_{O_2}}{P^{ref}}\right) \tag{3.27}$$

$$a_c^{eff} = \varepsilon_{active} \cdot ac \tag{3.28}$$

Where a_c is specific surface area of catalyst per unit volume, δ_{active} is the thickness of active reaction zone, C_{O2ref} is the oxygen concentration of reference state (same as $i_0^{ref,Air}$) and ε_{active} is effectiveness of gas transport to triple-phase boundary.

3.4.2 Ohmic Loss

The ohmic loss is expressed by ohmic's law. The total ohmic resistance (R_{ohmic}) is calculated from conductivity and resistivity of the chemical species and cell component involved. The anode conductivity is accounted by the solid species conductivity and mole fraction in solid electrode.

$$\eta_{ohmic} = i^{cell} \cdot A_{cell} \cdot R_{ohmic} \tag{3.29}$$

$$R_{ohmic} = R_{zinc} + R_{electrolyte} + R_{air} + R_{comp} \tag{3.30}$$

$$R_{ohmic} = \frac{\delta_{zinc}}{\sigma_{anode}A_{zinc}} + \frac{\delta_{electrolyte}}{\sigma_{electrolyte}A_{electrolyte}} + \frac{\delta_{air}}{\sigma_{cathode}A_{air}} + R_{comp} \tag{3.31}$$

$$\sigma_{anode} = \chi_{Zn}\sigma_{Zn} + \chi_{ZnO}\sigma_{ZnO} + \chi_{Carbon}\sigma_{Carbon} \tag{3.32}$$

Where σ is conductivity and χ is molar fraction of species in solid electrode.

Ion transport resistance in the separator also contributes to the ohmic potential loss. η_{ionic}^{Sep} is the separator loss which is calculated from potential gradient between zinc electrode and air electrode as explained from equation (3.34) (Schröder and Krewer 2014).

$$\eta_{ionic}^{Sep} = -\Delta\Phi \cdot \delta_{Sep} \tag{3.33}$$

$$\Delta\Phi = \frac{-i^{Cell} - \frac{F}{\delta_{Sep}} \cdot B_1 + \frac{F \cdot F_{conv} \cdot B_3}{\varepsilon^{Sep} A_{Sep}}}{\frac{F^2}{RT} B_2} \quad (3.34)$$

With: $B_1 = \sum_k z_k^{\pm} D_k \left(C_k^{air} - C_k^{zinc}\right)$ (3.34a)

$B_2 = \sum_k {z_k^{\pm}}^2 D_k \bar{C}_k$ (3.34b)

$B_3 = \sum_k z_k^{\pm} C_k^{zinc}$ (3.34c)

3.4.3 Concentration Loss

The concentration loss is the loss occurred from mass transfer limit of the reactant. In zinc-air case, the mass transfer limit is generally oxygen limit at the air electrode. The concentration loss is calculated from limiting current density (i_{lim}) which is computed from oxygen transfer rate limit at the air cathode (Spiegel 2008). In this work, limiting current density is modified with ε_{active} as expressed in equation (3.35).

$$i_{lim} = \frac{Z_{e,O2} F D_{O2,GDL}}{\delta_{GDL}} \cdot \varepsilon_{active} \cdot C_{O2} \quad (3.35)$$

$$\eta_{conc} = \frac{RT}{Z_{e,O2} F} \ln\left(1 - \frac{i^{cell}}{i_{lim}}\right) \quad (3.36)$$

Where $Z_{e,O2}$ is the number of exchanged electrons per one molecule of oxygen reacted. When the current density is getting close to limiting current density, the concentration loss will greatly increase.

There is another approach which can express the concentration loss. The exchange current density of cathode can be modified by limiting current density giving the modified exchange current density as equation (3.27a). The result equation combines the concentration loss into the activation loss term.

$$i_0^{Air} = i_0^{ref,Air} a_c^{eff} \delta_{active} \left(\frac{P_{O2}}{P^{ref}} \cdot \left(1 - \frac{i^{cell}}{i_{lim}}\right)\right) \quad (3.27a)$$

For electrolyzer, equation 3.20 can be used to calculated Nernst potential same as ZAFC. Because two cathodic reactions occur in zinc electrode, the zinc electrode activation loss is calculated in different way. Current densities of each cathodic reaction can be calculated from equation (3.21) as described in equation (3.21a) and (3.21b).

$$i_{Zn}^{Cell} = i_0^{zinc} \cdot \left[\exp\left(\frac{\alpha Z_e F}{RT} \eta_{zinc}\right) - exp\left(-\frac{(1-\alpha) Z_e F}{RT} \eta_{zinc}\right)\right] \quad (3.21a)$$

$$i_H^{Cell} = i_0^H \cdot \left[\exp\left(\frac{\alpha Z_e F}{RT} \eta_H\right) - exp\left(-\frac{(1-\alpha) Z_e F}{RT} \eta_H\right)\right] \quad (3.21b)$$

The overpotential of hydrogen evolution (η_H) is calculated from equation (3.37) and (3.38). In electrolyzer case, the exchange current density of zinc (i_0^{zinc}) does not only depend on hydroxide ion concentration but also depend on zincate ion concentration (Bockris, Nagy et al. 1972). Equation (3.39) is used to compute i_0^{zinc} instead of equation (3.23). The exchange current density of hydrogen evolution (i_0^H) can be calculated by equation (3.40). The charge balance equation (3.41) is an ODE which used to account for transient changes of zinc activation loss.

$$\eta_H = \eta_{zinc} + \Delta E \tag{3.37}$$

$$\Delta E = \left[-1.266 + \frac{RT}{Z_e^{zinc} \cdot F} ln \left(\frac{(C^{zinc}_{Zn(OH)_4^{2-}}/C^{ref})}{(C^{zinc}_{OH^-}/C^{ref})^4} \right) \right] - \left[-0.828 - \frac{RT}{Z_e^{H} \cdot F} ln \left(\frac{C^{zinc}_{OH^-}}{C^{ref}} \right) \right] \tag{3.38}$$

$$i_0^{zinc} = i_0^{ref,zinc} \left(\frac{(C^{zinc}_{Zn(OH)_4^{2-}}/C^{ref})}{(C^{zinc}_{OH^-}/C^{ref})} \right) \tag{3.39}$$

$$i_0^{H} = i_0^{ref,H} \left(\frac{C^{zinc}_{OH^-}}{C^{ref}} \right)^{-2} \tag{3.40}$$

$$\frac{d\eta^{zinc}}{dt} \cdot C_{DL}^{zinc} = i^{cell} - \frac{z_e^{zinc} \cdot F \cdot (r_{Zn} + r_H)}{A^{zinc}_{electrode}} \tag{3.41}$$

The equations used to describe ohmic loss can be used for electrolyzer except the separator loss does not include. The concentration loss is neglected in this electrolyzer model.

3.5 Model Parameters

The Table 3.1 and 3.2 consist of 5 parameter categories: Cell design parameter, Reaction Kinetic, Mass transport, Operating input miscellaneous constant and material properties. In the reference column, the parameters that is fixed due to cell design or nature of species are defined as “Given”.

To perform the simulation of ZAFC, three parameters were fitted, including the resistivity of cell component, the thickness of active zone and the effectiveness of gas transport to the active triple-phase boundary. The parameters fitted are defined as “fitted”. The fitted values can be different due to the different experiment data. In this thesis, the fitted parameters were fitted with the experimental polarization curve.

For the calculated parameter, the calculation method can be found in mathematical model section or appendix A. The gas diffusion coefficients with the porous GDL are calculated based on the Knudsen diffusion model (appendix A1). The diffusivity of hydroxide ion and conductivity of the electrolyte are calculated as the function of potassium hydroxide concentration (appendix A2 and A3). The concentration of oxygen dissolved in electrolyte is expressed by Tromans (1998) (appendix A4).

Table 3.1 Parameters for polarization and discharging simulation of ZAFC

Cell Parameters			
Parameter	Value	Units	Reference
A_{Sep}	0.1	dm2	Given
A_{zinc}	0.1	dm2	Given
A_{air}	0.1	dm2	Given
δ_{Sep}	1×10^{-3}	dm	Given

δ_{zinc}	0.1	dm	Given
δ_{GDL}	1.67×10^{-2}	dm	Given
ε^{Sep}	0.1	dimensionless	Given
ε^{GDL}	0.82	dimensionless	Given
R_{comp}	1.25	ohm	fitted
Kinetic Parameters			
Parameter	Value	Units	Reference
k_s	0.25	$dm^3 \cdot s^{-1}$	Schröder and Krewer (2014)
$i_0^{ref,Air}$	1.5×10^{-8}	$A \cdot dm^{-2}$	Mao and White (1992)
a_c	1×10^{5}	dm^2/dm^3	Mao and White (1992)
C_{O2ref}	$f(C_{KOH,ref}, P_{O_2})$	mol/dm^3	Tromans (1998)
δ_{active}	1×10^{-5}	dm	fitted
a_0	1.4×10^{4}	dm^2/dm^3	Jung, Kim et al. (2016)
ε_0	0.649	dimensionless	Jung, Kim et al. (2016)
$v_{Zn,1}$	-1	dimensionless	Given
$v_{OH^-,1}$	-4	dimensionless	Given
$v_{Zn(OH)_4^{2-},1}$	+1	dimensionless	Given
$v_{Zn(OH)_4^{2-},2}$	-1	dimensionless	Given
$v_{OH^-,2}$	+2	dimensionless	Given
$v_{ZnO,2}$	+1	dimensionless	Given
$v_{H_2O,2}$	+1	dimensionless	Given
$v_{O_2,3}$	-0.5	dimensionless	Given
$v_{H_2O,3}$	-1	dimensionless	Given
$v_{OH^-,2}$	+2	dimensionless	Given
$Z_{e,1}$	2	dimensionless	Given
$Z_{e,3}$	2	dimensionless	Given
$Z_{e,O2}$	4	dimensionless	Given

Transport Parameters			
Parameter	Value	Units	Reference
α_{zinc}	0.5	dimensionless	Assumed
α_{air}	0.5	dimensionless	Assumed
$D_{Zn(OH)_4^{2-},Elec}$	8.55×10^{-9}	dm^2/s	Krejčí, Vanýsek et al. (1993)
$D_{OH^-,Elec}$	$f(C_{KOH})$	dm^2/s	Calculated
$D_{H_2O,Elec}$	5.26×10^{-7}	dm^2/s	Newman and Thomas (2004)
$D_{K^+,Elec}$	1.2×10^{-7}	dm^2/s	Sunu and Bennion (1980)
$D_{O_2,Air}$	2.3×10^{-3}	dm^2/s	Bird, Stewart et al. (2002)
ε^{active}	0.2191	dimensionless	fitted
Operating Parameters			
Parameter	Value	Units	Reference
T	298.15	K	Chosen
P_{O_2}	0.21	atm	Chosen
C_{KOH}	Studied	mol/dm^3	Vary
N_{carbon}	Studied	mole	Vary
N_{Zn}	Studied	mole	Vary
N_{ZnO}	Studied	mole	Vary
$Space\ Velocity$	Studied	h^{-1}	Vary
Miscellaneous constants / Properties			
Parameter	Value	Units	Reference
R	8.314	J/mol·K	Dean and Lange (1999)
F	96,485	C/mol	Dean and Lange (1999)
$z_{K^+}^{\pm}$	+1	dimensionless	Given
$z_{OH^-}^{\pm}$	-1	dimensionless	Given
$z_{Zn(OH)_4^{2-}}^{\pm}$	-2	dimensionless	Given
σ_{Zn}	2×10^{6}	S/dm	Sunu and Bennion (1980)
σ_{ZnO}	1×10^{-9}	S/dm	Sunu and Bennion (1980)
σ_{Carbon}	2×10^{5}	S/dm	Pierson (1993)
$\sigma_{electrolyte}$	$f(C_{KOH})$	S/dm	calculated

$\sigma_{Cathode}$	5×10^{3}	S/dm	Given
$\bar{V}_{Zn}$	9.15×10^{-3}	dm^3/mol	Sunu and Bennion (1980)
$\bar{V}_{ZnO}$	1.45×10^{-2}	dm^3/mol	Sunu and Bennion (1980)
$\bar{V}_{Carbon}$	5.3×10^{-3}	dm^3/mol	Pierson (1993)
$\bar{V}_{K^+}$	3.6×10^{-3}	dm^3/mol	Marcus (2009)
$\bar{V}_{OH^-}$	7.89×10^{-3}	dm^3/mol	Mathias (2004)
$\bar{V}_{Zn(OH)_4^{2-}}$	1.86×10^{-2}	dm^3/mol	Schröder and Krewer (2014)
$\bar{V}_{H_2O}$	1.78×10^{-2}	dm^3/mol	Kimble and White (1991)

Table 3.2 Parameters for polarization and charging simulation of zinc electrolyzer

Cell Parameters			
Parameter	Value	Units	Reference
A_{zinc}	0.1	dm^2	Given
A_{air}	0.1	dm^2	Given
$\delta_{electrolyte}$	0.1	dm	Given
δ_{GDL}	1.67×10^{-2}	dm	Given
R_{comp}	0.2	ohm	fitted
Kinetic Parameters			
Parameter	Value	Units	Reference
k_s	0.25	$dm^3 \cdot s^{-1}$	Schröder and Krewer (2014)
$i_0^{ref,Zn}$	6.3	$A \cdot dm^{-2}$	Bockris, Nagy et al. (1972)
$i_0^{ref,H}$	1×10^{-7}	$A \cdot dm^{-2}$	Saleh, Weidner et al. (1995)
$i_0^{ref,Air}$	1.5×10^{-8}	$A \cdot dm^{-2}$	Mao and White (1992)
a_c	1×10^{5}	dm^2/dm^3	Mao and White (1992)
C_{O2ref}	$f(C_{KOH,ref}, P_{O_2})$	mol/dm^3	Tromans (1998)
a_0	1.4×10^{4}	dm^2/dm^3	Jung, Kim et al. (2016)
ε_0	0.649	dimensionless	Jung, Kim et al. (2016)
$v_{Zn,1}$	-1	dimensionless	Given

$v_{OH^-,1}$	-4	dimensionless	Given
$v_{Zn(OH)_4^{2-},1}$	+1	dimensionless	Given
$v_{Zn(OH)_4^{2-},2}$	-1	dimensionless	Given
$v_{OH^-,2}$	+2	dimensionless	Given
$v_{ZnO,2}$	+1	dimensionless	Given
$v_{H_2O,2}$	+1	dimensionless	Given
$v_{O_2,3}$	-0.5	dimensionless	Given
$v_{H_2O,3}$	-1	dimensionless	Given
$v_{OH^-,2}$	+2	dimensionless	Given
$Z_{e,1}$	2	dimensionless	Given
$Z_{e,3}$	2	dimensionless	Given
$Z_{e,O2}$	4	dimensionless	Given
Transport Parameters			
Parameter	Value	Units	Reference
α_{zinc}	0.5	dimensionless	Assumed
α_{air}	0.5	dimensionless	Assumed
$D_{Zn(OH)_4^{2-},Elec}$	8.55×10^{-9}	dm^2/s	Krej et al., 1993
$D_{OH^-,Elec}$	$f(C_{KOH})$	dm^2/s	Calculated
$D_{H_2O,Elec}$	5.26×10^{-7}	dm^2/s	Newman and Thomas (2004)
$D_{K^+,Elec}$	1.2×10^{-7}	dm^2/s	Sunu and Bennion (1980)
$D_{O_2,Air}$	2.3×10^{-3}	dm^2/s	Bird, Stewart et al. (2002)
Operating Parameters			
Parameter	Value	Units	Reference
T	298.15	K	Chosen
P_{O_2}	0.21	atm	Chosen
C_{KOH}	Studied	mol/dm^3	Vary
N_{carbon}	Studied	mole	Vary
N_{Zn}	Studied	mole	Vary
N_{ZnO}	Studied	mole	Vary
$Flow$	Studied	ml/min	Vary

Miscellaneous constants / Properties			
Parameter	Value	Units	Reference
C_{DL}^{zinc}	250	F/dm	Schröder and Krewer (2014)
R	8.314	J/mol·K	Dean and Lange (1999)
F	96,485	C/mol	Dean and Lange (1999)
$z_{K^+}^{\pm}$	+1	dimensionless	Given
$z_{OH^-}^{\pm}$	-1	dimensionless	Given
$z_{Zn(OH)_4^{2-}}^{\pm}$	-2	dimensionless	Given
σ_{Zn}	2×10^{6}	S/dm	Sunu and Bennion (1980)
σ_{ZnO}	1×10^{-9}	S/dm	Sunu and Bennion (1980)
σ_{Carbon}	2×10^{5}	S/dm	Pierson (1993)
$\sigma_{electrolyte}$	$f(C_{KOH})$	S/dm	calculated
$\sigma_{Cathode}$	5×10^{3}	S/dm	Given
$\bar{V}_{Zn}$	9.15×10^{-3}	dm^3/mol	Sunu and Bennion (1980)
$\bar{V}_{ZnO}$	1.45×10^{-2}	dm^3/mol	Sunu and Bennion (1980)
$\bar{V}_{Carbon}$	5.3×10^{-3}	dm^3/mol	Pierson (1993)
$\bar{V}_{K^+}$	3.6×10^{-3}	dm^3/mol	Marcus (2009)
$\bar{V}_{OH^-}$	7.89×10^{-3}	dm^3/mol	Mathias (2004)
$\bar{V}_{Zn(OH)_4^{2-}}$	1.86×10^{-2}	dm^3/mol	Schröder and Krewer (2014)
$\bar{V}_{H_2O}$	1.78×10^{-2}	dm^3/mol	Kimble and White (1991)

After modelling, the mathematical models are simulated to study the parameter. This work focuses on the electrolyte composition. The investigated parameters are feed flowrate and compositions of zinc, ZnO, KOH and conductive carbon as shown in table 3.3.

Table 3.3 Studied parameters

Parameter	**Values**	
	ZAFC	**Electrolyzer**
KOH concentration	4 – 14 M	4 – 14 M
Zinc and ZnO concentration	0 – 2 times ZnO solubility	0.1 – 1.1 M Zincate ion
Electrolyte flowrate (space velocity)	0 – 5 h^{-1}	-
Conductive carbon	0 – 30 %	-

CHAPTER IV

EXPERIMENTAL

The polarization curve data was employed to support the proposed model and its subsequent parameter estimation. Experimental ZAFC is designed as a tubular cell. The design parameters and cell component are shown in table 1.1 and 1.2. To investigate the polarization curve of the cell, the BA500 battery analyzer was employed with BA500WIN software. The polarization curve is obtained by varying current density drawn and measuring cell potential.

For alkaline zinc electrolyzer, the electrolyzer model is validated by the experiment of Zn electrolysis. The experiment took place in a 200ml beaker. KOH solution is used as electrolyte same as ZAFC experiment. The polarization curve is obtained by the same method as ZAFC.

4.1 Zinc-air fuel cell (ZAFC)

As shown in table 1.1 and 1.2, ZAFC was designed as a tubular cell. Zinc powder (UNIVAR) was used as anode electrode with stainless steel mesh current collector. The cathode was oxygen in the air. The gas diffusion layer (GDL) / catalytic layer (CL) material was graphite mixed with polytetrafluoroethylene (PTFE, Sigma Aldrich) as hydrophobic filler and MnO_2 (Sigma Aldrich) as catalyst. The current collector for cathode was nickel foam (MTI corp.). Nylon membrane filter (Steritech, pore size 0.1 μm, nominal thickness 65-125 μm) was used as a separator. 9 M Potassium hydroxide (KOH pellets form UNIVAR) solution was used as electrolyte. The active surface area of the cell was 10 cm^2.

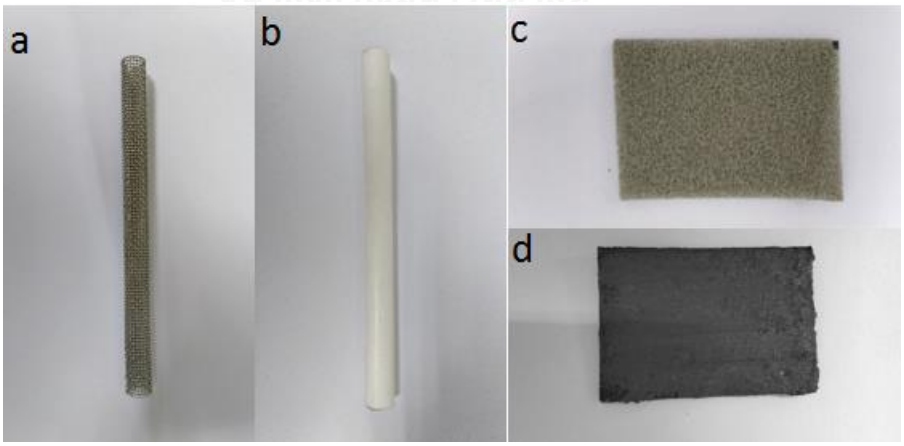

Figure 4.1 Cell components a) stainless steel mesh b) stainless steel mesh wrapped with nylon membrane c) nickel foam and d) nickel foam coated with GDL / CL

The current collector of anode was stainless steel mesh which was rolled into tubular shape as shown in figure 4.1a then the current collector was wrap with nylon membrane as separator (figure 4.1b). For cathode, the current collector was 2×5 cm^2 nickel foam (figure 4.1c) which was coated with GDL / CL material (figure 4.1d). To

prepared the GDL / CL material, graphite, PTFE and MnO_2 catalyst were mixed together with binder. The binder was Poly(styrene-Co-butadiene) (Sigma Aldrich) dissolved in toluene solvent. The GDL / CL composition of graphite, PTFE, catalyst and binder were 67, 10, 20 and 3%, respectively. The well-mixed GDL / CL material was viscous and paste-like. The prepared GDL / CL paste was coated on the one side nickel foam and then dried in the oven at 85 °C for 10 min. The coating and drying processes were repeated 3 times. The prepared catalytic nickel foam was employed in the ZAFC as cathode. 9M KOH solution was prepared by dissolving KOH pellets in the distilled water. To make zinc flow with electrolyte, Carbopol 940 was used as gelling agent and added into electrolyte by 1.4%. The electrolyte and gelling agent were mixed for about 6 hours in order to become gelled completely. Zinc powder was added to the electrolyte by 5%. Peristaltic pump (Lead fluid) was used to drive the electrolyte to flow. The flowrate of 50 ml/min was used. The schematic diagram and photo of the experiment were shown in figure 4.2 and 4.3, respectively.

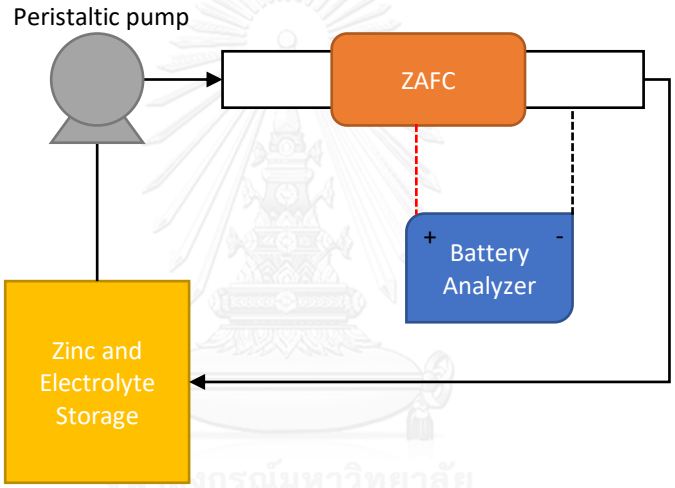

Figure 4.2 schematic diagram of ZAFC experiment

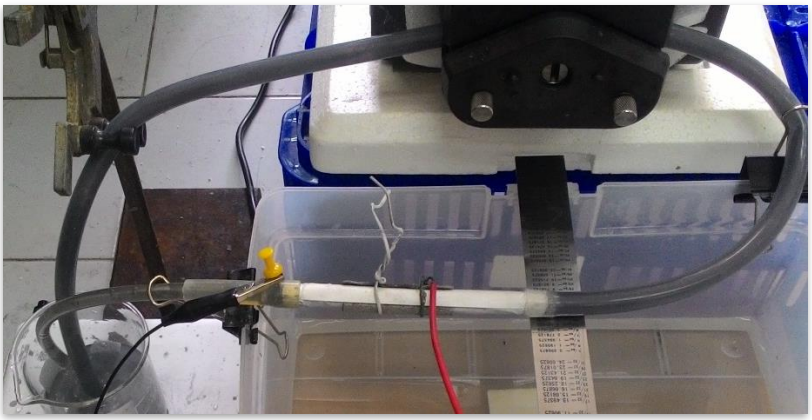

Figure 4.3 photo of ZAFC experiment

4.2 Alkaline Zinc Electrolysis

The experimental conditions and parameters were applied as shown in table 1.3. The experiment took place in a 100-ml beaker. The current collector of cathode was copper plate with active area 8 cm^2 and anode collector was nickel foam with the same amount of active area. Both electrodes were dripped in the electrolyte with the distance between the electrode of 10 mm. 100g of 9M KOH solution was used as electrolyte. The electrolyte was stirred continuously by magnetic stirrer. There was no catalyst used in this experiment. ZnO was used as reactant of the electrolysis process. 12.75g of ZnO was added into the electrolyte which produced 1.05 M zincate solution. The ZnO was dissolved in KOH solution and white liquid electrolyte was obtained. When the current was applied to the cell, the electrodeposited zinc attached on the dipped surface of the copper current collector. On the nickel current collector, oxygen was generated instead. The schematic diagram of this experiment was shown in figure 4.3.

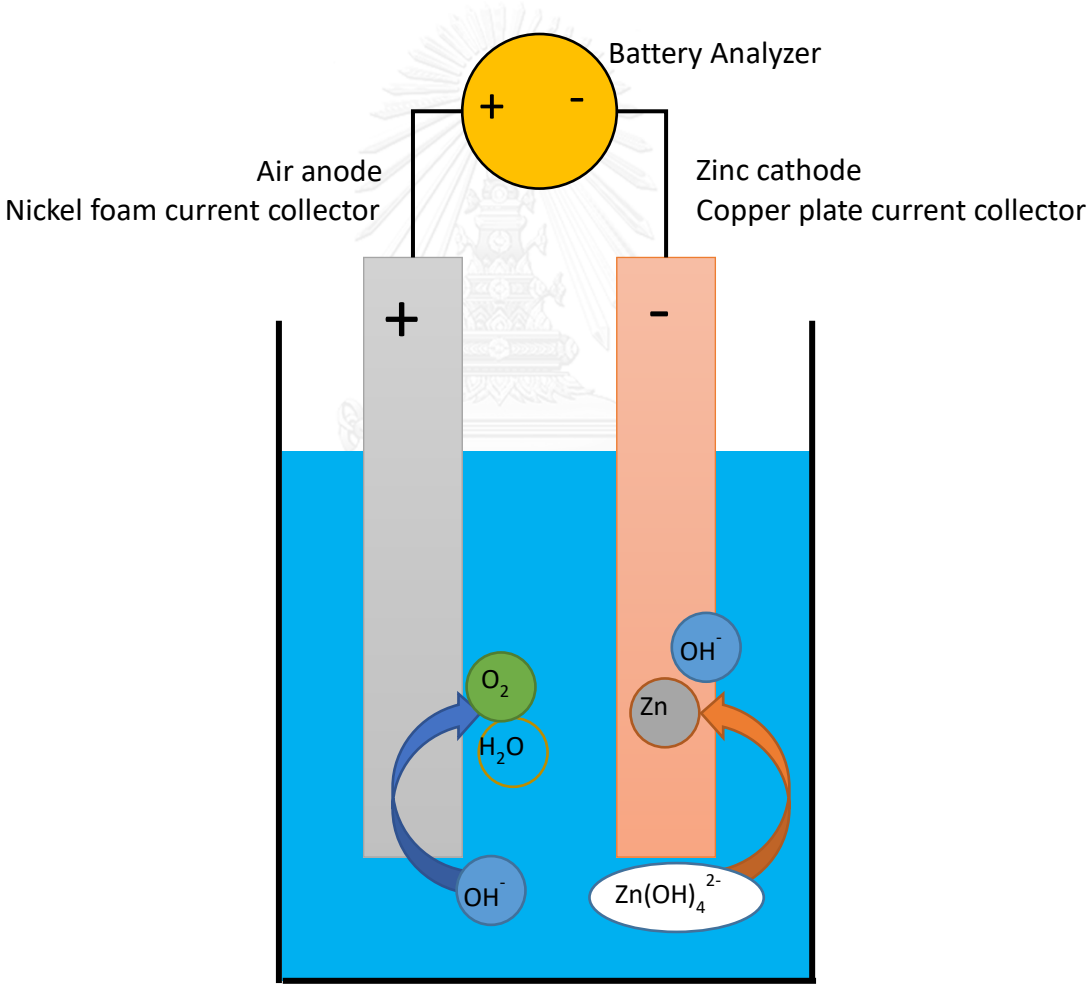

Figure 4.4 schematic diagram of alkaline zinc electrolyzer experiment

4.3 Polarization curve characterization

To characterize the polarization curve of ZAFC and Zn electrolysis, the BA500 battery analyzer was employed with the BA500WIN software. This analyzer can measure the cell voltage at constant current. Battery operation mode can be selected between charge and discharge mode. In discharge mode, the current drawn can be adjusted manually and cell voltage is measured at the selected current continuously. For charge mode, the analyzer can supply current to the battery and measure the cell voltage.

In this work, the data of cell voltage was collected 1 value per second. For one current value, the voltage data had been collected for 10 seconds. After that, the current value was changed to the next value. For one current value, 10 voltage values were used to calculated the average cell voltage. The values were plotted on the voltage versus current density graph. For ZAFC, the current value was increased until the values shown in the battery analyzer did not change.

CHAPTER V

RESULT AND DISCUSSION

In the following, all simulations were performed in MATLAB. The ODE models were solved with ode15s solver. Polarization curve was obtained by plotting cell voltage at any current density varied. The polarization curve data were collected at the holding time of 60 seconds. Charge / discharge curves were simulated with galvanostatic condition with selected current density and holding time. The charge / discharge curve data were collected 1 point per 60 seconds.

This chapter consisted of 2 main sections: ZAFC Modelling and Alkaline Zinc Electrolyzer Modelling.

5.1 ZAFC Modelling

5.1.1 ZAFC Model Parameter Estimation and Validation

From section 3.5, there are 3 parameters that need to be fitted with the experimental data including the resistivity of cell component (R_{comp}), the thickness of active zone (δ_{active}) and the effectiveness of gas transport to the active zone (ε_{actve}). The polarization curve from simulation was compared with from the experimentation. The three parameters can be adjusted properly to make the simulated polarization curve fitted with the experimental polarization curve. R_{comp} was adjusted to characterize the ohmic loss. δ_{active} was adjusted to determine the influence of activation overpotential of cathode. Because the oxygen reduction reaction (ORR) in ZAFC is three-phase reaction, the reactive zone is located at the interface of GDL/CL layer and electrolyte layer. The thickness of active zone is very small compare with cathode thickness. The cathode with high thickness of active zone has low activation overpotential and provides good performance. The last fitted parameter is ε_{actve} which affects the limiting oxygen transport and the active area of cathode reaction. Due to the triple-phase boundary theory, actual reactive area occurs at the interface of solid catalyst, electrolyte and gas which is very small. ε_{active} is applied as effectiveness factor defining the proportion of reactive area in full electrode area.

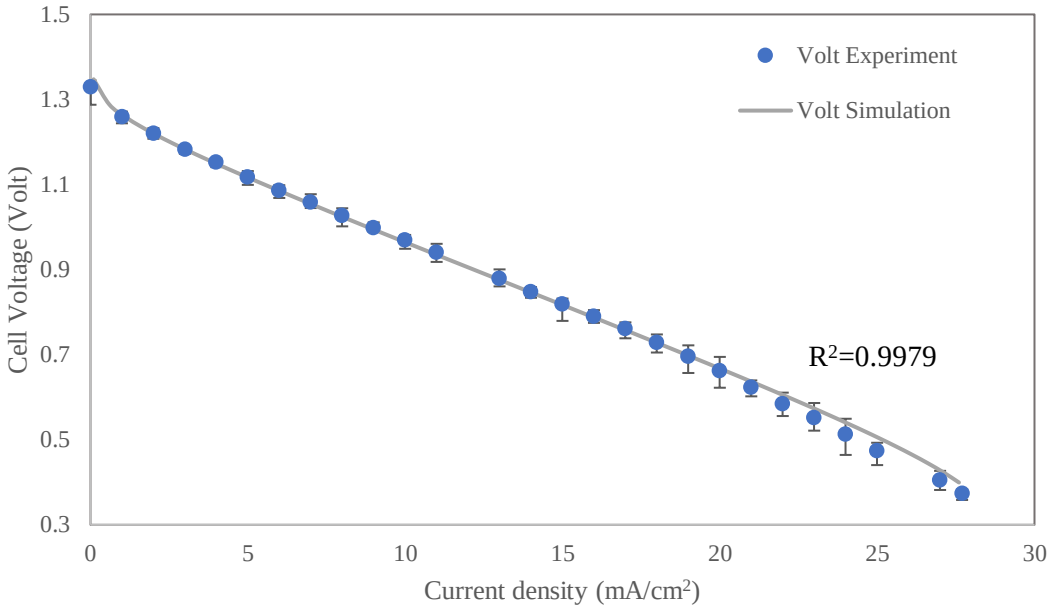

Figure 5.1 Comparison of polarization curve of ZAFC between experiment data and simulation data

The polarization curve comparison between experiment and simulation was depicted in figure 5.1. The simulation curve was predicted from the proposed model with the parameter fitted. The fitted values of R_{comp}, δ_{active} and ε_{actve} were 1.25 Ω, 1 μm and 0.2191, respectively. The predicted polarization curve was in an acceptable agreement with experimental data. At high current density, small offset was observed but the predicted and experimental curve were well-fitted at low current density especially at ohmic region which normally is operating point of the cell (R^2=0.9979). This small offset occurred because oxygen concentration loss has greater effect in the experiment. In this model, oxygen concentration loss computed from limiting current density which did not change from the initial stage. In the experiment, air electrode had changed along the operation time. For instance, penetration of electrolyte to air electrode caused changing in the GDL. However, the model parameters related to concentration loss were constant along the operation. The parameter changed with time could eliminate this offset. The fitted model was used to study the parameters in next section.

For validation of the ZAFC model, the parameters was estimated with the experiment data of Sapkota and Kim (2010). At first, the model was fitted with literature data of 8M KOH. Then, the concentration of KOH was changed to 4 and 8M to validate the predicted result. The polarization curve comparison between the literature data and the predicted data was shown in figure 5.2. The fitted values of R_{comp}, δ_{active} and ε_{actve} were 5 mΩ, 420 μm and 0.25, respectively. The comparison of literature and simulation was acceptable for all compared KOH concentration. The values of R^2 of the predicted data with 4M, 8M and 16M KOH concentration were 0.9834, 0.9753 and 0.9935, respectively.

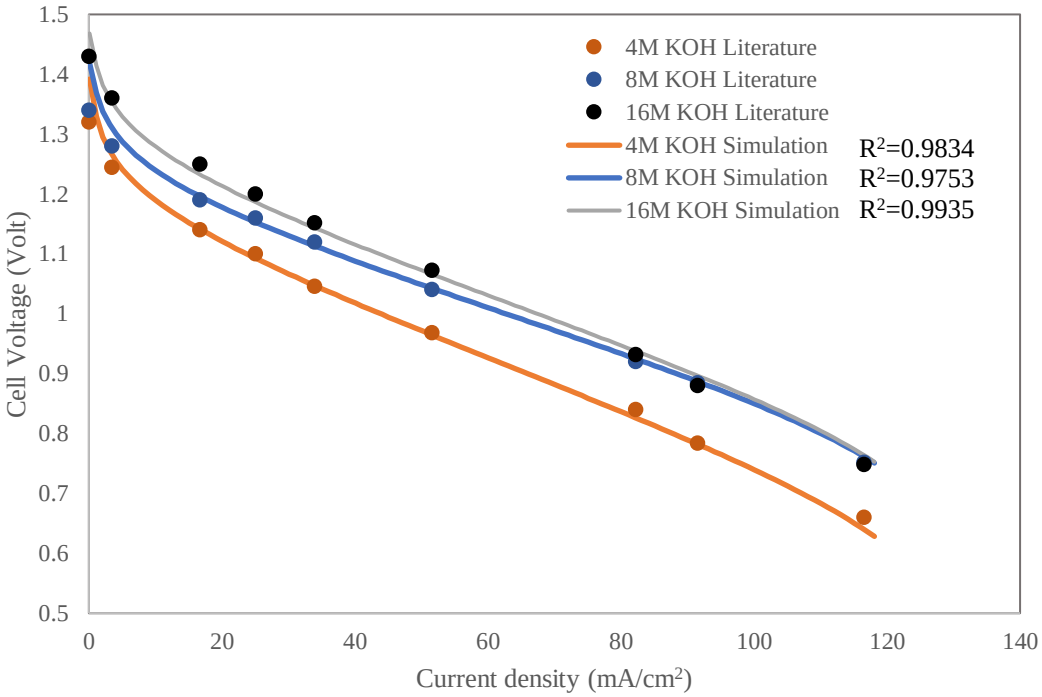

Figure 5.2 Comparison of polarization curve of ZAFC between experiment data of Sapkota and Kim (2010) and predicted data of this simulation.

5.1.2 Effect of Potassium Hydroxide Concentration on ZAFC

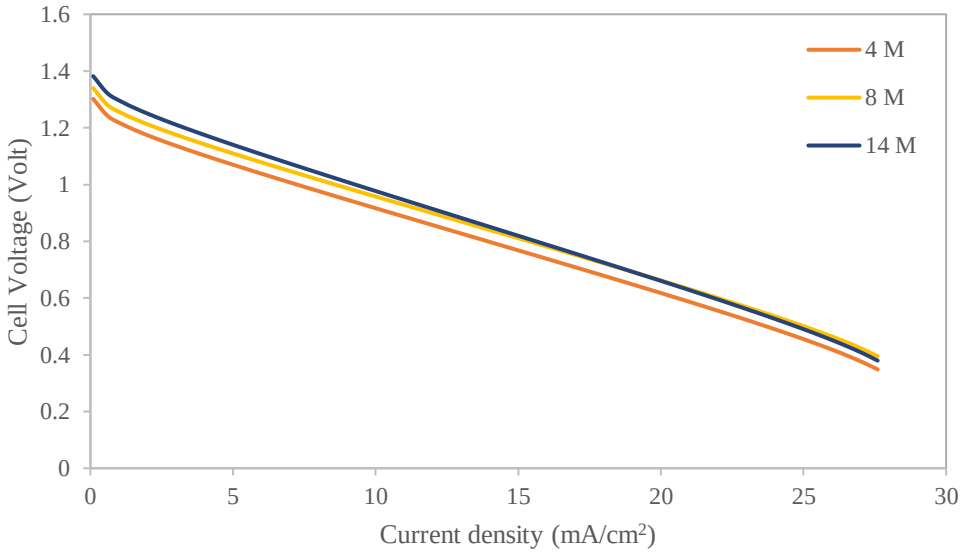

Figure 5.3 Comparison of polarization curve between 4,8 and 14M KOH concentration

Effect of KOH concentration was investigated by varying the KOH concentration of the feed flow. Electrolyte concentration has a significant influence on some parameters in ZAFC which affect the cell performance. Comparison of cell

performance between 4, 8 and 14 M KOH concentration was illustrated in figure 5.3. Generally, open circuit voltage (OCV) is calculated from Nernst equation (equation (3.20)) including hydroxide concentration term therefore higher KOH concentration is provide higher OCV as shown in Figure 5.4.

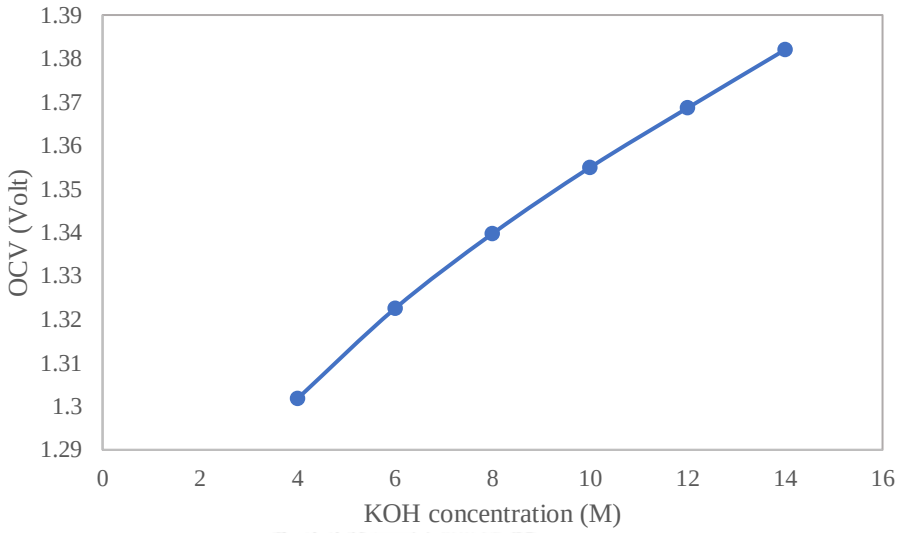

Figure 5.4 Comparison of OCV between various KOH concentration

The low current density region is normally dominated by activation loss particularly cathode activation loss. Appleby and Marie (1979) investigated kinetic of ORR on carbon material in alkaline solution. The research proposed that the reaction orders of ORR were first and zero order respect to oxygen and hydroxide, respectively. The cathode activation loss was independent of KOH concentration therefore the cathode activation loss from simulation was similar for all concentration. For anode, increasing in KOH concentration from 4 to 8 M decreased the activation loss, however, higher activation loss was observed at 14 M (figure 5.5). This occurred because the reference exchange current density ($i_0^{Zn,ref}$) of anode is the function of KOH concentration. In this work, the correlation fitted with experiment data by Dirkse and Hampson (1972) was used to estimate $i_0^{Zn,ref}$ as depicted in figure 5.6. It was observed that $i_0^{Zn,ref}$ increased along with KOH concentration until the maximum point which was about 7 M. Increasing KOH concentration further resulted in declining of $i_0^{Zn,ref}$.

At high current density range, high KOH concentration showed low cell performance (figure 5.7). The major reason was ohmic potential loss which was mainly effected by KOH concentration. Ionic conductivity of electrolyte is a function of KOH concentration. In this work, the conductivity was calculated from the correlation of KOH solution conductivity and concentration proposed by See and White (1997). It was showed that the conductivity of KOH solution was increased along with concentration until the maximum point which was about 6 M. Increasing KOH concentration after maximum point showed decreasing in the conductivity. For comparison, ionic conductivities of KOH solution at 4, 8 and 14 M were 0.55, 0.621 and 0.367 S/cm. Lower ionic conductivity of electrolyte resulted in higher ohmic resistance and potential loss particularly at high current density region.

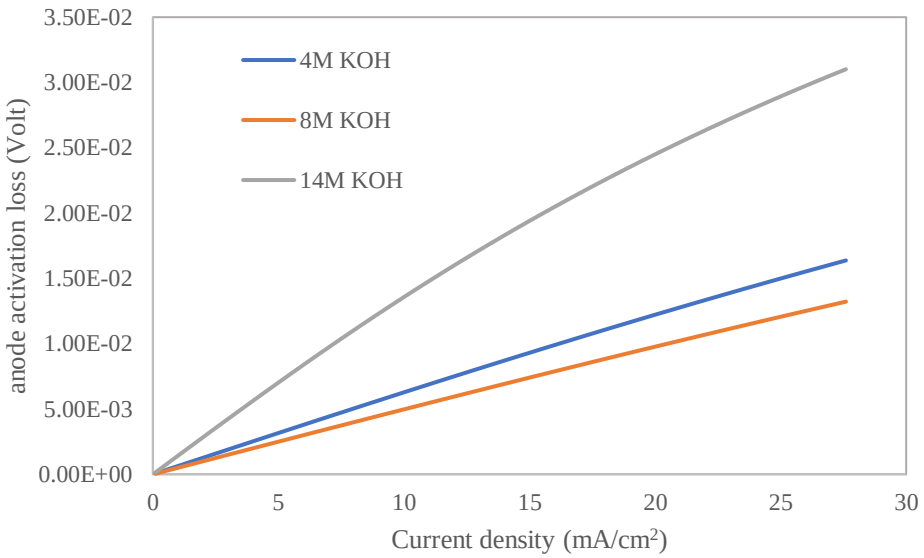

Figure 5.5 Comparison of anode activation loss between 4,8 and 14M KOH concentration

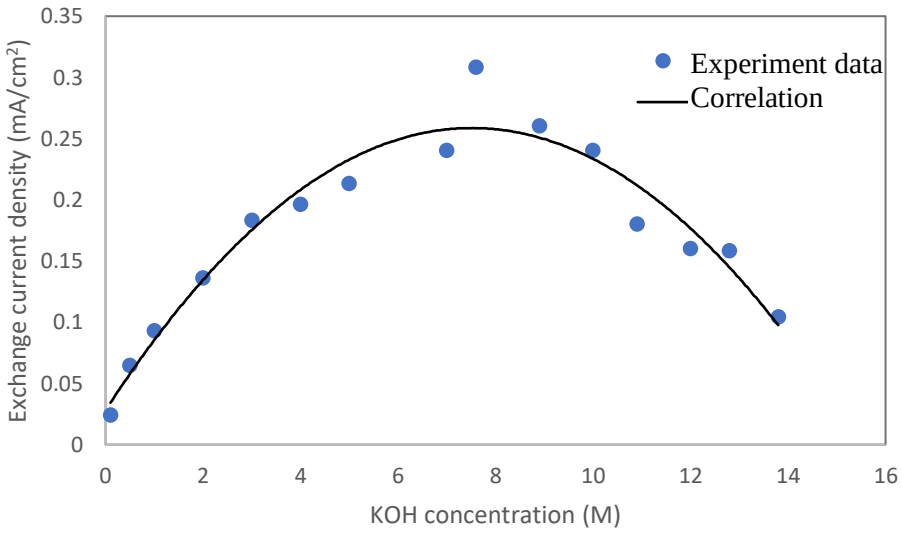

Figure 5.6 Reference exchange current density at various KOH concentration (Dirkse and Hampson 1972)

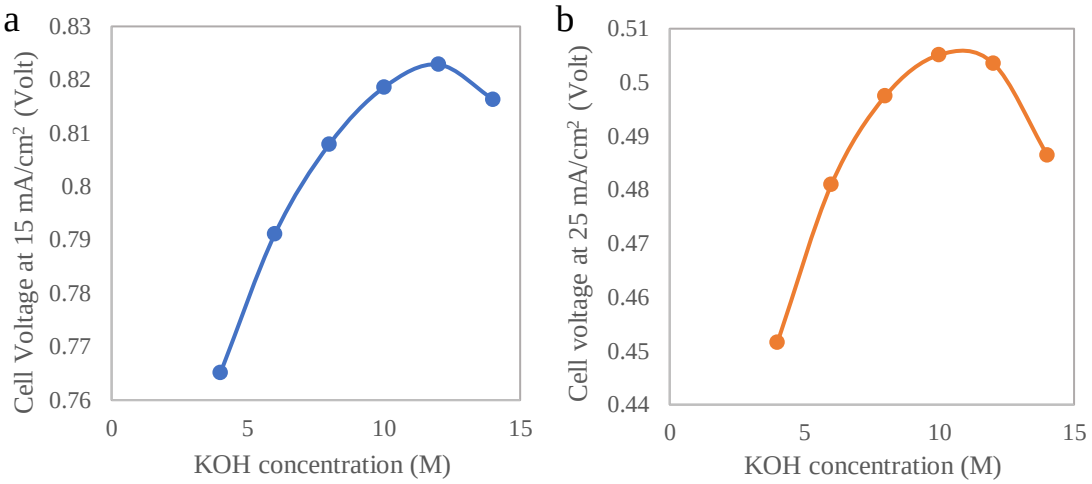

Figure 5.7 Comparison of cell voltage between various KOH concentration at a) 15 mA/cm^2 and b) 25 mA/cm^2

To summarize the effect of KOH concentration on ZAFC performance, increasing KOH concentration provided higher Nernst potential. However, the exchange current density and ionic conductivity was lower after maximum point at 6 - 7 M KOH concentration. For that reason, using KOH concentration too high was not optimum. The simulation result demonstrated the same way as the previous experiment by Sapkota and Kim (2010). The previous study also showed that increasing KOH concentration too high provided no improvement to the cell performance. The widely-used KOH concentration was 7 to 9 M because of good conductivity and high activity of hydroxide ion (Xu, Ivey et al. 2015).

5.1.3 Effect of Flow on ZAFC

In order to account effect of flow, discharge curve was examined together with polarization curve. Polarization curve was unable to obviously analyze the difference of the simulation result because the polarization curve used data at 60 seconds from the start while the effect of flow cannot be noticed in this range of time. The discharge curve was able to analyze long-time operation performance of the ZAFC.

Figure 5.8 showed the comparison between electrolyte flowrate (space velocity) of 0 to 0.5 per hour (h^{-1}) at discharge current density of 15 mA/cm^2. Cell voltage (figure 5.8a) related with moles of zinc in ZAFC (figure 5.8b). The non-flowing cell operated like a battery which has finite amount of zinc in the cell. Zinc in the cell decreased along the time and depleted. The depletion of zinc caused cell voltage to drop. From the result at discharge current density of 15 mA/cm^2, the non-flowing cell was able to last for about 3.5 h. Increasing flowrate resulted in extension of discharge duration before zinc depletion as the cell with higher flowrate lasted longer than the lower flowrate cell. The depletion of zinc was still occurred unless the inlet flowrate of zinc was greater than zinc consumption rate. Nevertheless, the consumption rate varied with the discharge current density and discharge duration was also different as shown in figure 5.9.

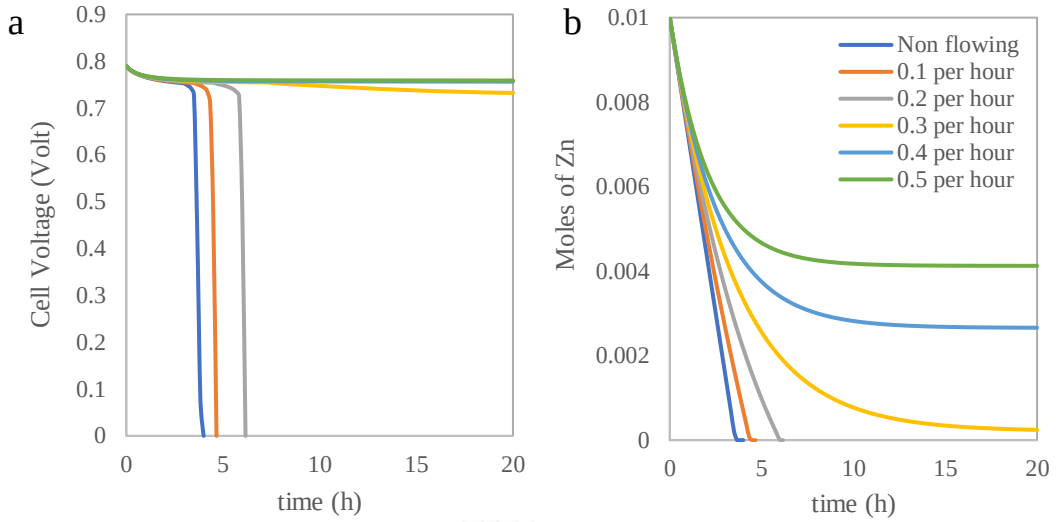

Figure 5.8 Comparison of a) voltage and b) moles of zinc between various electrolyte flowrate at discharge current of 15 mA/cm^2

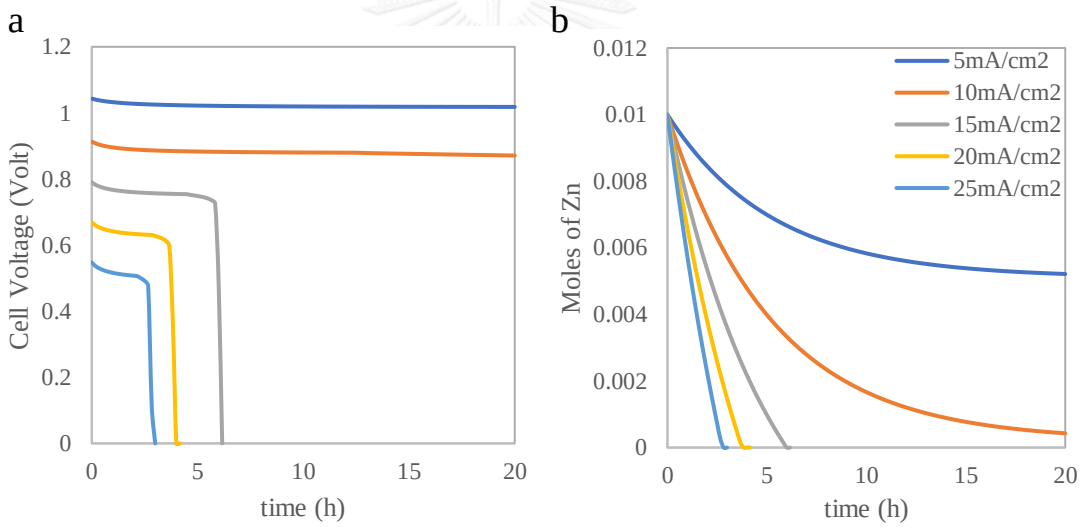

Figure 5.9 Comparison of a) voltage and b) moles of zinc between various discharge current at electrolyte flowrate of 0.2 h^{-1}.

Figure 5.10 showed the comparison of polarization curve between electrolyte flowrate of 0 to 5 h^{-1} at operation time of 10 hours. By extending the collecting data time from 60 seconds to 10 hours, polarization curve can be used to illustrate the effect of flow. The result showed that using the higher electrolyte flowrate maintained the cell performance for long-time operation. The cells with non-flowing electrolyte and low electrolyte flowrate had maximum discharge current density lower than the maximum performance cell as shown in figure 5.11. The overpotential at high current density occurred from the depletion of zinc as depicted in figure 5.11a. Moreover, increasing flowrate provided higher overall cell voltage because the higher hydroxide concentration was maintained at higher electrolyte flowrate as described in figure 5.11b. However, at high enough flowrate, difference in cell performance was unable to clearly observe. As considered the result with 0.1 and 0.5 h^{-1} in figure 5.10 and 5.11,

moles of zinc and hydroxide concentration of both 1 and 5 h^{-1} cells were different but the cell voltage of both cells were equally same.

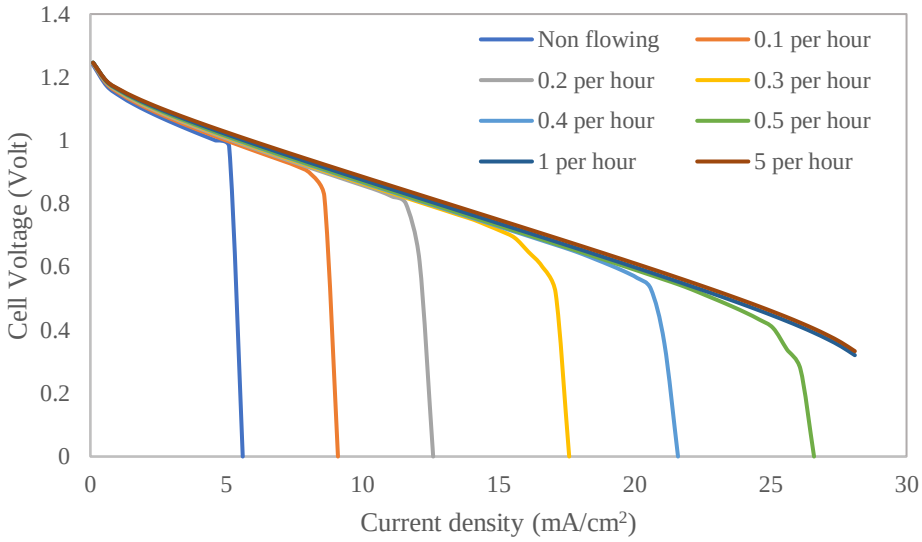

Figure 5.10 Comparison of polarization curve between various electrolyte flowrate at operation time of 10 h.

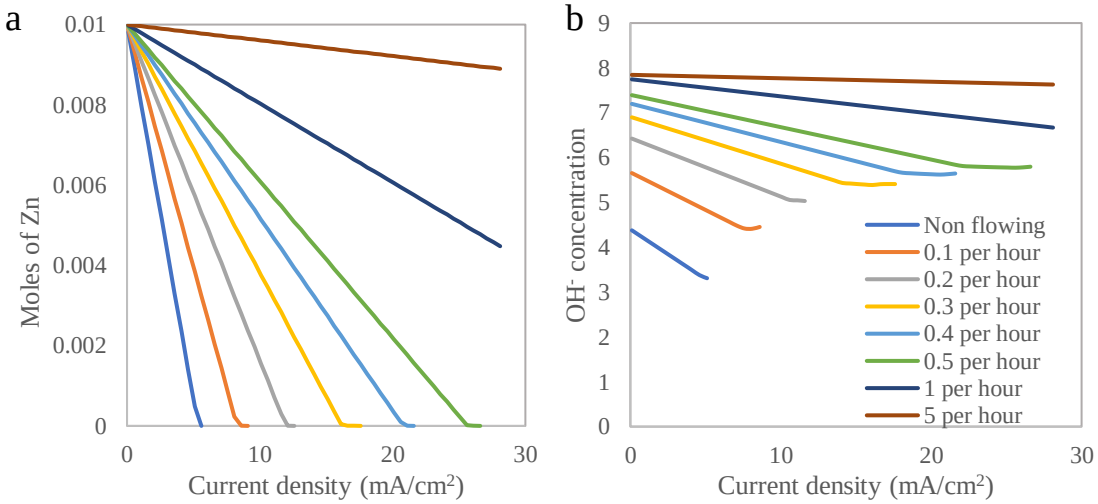

Figure 5.11 Comparison of a) Moles of Zn and b) OH^- concentration between various electrolyte flowrate at operation time of 10 h.

To conclude the effect of flow on ZAFC performance, increasing electrolyte flowrate provided higher cell performance for long-time operation. At high enough electrolyte flowrate, moles of zinc and hydroxide concentration which are anode reactant of ZAFC was maintained at high amount therefore the cell voltage was also maintained. This introduced that controlling electrolyte flowrate could control the amount of reactant and performance of ZAFC. The result was concluded the same way as the previous experiment by Puapattanakul, Therdthianwong et al. (2013). The research showed that ZAFC with flowing electrolyte provided 27% higher average current than that with non-flowing electrolyte. The patent by Kim, Suh et al. (2013)

also explained that the circulation of electrolyte enhanced the cell performance comparing to the non-circulation cell but increasing circulation rate too high did not provide significant improvement in cell performance.

5.1.4 Effect of Zincate Ion Concentration and zinc oxide content on ZAFC

Effect of zincate ion concentration and ZnO content was investigated by varying the initial zincate ion concentration of the feed flow. The concentration of zincate ion was varied relatively with ZnO chemical solubility in electrolyte. The correlation of ZnO solubility in KOH solution was fitted from the literature of Dyson, Schreier et al. (1968). The initial ZnO content of all case was 0 and ZnO generated when zincate ion was over solubility limit.

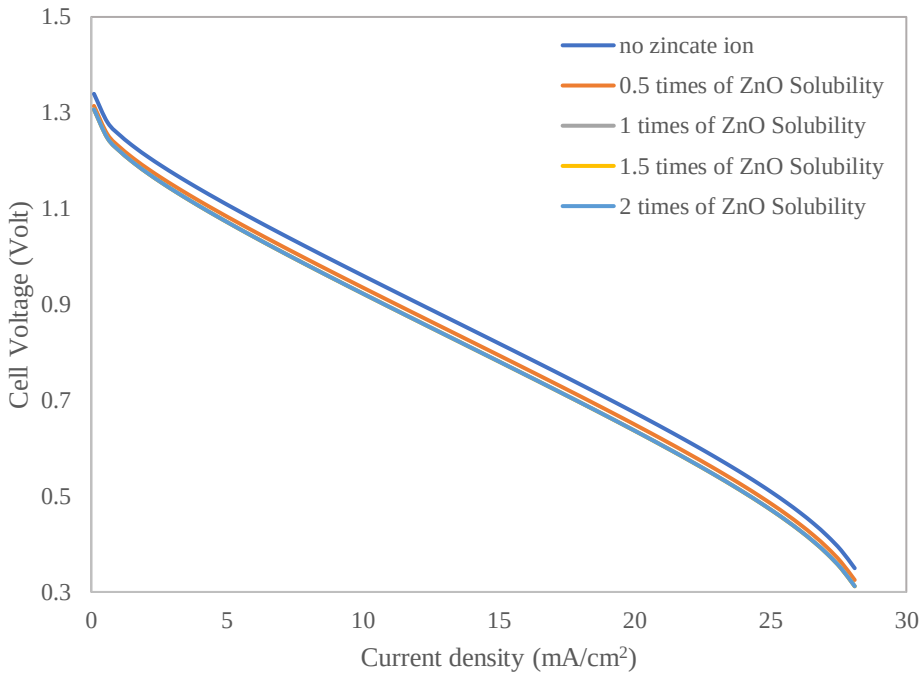

Figure 5.12 Comparison of polarization curve between various initial zincate ion concentration which relatively varied with ZnO solubility in KOH solution.

Comparison of cell performance between the initial zincate ion concentration of 0, 0.5, 1, 1.5 and 2 times of ZnO solubility was shown in figure 5.12. The overall performance of the cell with no initial zincate ion was higher than the others with initial zincate ion and the higher initial zincate ion concentration provided lower cell performance. In the model, concentration of zincate ion directly affected the Nernst potential. Increasing in zincate ion concentration decreased the anodic standard potential resulted in lower Nernst potential. Moreover, change of zincate ion also affected the concentration of hydroxide ion because of electroneutrality assumption. In real experiment, changing of initial zincate ion concentration was done by discharging of zinc or adding ZnO therefore the hydroxide ion was also consumed. The higher initial zincate ion concentration resulted in the lower initial hydroxide ion and cell potential. Figure 5.13 demonstrated the comparison of OCV and anodic composition at various initial zincate ion concentration. At the range of initial zincate ion lower than ZnO

solubility limit, cell voltage and hydroxide concentration decreased due to increasing of zincate ion. However, the cell behavior was different at the range of initial zincate ion higher than ZnO solubility limit. Because saturated zincate immediately transformed into ZnO, the hydroxide ion and actual zincate ion was not significantly different (figure 5.13b - c). For that reason, OCV was also not much different at this range of initial zincate ion as shown in figure 5.13a.

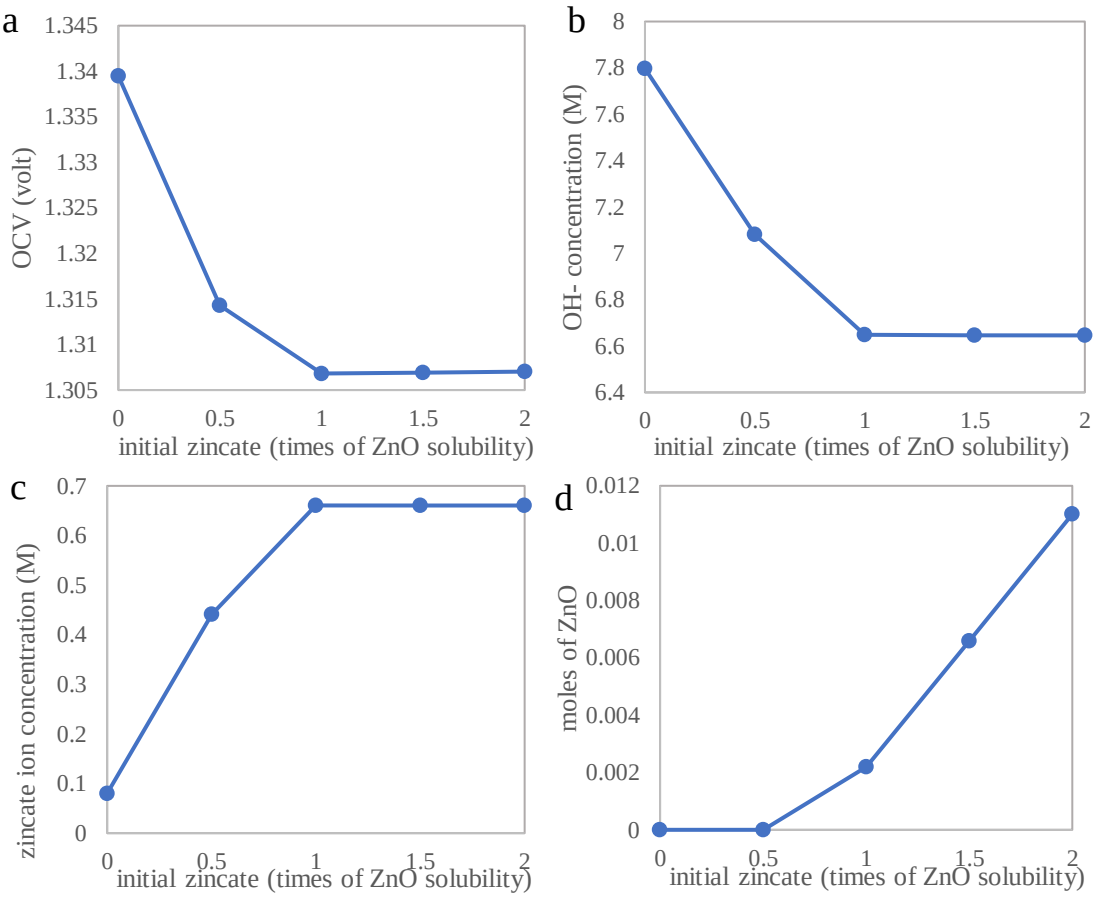

Figure 5.13 Comparison of a) OCV, b) hydroxide ion concentration c) zincate ion concentration and d) ZnO content between various initial zincate ion concentration (at open circuit).

Long-time operation result was presented in figure 5.14. The result also showed that increasing in initial zincate ion decreased cell performance at non-saturated range but the cell performance was not significantly different after zincate ion saturation (figure 5.14a). From no initial zincate ion case, cell voltage behavior changed after zincate ion became saturated and began to generate ZnO. In the saturated zone, cell voltage tended to decline even though the concentration of hydroxide ion and zincate ion did not change much in this zone. As compared between other case, increasing in initial zincate ion decreased cell voltage at the beginning of the operation because higher zincate ion and lower hydroxide ion concentration provided lower Nernst potential and higher anode activation loss (figure 5.14e and f). After a period of operation time, the concentration of hydroxide and zincate ion became steady and equal between all case therefore the Nernst potential and the activation loss was also not

different between all other case. The higher initial zincate ion provided higher ZnO generated than the lower (figure 5.14d). However, Increasing in ZnO did not provided significant change in this operation case.

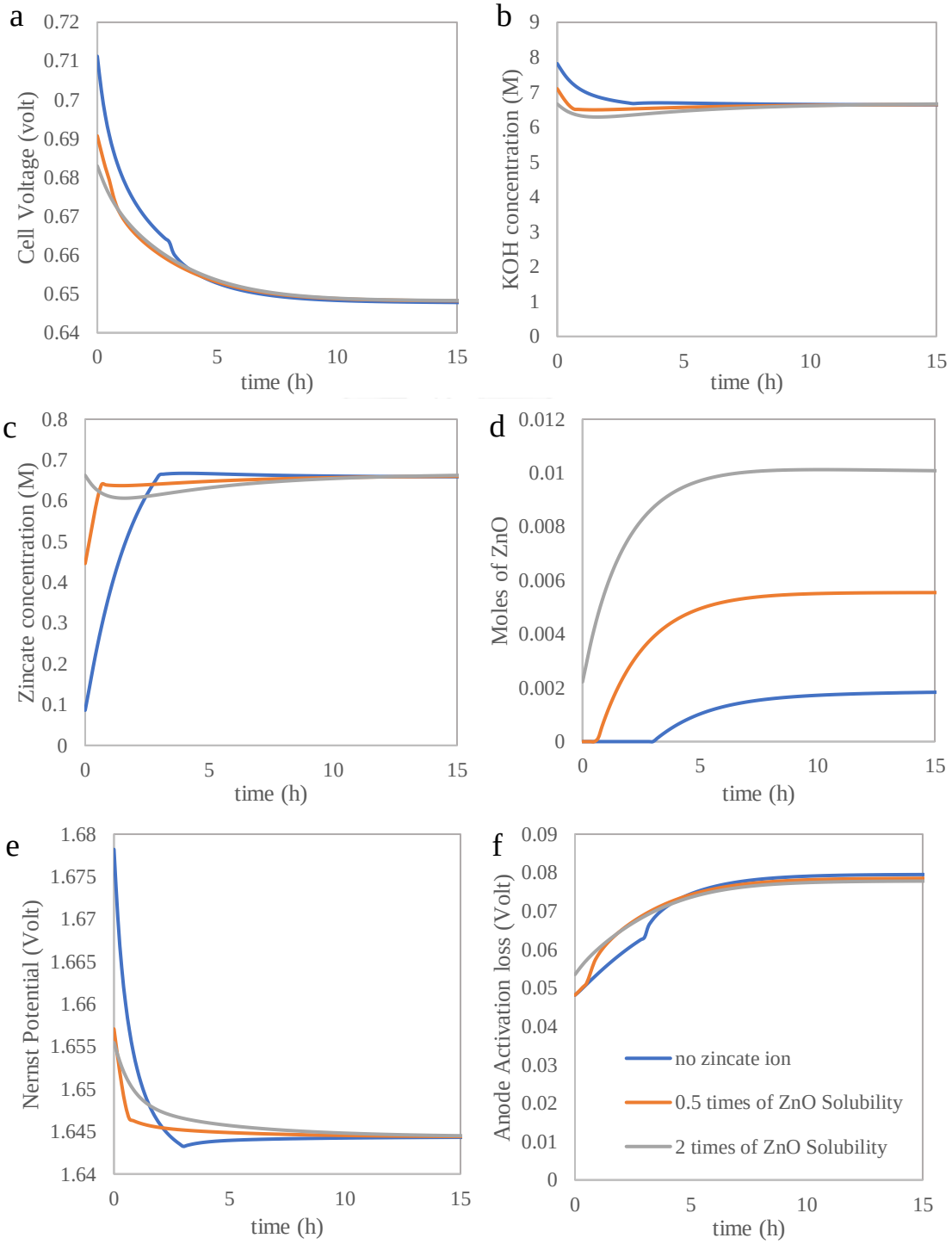

Figure 5.14 Comparison of a) cell voltage, b) hydroxide ion concentration c) zincate ion concentration, d) ZnO content, e) conductivity of solid electrode and f) zinc volume fraction between various initial zincate ion concentration at the discharge current of 20 mA/cm^2 in long-time operation.

Effect of ZnO was experimentally studied in many previous literatures. It was claimed that ZnO had low conductivity and contributed to ohmic voltage loss of zinc-air system. In this research, ZnO content directly affected to the conductivity of anode. The anode conductivity was also affected by its porosity because pores of electrode was filled with the electrolyte which decreased the anode conductivity. To investigate the anode conductivity, ZnO content was studied together with porosity of anode. Figure 5.15 showed effect of anode porosity and ZnO content on cell voltage. From figure 5.15a, OCV was increased along with porosity until the maximum point (0.65 for 90% ZnO and 0.8 for the others). After this point, OCV tended to decrease instead. This occurred because the higher porosity provided the greater amount of hydroxide ion inside anode pores which resulted in the higher Nernst potential. However, the excessive porosity resulted in high anode activation loss which affected the overall cell voltage. For the effect of ZnO on OCV, increasing ZnO content decreased the OCV for all case because the higher amount of ZnO meant lower amount of zinc in the same porosity. Decreasing in zinc content led to increasing in activation loss of anode. At the current density of 20 mA/cm^2 (figure 5.15b), increasing in porosity resulted in decreasing in cell voltage since the higher amount of pore filled with higher amount of electrolyte which had low conductivity. Low conductivity provided high ohmic loss which was dominant loss in the high current region. Moreover, the higher porosity also provided the higher activation loss. ZnO affected both activation loss and ohmic loss same as the porosity. From comparison of cell voltage between at OCV and 20 mA/cm^2, porosity and ZnO provided greater influence at current density of 20 mA/cm^2 than at OCV because ohmic loss and activation loss increased along with the current density.

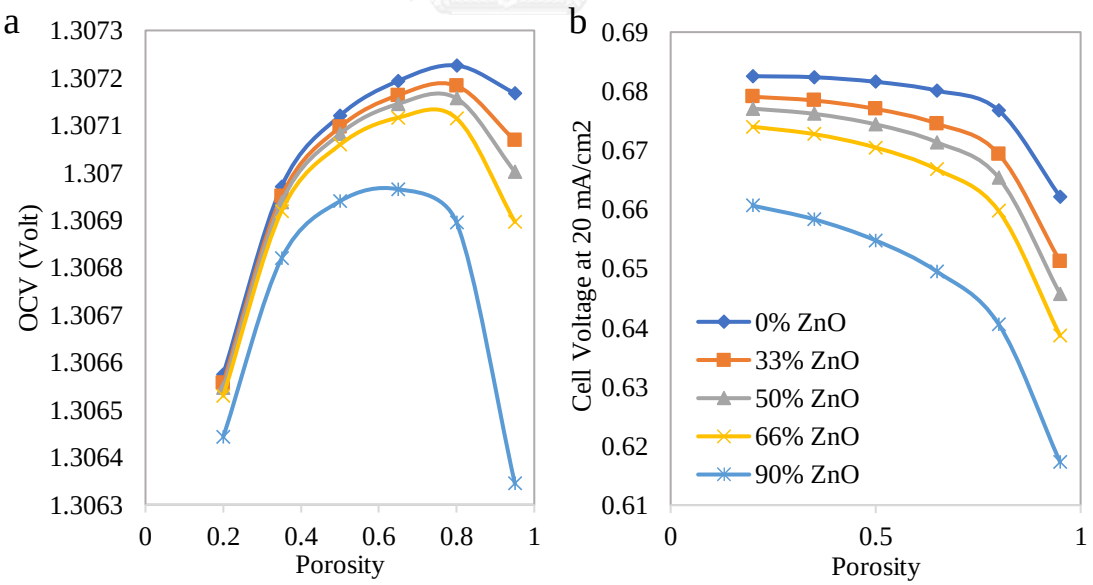

Figure 5.15 Comparison of cell voltage at a) open circuit and b) 20 mA/cm^2 between various anode porosity and ZnO content

To summarize the effect of zincate ion and zinc oxide, increasing in zincate ion concentration decreased overall cell performance. The higher zincate ion provided lower Nernst potential resulted in lower overall cell voltage. The saturated zincate transformed into ZnO. ZnO had low conductivity and was inactive in discharge reaction led to higher ohmic overpotential and anodic activation overpotential. From this

simulation, it was observed that ZnO slightly reduced overall cell performance because change in ohmic loss had low impact in this model. In the other studies, ZnO formed on the surface of zinc particle which act as electrical insulation. This phenomenon is called passivation of zinc which decreases zinc electrode utilization. This model did not include the effect of passivation therefore the negative effect of ZnO was less than the real case. However, different operation procedure based on existing of ZnO should be considered. There are some literatures that studied about this. Kim, Kim et al. (2015) proposed that the precipitation of ZnO showed negative effect to ZAB charge-discharge cycling stability and suggested that preventing ZnO from precipitation could prolong ZAB life cycle. Zhu, Duch et al. (2015) used calcium hydroxide to scavenge zincate ion resulted in higher dissolution of ZnO and improvement of cell performance and capacity. However, some studies suggested that high dissolution of ZnO was not preferred because zincate ions or other zinc discharge species caused dendrite formation and zinc shape change in rechargeable ZAB (Xu, Ivey et al. 2015). In ZAFC, dendrite formation and shape change were handled by mechanical recharging outside the cell therefore controlling zincate ion and ZnO low could optimize the cell performance.

5.1.5 Effect of Conductive carbon on ZAFC

Effect of conductive carbon was investigated by varying ratio of carbon. Adding conductive carbon could improve performance in the part of conductivity. It was assumed that the carbon added was mixed into the solid electrode. Conductive carbon was varied from 0 to 30% of solid electrode weight. The conductivity of anode (solid plus electrolyte), cell voltage at 20 mA/cm^2, OCV and zinc active surface fraction (X_{Zn}) were showed in figure 5.16. Adding carbon showed no significant difference in anode conductivity except at 90% ZnO content (figure 5.16a). At high ZnO content, the conductivity of solid electrode was low because ZnO has low conductivity (1×10^{-9} S/dm). Adding carbon, which has conductivity of 2×10^{5} S/dm, improved the conductivity of the electrode. At low ZnO content, the solid electrode has high zinc content which has higher conductivity (2×10^{6} S/dm) than carbon therefore adding carbon did not improve the anode conductivity at this condition. Although adding carbon increased anode conductivity at high ZnO content, the cell voltage was decreased at all condition (figure 5.16b and c). It was observed that zinc active surface fraction was also reduced by adding carbon into zinc electrode. The lower active surface fraction resulted in the higher anode activation loss and lower cell voltage.

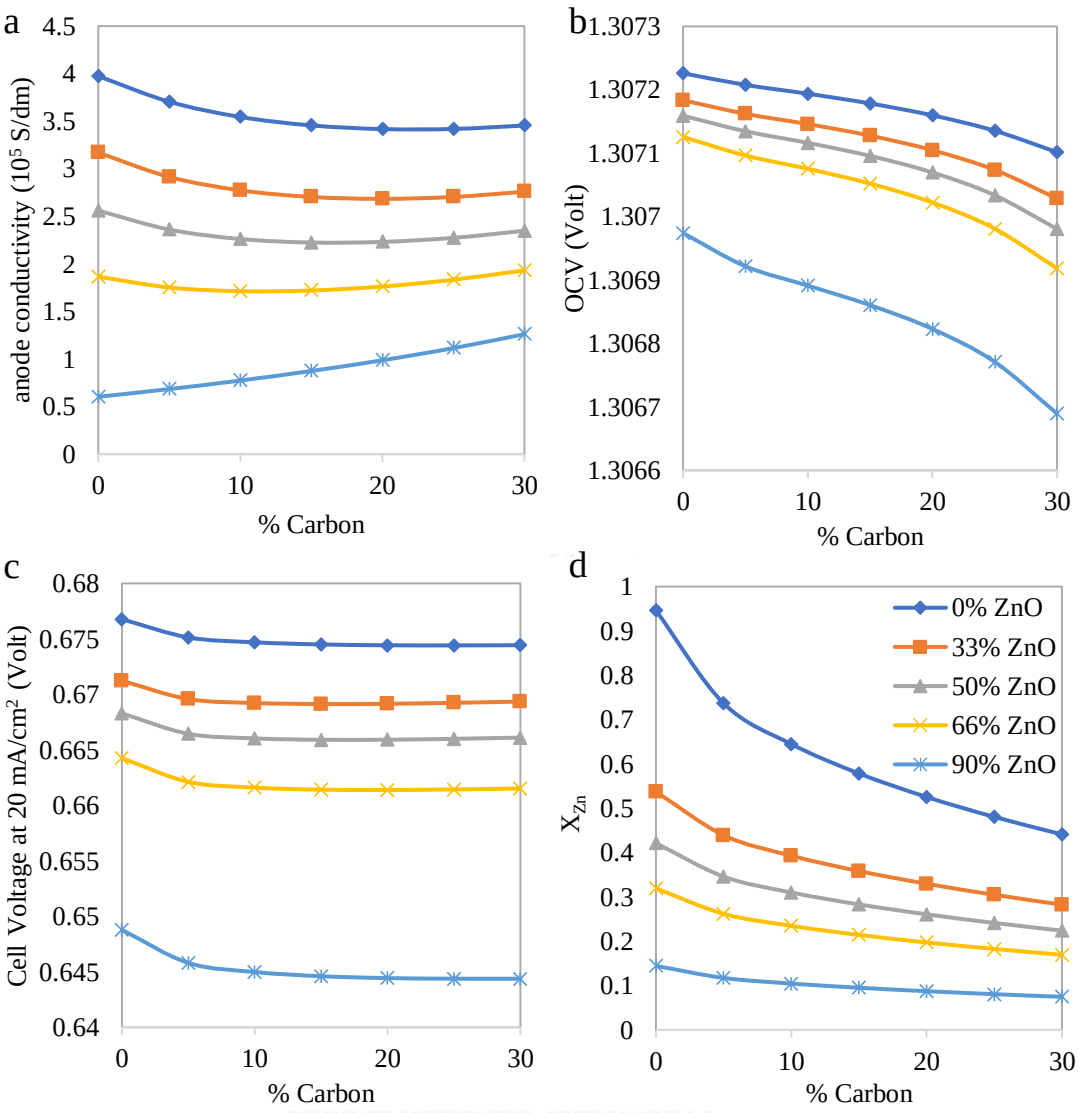

Figure 5.16 comparison of a) anode conductivity, b) OCV, c) cell voltage at 20 mA/cm^2 and d) X_{Zn} between adding conductive carbon of 0 to 30 % of solid electrode weight.

The long-time operation at current density of 20 mA/cm^2 was simulated and the result was illustrated in figure 5.17. At initial state, the anode conductivity of the case with 0% carbon was highest among other case. Then, ZnO was generated along the time which contributed to lower conductivity of anode as shown in figure 5.17a but It showed less effect on the higher carbon added case. After the system approached steady state, the conductivity of higher carbon added case was higher than the lower case. It was observed that higher carbon added assisted the system with high ZnO content to maintain anode conductivity high. However, the overall cell voltage was reduced by adding carbon. Adding carbon reduced active surface fraction of zinc and provided higher activation loss.

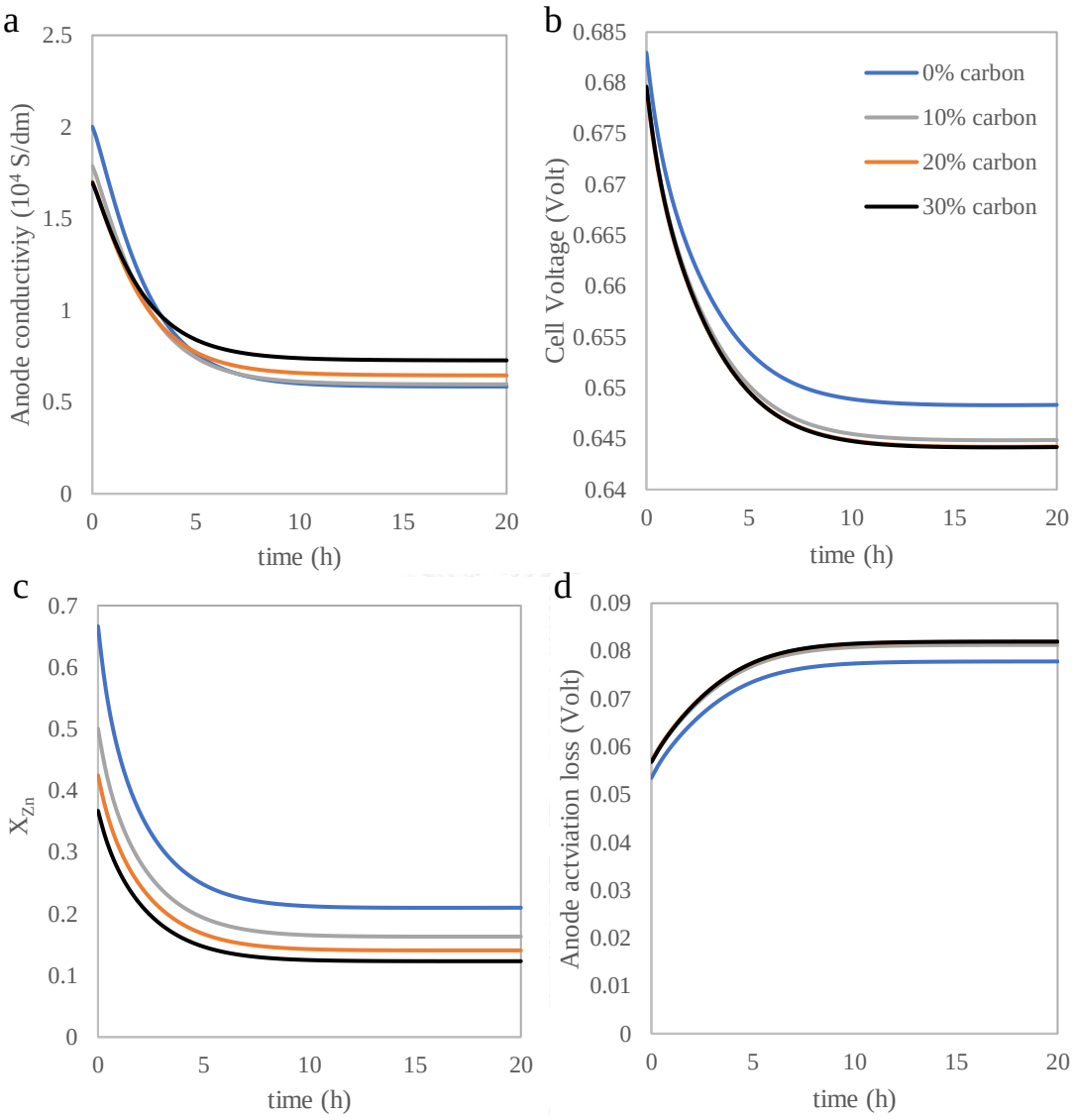

Figure 5.17 comparison of a) anode conductivity, (b) cell voltage at 20 mA/cm^2, c) X_{Zn} and d) anode activation loss between adding conductive carbon of 0 to 30% of electrolyte weight by discharge current density of 20 mA/cm^2 at long-time operation

5.2 Alkaline Zinc Electrolyzer Modelling

5.2.1 Electrolyzer Model Validation

To examine the validity of zinc electrolyzer model, the predicted polarization curve was compared with experimental data as showed in figure 5.18. The compared data was operated at KOH concentration of 9 M, zincate ion concentration of 1.05 M (saturated) and non-flowing electrolyte. The other design variables and operating condition was given in table 3.2. The result showed that the simulated polarization curve was in an acceptable agreement with the experimental data (R^2 = 0.9813). At low current density region, the predicted data and experiment data were in line within a small margin. At high current density region, the predicted result appeared to be higher than the experimental result because the experimental conditions were not constant

along the measuring period. The points in high current density range were collected after the lower range for a period. The generated zinc on the electrode caused lower resistivity in the high range therefore the experimental cell voltage was lower than predicted cell voltage in this range.

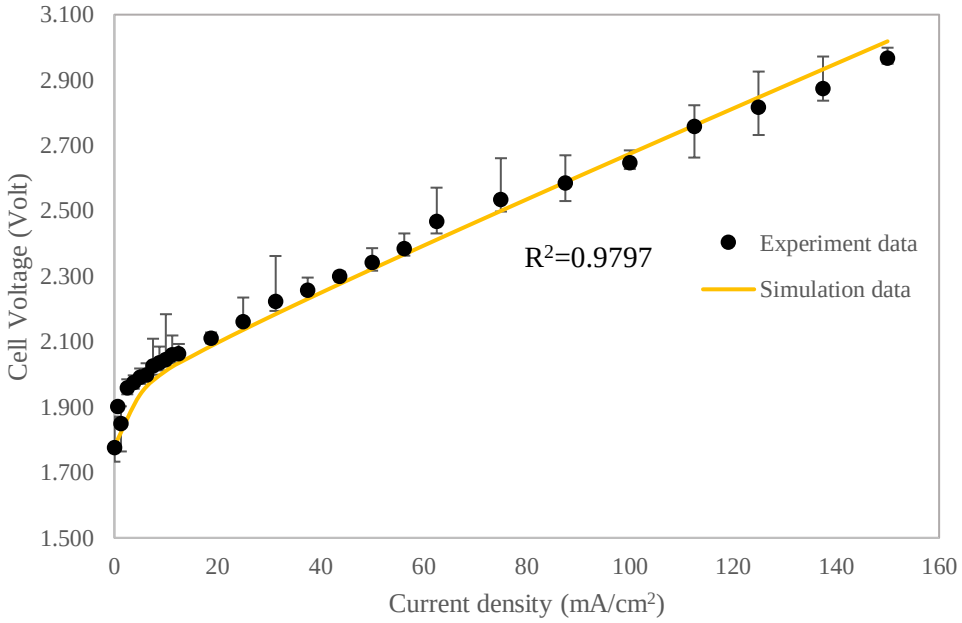

Figure 5.18 Comparison of polarization curve of alkaline zinc electrolyzer between experiment and simulation

5.2.2 Effect of Potassium Hydroxide Concentration on Zinc Electrolyzer

To account the effect of KOH concentration on zinc electrolyzer performance, comparison between various KOH concentration was performed. The cell voltage result was shown in figure 5.19. It was observed that increasing KOH concentration provided increasing in OCV (figure 5.19a) because of increasing in Nernst potential. However, cell voltage at 150 mA/cm^2 showed different trend. Increasing KOH concentration from 4 to 6 M reduced the cell voltage but increasing KOH concentration above 6 M increased the cell voltage instead. Since the highest ionic conductivity of electrolyte was observed at the KOH concentration of 6 M, the ohmic loss was lowest at this point (figure 5.20a). Figure 5.20 showed the comparison of ohmic loss and cathode activation loss based on zinc regeneration reaction. Cathode activation loss negatively increased with the increasing of KOH concentration because increasing hydroxide ion reduced the cathodic exchange current density of zinc cathode reaction. From figure 5.20b, all values except at OCV have negative sign which means the voltage was lost to regenerate zinc from zincate ion (reaction 2.6). At OCV, the values were positive which mean the reaction did not normally occur in charging mode.

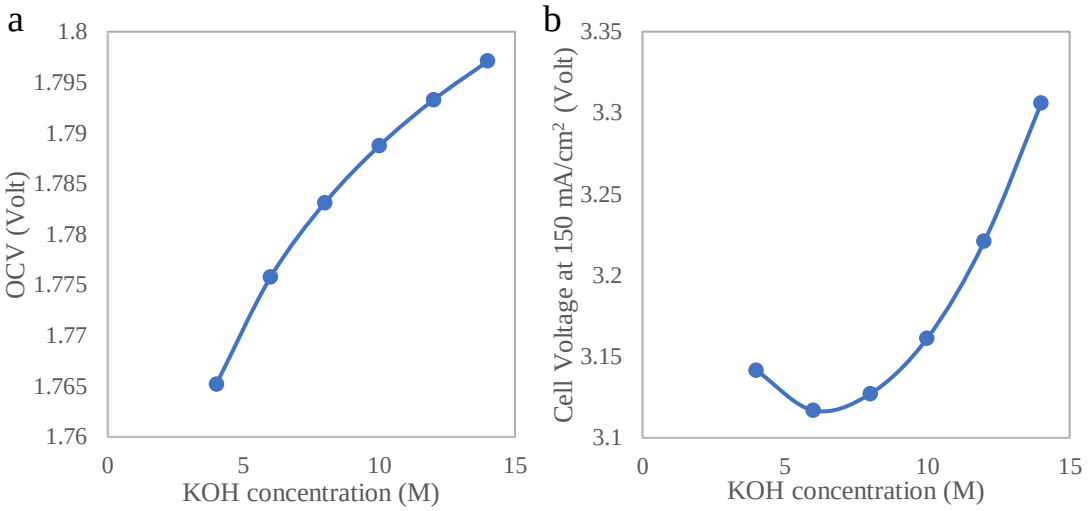

Figure 5.19 Comparison of a) OCV and b) cell voltage at 150 mA/cm^2 with 0.1M zincate ion concentration, no initial zinc and various KOH concentration.

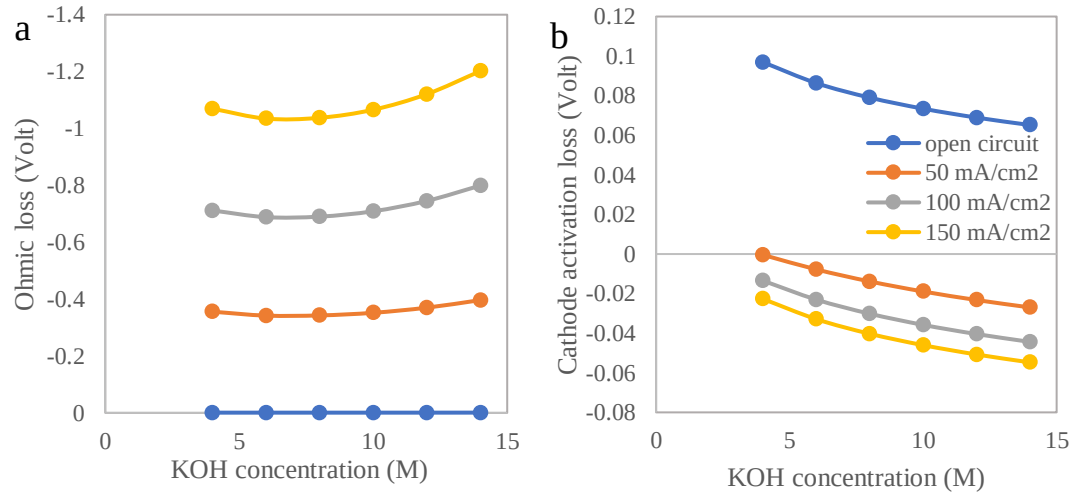

Figure 5.20 Comparison of a) ohmic loss and b) cathode activation loss (zinc regeneration) with 0.1M zincate ion concentration, no initial zinc at various KOH concentration and current density.

To describe the cathode reaction behavior, cathode activation loss vs zinc regeneration was compared with the loss vs hydrogen evolution reaction (HER) as shown in figure 5.21. In this simulation, the cathodic reaction included zinc regeneration reaction (reaction 2.6) and HER (reaction 2.9). The rates of reaction were the function of activation loss. At the low current density in figure 5.21a, the activation losses were positively high especially at low KOH concentration. The current supplied was too low to activate the zinc regeneration reaction therefore the only reaction occurred was HER. At standard state, the standard potential of zinc regeneration reaction and HER are -1.287 and -0.828 volt vs standard hydrogen electrode (SHE), respectively. This means HER has more overpotential than zinc regeneration reaction about 0.459 volt at standard state. Even though the zinc activation losses were positively high at low current density region, the HER activation loss were still negative at any current density (figure 5.21b).

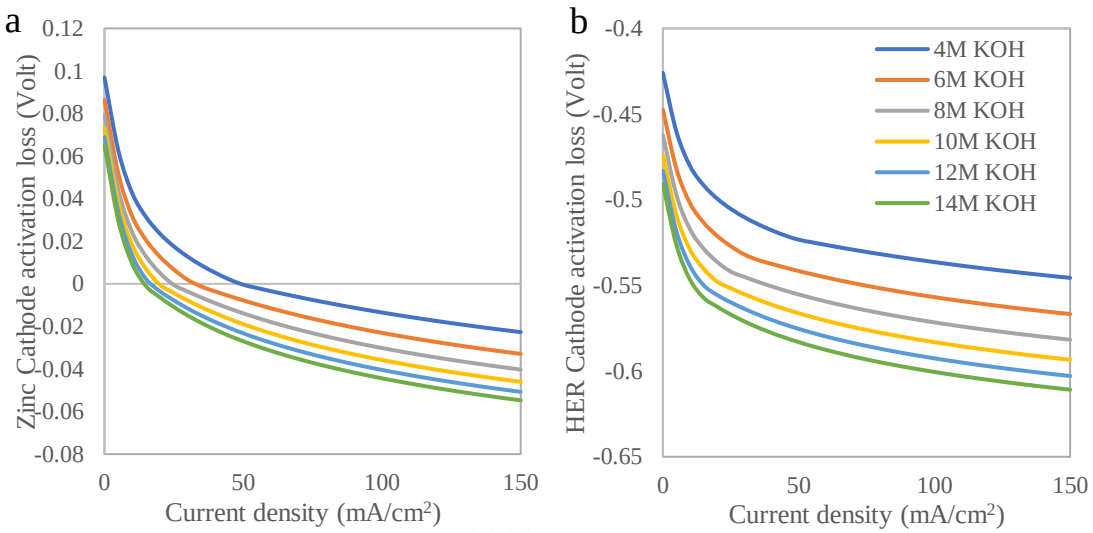

Figure 5.21 Comparison of cathode activation loss between a) zinc regeneration reaction and b) HER with 0.1M zincate ion concentration, no initial zinc and various KOH concentration.

For no initial zinc case, the current supplied to regenerate zinc from zincate ion and generate hydrogen from water. If the zinc regeneration was not active, only HER was active in cathode. For the case with initial zinc, there was another reaction that can be activated. Oxidation of zinc to zincate ion (reaction 2.1) which typically occurred in discharging mode was activated in this case. Figure 5.22 showed current density of zinc regeneration reaction and HER in case of 1×10^{-4} moles of initial zinc. In this figure, positive current density means current supplied and negative current density means current discharged. At low current density region, current densities of zinc were negative while HER current densities were higher than supplied current density. The current from zinc discharging was supplied to HER. Combination of zinc oxidation reaction (reaction 2.1) and HER (reaction 2.9) gives zinc corrosion reaction (reaction 2.10). The result showed that increasing in KOH concentration increased current supplied to zinc regeneration and decreased current supplied to HER. From figure 5.23, the activation losses of 1×10^{-4} moles of initial zinc case were lower than no initial zinc case at low current density region (figure 5.21) because zinc discharging reaction also occurred in this case.

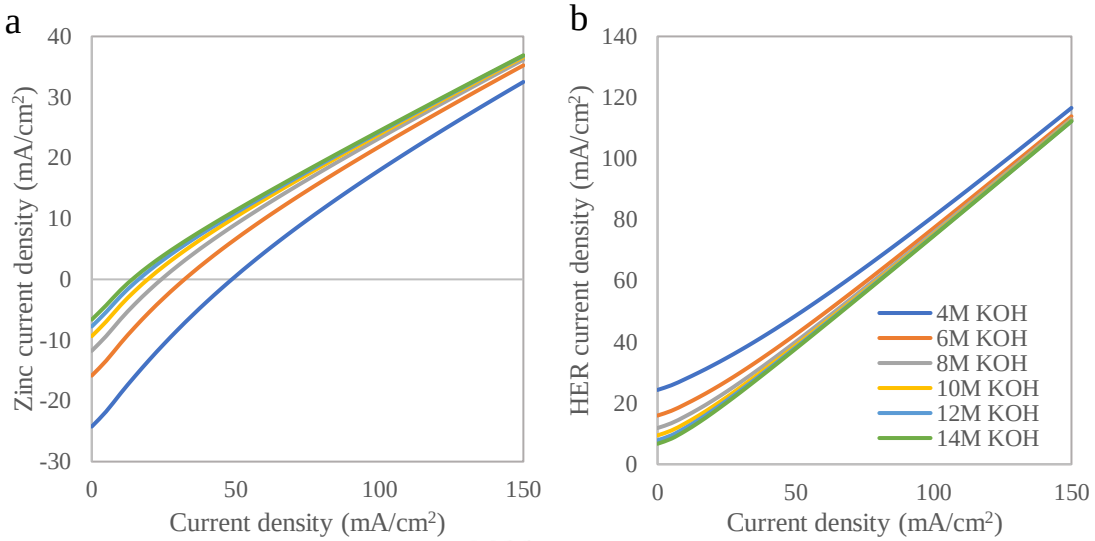

Figure 5.22 Comparison of current density of a) zinc regeneration reaction and b) HER with 0.1M zincate ion concentration, 1×10^{-4} moles of initial zinc and various KOH concentration.

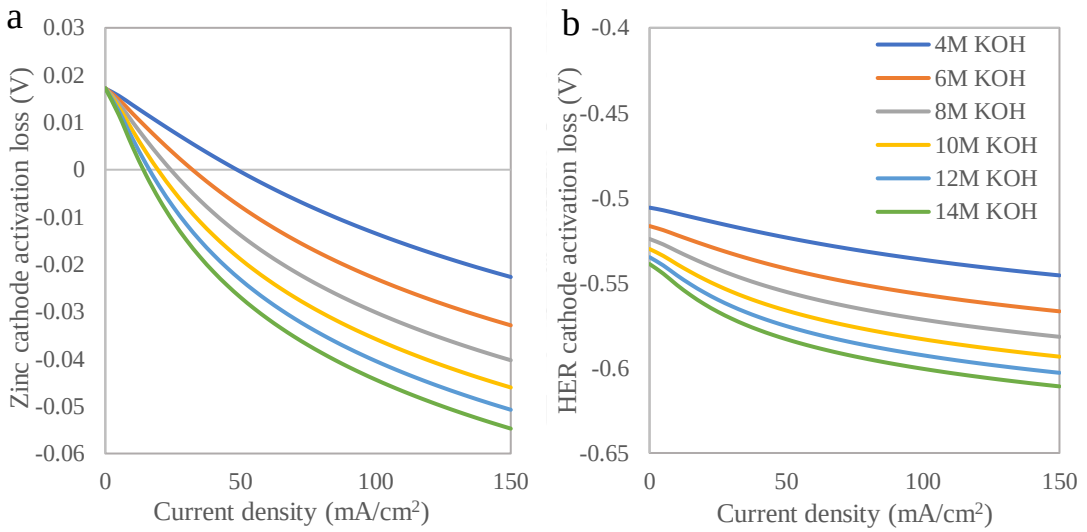

Figure 5.23 Comparison of cathode activation loss between a) zinc regeneration reaction and b) HER with 0.1M zincate ion concentration, 1×10^{-4} moles of initial zinc and various KOH concentration.

For alkaline zinc electrolyzer, the cell performance evaluation other than cell voltage is current efficiency. Current efficiency (C.E.) is the ratio of the electrochemical equivalent current for the specific reaction to the total applied current. In this simulation, C.E. was defined as the ratio of zinc current density to the total current density applied. Figure 5.24 showed the effect of KOH concentration on C.E. The C.E. behaved same as the current of zinc regeneration reaction shown in figure 5.22a. Increasing in current density increased C.E. as shown in figure 5.24a. The increasing of C.E. in the high current density region was lower than the lower current density region. For effect of KOH concentration, the higher KOH concentration provided higher C.E. as shown in figure 5.24b. However, the increasing of C.E. in the higher

KOH concentration range was lower than lower KOH concentration range. Sharifi, Mojtahedi et al. (2009) studied about alkaline electrolysis condition. The previous work concluded the same way as this work for the effect of current density. The effect of KOH concentration on C.E. was proposed differently from this work. They proposed that the C.E. decreased when increasing the KOH concentration. By adding more KOH to solution, the potassium ion concentration rises which increased hydrogen generation via the proposed mechanism. However, there was other literature that was contrast with Sharifi's work. Einerhand, Visscher et al. (1988) found that hydrogen production decreases with increasing KOH concentration which is according to the result of this work.

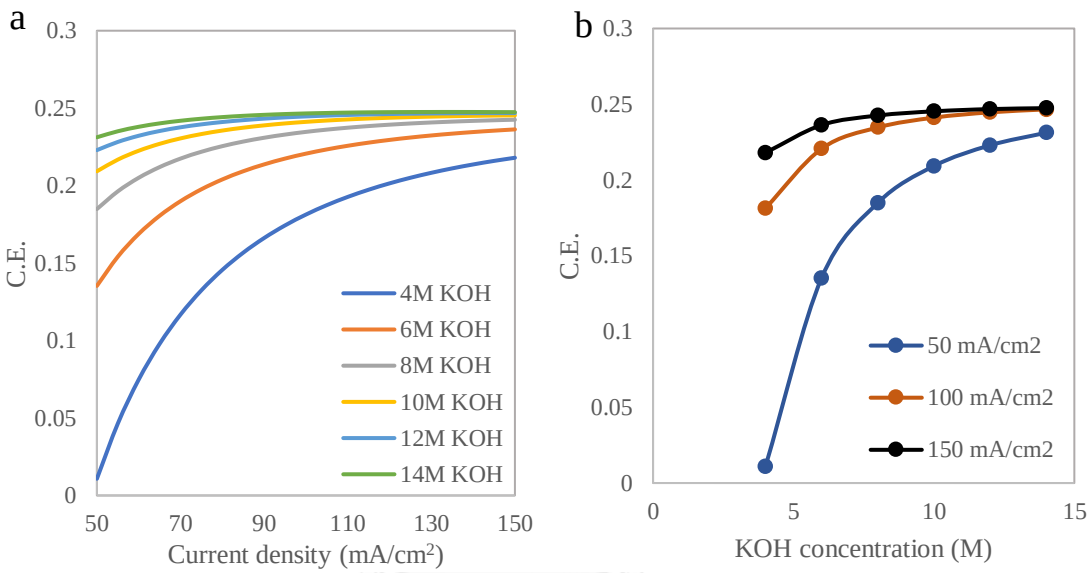

Figure 5.24 Comparison of current efficiency with 0.1M zincate concentration, no initial zinc, various KOH concentration.

5.2.3 Effect of Zincate Ion Concentration on Zinc Electrolyzer

To clarify the effect of zincate ion on alkaline zinc electrolyzer, the simulations with different initial zincate ion concentration were compared. The simulations were performed with 8 M KOH concentration and no initial zinc. The comparison of OCV and cell voltage at 150 mA/cm^2 was shown in figure 5.25. The result showed that increasing in zincate ion concentration reduced cell voltage. From figure 5.25, cell voltage decreased along with initial zincate ion concentration increasing until 0.7 M of initial zincate ion. After 0.7 M of initial zincate ion, the cell voltage was almost the same. This happened because zincate ion was saturated at about 0.66 M for this condition. The concentration of zincate ion above saturated concentration precipitated into ZnO therefore increasing zincate ion over ZnO solubility limit did not directly affect the cell performance. The ZnO solubility limit depends on hydroxide ion concentration thus increasing KOH concentration can increase the saturation limit of zincate ion.

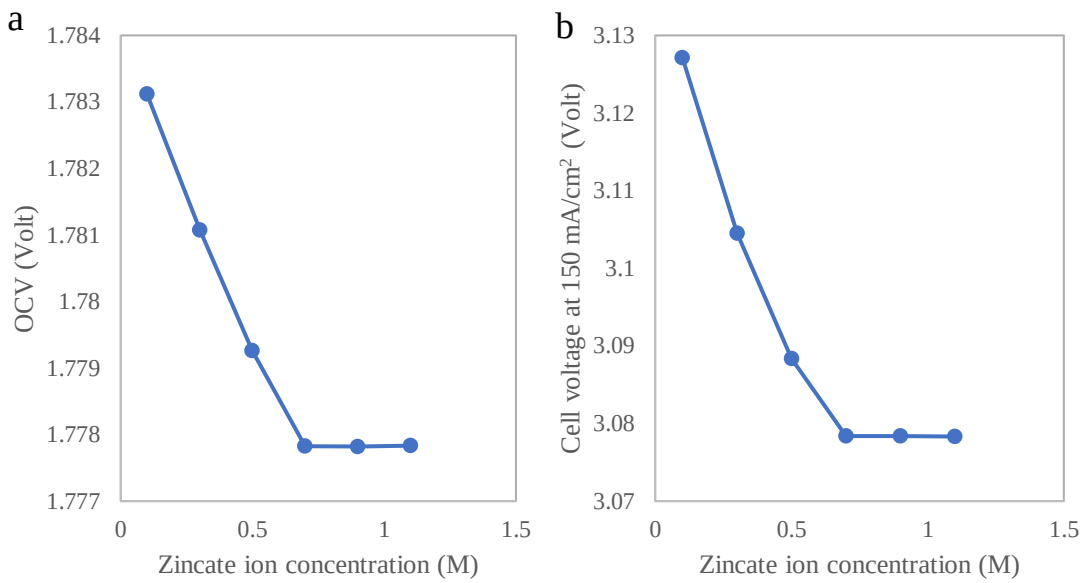

Figure 5.25 Comparison of a) OCV and b) cell voltage at 150 mA/cm^2 with 8 M KOH concentration, no initial zinc and various initial zincate ion concentration.

For cathode activation loss, the effect of zincate ion showed the same trend as cell voltage (figure 5.26b). According to Bockris, Nagy et al. (1972), the cathodic reaction orders were 1 for zincate ions and -1 for hydroxide ions therefore increasing zincate ion concentration increased the exchange current density and reduced the activation loss. For ohmic loss, increasing zincate ion concentration did not provide significant effect on the ohmic loss (figure 5.26a). In this model, zincate ion did not involve in the conductivity of electrolyte therefore the result showed no different. The more zincate ion above the saturation limit provided more ZnO which has the effect on the electrode conductivity. However, the ZnO amount was too small to provide significant different.

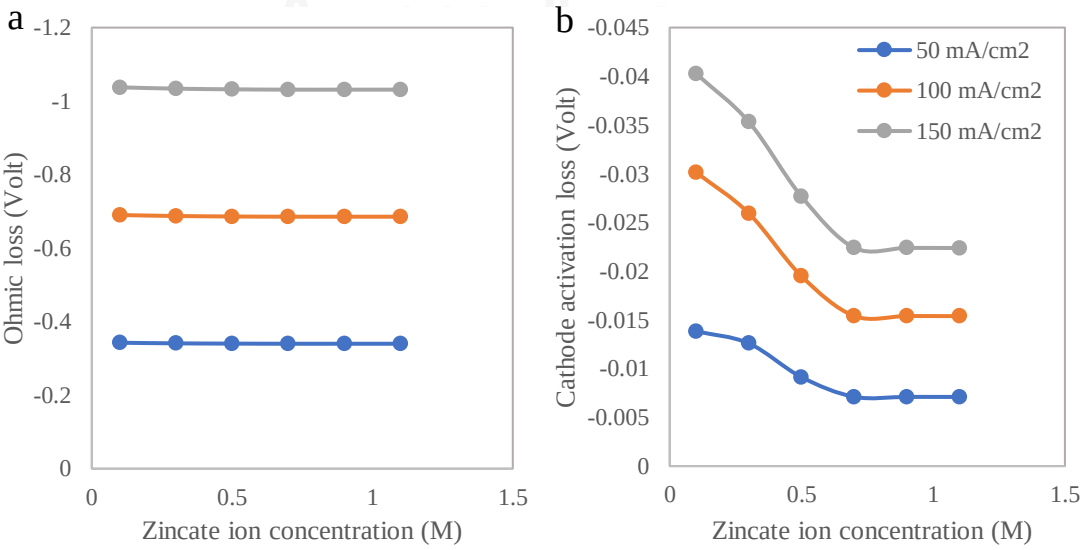

Figure 5.26 Comparison of a) ohmic loss and b) cathode activation loss at 150 mA/cm^2 with 8 M KOH concentration, no initial zinc and various initial zincate ion concentration.

To describe the effect of zincate ion on C.E., comparison of C.E. and HER current density was conducted in figure 5.27. The result showed that higher zincate ion concentration provided higher C.E. and lower HER current density. Increasing zincate ion more than the saturation limit did not affected C.E. and HER current density same as cell voltage and the activation loss. From figure 5.27b, increasing the zincate ion concentration suppressed hydrogen evolution even though the zincate ion did not directly affect exchange current density of HER. Increasing zincate ion concentration increased the exchange current density of zinc regeneration and consequently increased the current of zinc regeneration reaction. Because zinc regeneration and HER are competitive reactions, HER rate declined when zinc regeneration rate rose. According to the previous work of Sharifi, Mojtahedi et al. (2009), increasing zincate ion concentration also increased C.E. same as this result. Einerhand, Visscher et al. (1988) was also found that the hydrogen production increased with decreasing zincate ion concentration.

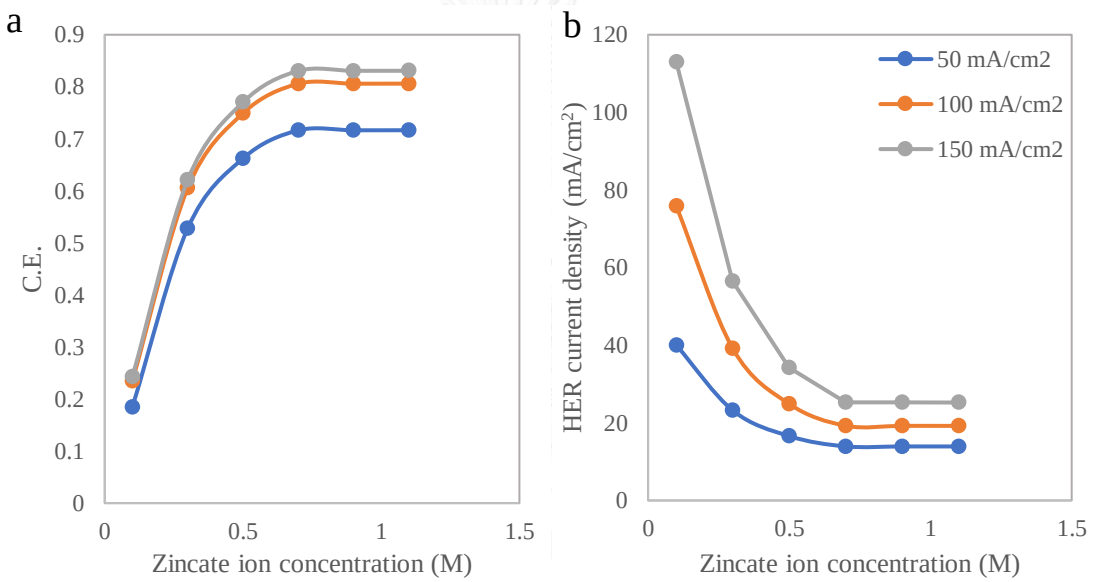

Figure 5.27 Comparison of a) current efficiency and b) HER current density with 8 M KOH concentration, no initial zinc and various initial zincate ion concentration.

CHAPTER VI
CONCLUSIONS

6.1 Conclusions

In this research, mathematical dynamic models of zinc-air fuel cell (ZAFC) and alkaline zinc electrolyzer were developed. For ZAFC, the model has 3 parameters which estimated by fitting from the experimental result. The model was validated with literature data. After parameter fitting, the predicted polarization curve of ZAFC indicated good agreement with the literature data. There are 4 parameters which was investigated the effect on the ZAFC performance: potassium hydroxide (KOH) concentration, flow of electrolyte, zincate ion concentration and conductive carbon. For the effect of KOH concentration, overall cell voltage increased when KOH concentration increased but increasing KOH concentration too high showed reduction of cell performance. Increasing KOH concentration more than about 7 M decreased ionic conductivity of electrolyte and anodic exchange current density. For the effect of flow, increasing electrolyte flowrate could maintain the amount of zinc and electrolyte concentration for long-time operation and consequently improved the cell performance. However, increasing flowrate higher than space velocity of 1 h^{-1} did not provide significant improvement for this simulation. Selecting electrolyte flowrate also related with the discharging current density. High current density also needed high flowrate to maintain the cell performance. For zincate ion concentration, increasing zincate ion decreased Nernst potential resulted in reduction of cell voltage. Increasing zincate ion concentration over the saturation limit produced zinc oxide (ZnO) which decreased conductivity and active area of zinc electrode. For conductive carbon, adding carbon into zinc electrode did not provide significant improvement to the cell performance. Furthermore, the cell voltage tended to decrease when carbon content increased because zinc active surface area was reduced resulted in higher activation loss.

The alkaline zinc electrolyzer model was developed and validated with the experiment data. The predicted polarization of electrolyzer demonstrated acceptable agreement with the experimental result. The studied parameters for zinc electrolyzer were KOH concentration and zincate ion concentration. The result showed that increasing KOH concentration increased Nernst potential and cathode activation loss resulted in increasing of overall cell voltage. However, the minimum ohmic loss was observed at 6 to 7 M of KOH due to the maximum conductivity of electrolyte. Consequently, the minimum cell voltage was also observed at 6 to 7 M of KOH in the high current density region. Increasing KOH concentration above 7 M resulted in increasing of ohmic loss and the cell voltage. For current efficiency (C.E.), increasing in current density increased C.E. for all conditions. C.E. increased when KOH concentration increased especially in the low range of KOH concentration. Increasing KOH concentration showed less improvement on C.E. in the high KOH concentration range. For the effect of zincate ion, increasing zincate ion concentration decreased Nernst potential and activation loss led to decreasing of cell voltage. C.E. increased when zincate ion concentration increased. Same as ZAFC, increasing zincate ion concentration higher than the saturation limit also generated ZnO. Increasing zincate

ion concentration further than this limit provided no significant effect to the cell performance. Zincate saturation limit can be increased by increasing concentration of KOH.

6.2 Recommendations and further studies

The mathematical models developed in this study exhibits acceptable agreement with experimental data for polarization curve. However, these models are zero-dimensional and have many assumptions. This work can be expanded by various ways:

1. These models can be used for further studies that want to evaluated system performance. For example, an integrated system of ZAFC and zinc electrolyzer was used as an energy storage for photovoltaic systems.
2. The models proposed are zero-dimensional models. To expand this work, the models should be modified in to multi-dimensional model. The distance and direction should be investigated to understand the behavior inside the cells and other problems such as passivation. Some parameters should also be change into time and dimension dependent parameters.
3. The mechanism of zinc reduction was assumed to be simple. The zincate ion in this work only consisted of $Zn(OH)^{2-}_4$. However, in the real case, the mechanism of zinc reduction was very complicated and zinc soluble species was not only consisted of $Zn(OH)^{2-}_4$. Modifying the model to include the mechanism and other zinc soluble species might improve the model prediction and explain other problems.
4. These models less concerned about the air electrode but the impact of the air electrode was very significant. More carefully investigation of the air electrode must be made.
5. Other side reaction should be considered in the models because some side reactions also affect to the cell performance. For instance, corrosion of zinc can occur while discharging. Carbonation of the electrolytes may cause some failure in the operation.

REFERENCES

Appleby, A. J. and M. Jacquier (1976). "The C.G.E. circulating zinc/air battery: A practical vehicle power source." Journal of Power Sources **1**(1): 17-34.

Appleby, A. J. and J. Marie (1979). "Kinetics of oxygen reduction on carbon materials in alkaline solution." Electrochimica Acta **24**(2): 195-202.

Bird, R. B., W. E. Stewart and E. N. Lightfoot (2002). Transport Phenomena. Danvers, United States of America, John Wiley & Sons.

Bockelmann, M., U. Kunz and T. Turek (2016). "Electrically rechargeable zinc-oxygen flow battery with high power density." Electrochemistry Communications **69**: 24-27.

Bockris, J. O. M., Z. Nagy and A. Damjanovic (1972). "On the Deposition and Dissolution of Zinc in Alkaline Solutions." Journal of The Electrochemical Society **119**(3): 285-295.

Cooper, J. F. and R. Krueger (2006). The Refuelable Zinc-air Battery: Alternative Techniques for Zinc and Electrolyte Regeneration, ; Lawrence Livermore National Laboratory (LLNL), Livermore, CA**:** Medium: ED; Size: PDF-file: 31 pages; size: 30.37 Mbytes.

Dean, J. A. and N. A. Lange (1999). Lange's handbook of chemistry. New York :, McGraw-Hill.

Deiss, E., F. Holzer and O. Haas (2002). "Modeling of an electrically rechargeable alkaline Zn–air battery." Electrochimica Acta **47**(25): 3995-4010.

Dirkse, T. P. and N. A. Hampson (1972). "The Zn(II)/Zn exchange reaction in KOH solution—I. Exchange current density measurements using the galvanostatic method." Electrochimica Acta **17**(1): 135-141.

Dyson, W. H., L. A. Schreier, W. P. Sholette and A. J. Salkind (1968). "Physical-Chemical Studies of KOH - ZnO Electrolytes." Journal of The Electrochemical Society **115**(6): 566-569.

Einerhand, R. E. F., W. H. M. Visscher and E. Barendrecht (1988). "Hydrogen production during zinc deposition from alkaline zincate solutions." Journal of Applied Electrochemistry **18**(6): 799-806.

Farr, J. P. G. and N. A. Hampson (1967). "Evaluation of the characteristics of exchange reactions." Journal of Electroanalytical Chemistry and Interfacial Electrochemistry **13**(4): 433-441.

Gavrilović-Wohlmuther, A., A. Laskos, C. Zelger, B. Gollas and A. H. Whitehead (2015). "Effects of Electrolyte Concentration, Temperature, Flow Velocity and Current Density on Zn Deposit Morphology." Journal of Energy and Power Engineering **9**: 10.

Hampson, N. A., G. A. Herdman and R. Taylor (1970). "Some kinetic and thermodynamic studies of the system Zn/Zn(II), OH−." Journal of Electroanalytical Chemistry and Interfacial Electrochemistry **25**(1): 9-18.

Huh, T., G. Savaskan and J. W. Evans (1992). "Further studies of a zinc-air cell employing a packed bed anode part II: Regeneration of zinc particles and electrolyte by fluidized bed electrodeposition." Journal of Applied Electrochemistry **22**(10): 916-921.

Isaacson, M. J., F. R. McLarnon and E. J. Cairns (1990). "Current Density and ZnO Precipitation-Dissolution Distributions in Zn - ZnO Porous Electrodes and Their Effect on Material Redistribution: A Two-Dimensional Mathematical Model." Journal of The Electrochemical Society **137**(7): 2014-2021.

Jiratchayamaethasakul, C., N. Srijaroenpramong, T. Bunyangyuen, W. Arpavate, N. Wongyao, A. Therdthianwong and S. Therdthianwong (2014). "Effects of anode orientation and flow channel design on performance of refuelable zinc-air fuel cells." Journal of Applied Electrochemistry **44**(11): 1205-1218.

Jiricny, V., S. Siu, A. Roy and J. W. Evans (2000). "Regeneration of zinc particles for zinc–air fuel cells in a spouted-bed electrode." Journal of Applied Electrochemistry **30**(6): 647-656.

Jung, C.-Y., T.-H. Kim, W.-J. Kim and S.-C. Yi (2016). "Computational analysis of the zinc utilization in the primary zinc-air batteries." Energy **102**: 694-704.

Kim, H.-I., E.-J. Kim, S.-J. Kim and H.-C. Shin (2015). "Influence of ZnO precipitation on the cycling stability of rechargeable Zn–air batteries." Journal of Applied Electrochemistry **45**(4): 335-342.

Kim, H. G., D. J. Suh, C. S. Kim, H. J. Lee and B. K. Min (2013). Zinc air fuel cell with enhanced cell performance, Google Patents.

Kim, H. S., Y. N. Jo, W. J. Lee, K. J. Kim and C. W. Lee (2015). "Coating on Zinc Surface to Improve the Electrochemical Behavior of Zinc Anodes for Zinc-Air Fuel Cells." Electroanalysis **27**(2): 517-523.

Kimble, M. C. and R. E. White (1991). "A Mathematical Model of a Hydrogen/Oxygen Alkaline Fuel Cell." Journal of The Electrochemical Society **138**(11): 3370-3382.

Krejčí, I., P. Vanýsek and A. Trojánek (1993). "Transport of $Zn(OH)_4^{2-}$ Ions across a Polyolefin Microporous Membrane." Journal of The Electrochemical Society **140**(8): 2279-2283.

Kriegsmann, J. J. and H. Y. Cheh (1999). "The importance of the equilibrium zincate ion concentration in modeling a cylindrical alkaline cell." Journal of Power Sources **84**(1): 52-62.

Lee, C. W., K. Sathiyanarayanan, S. W. Eom, H. S. Kim and M. S. Yun (2006). "Effect of additives on the electrochemical behaviour of zinc anodes for zinc/air fuel cells." Journal of Power Sources **160**(1): 161-164.

Li, G., K. Zhang, M. A. Mezaal, R. Zhang and L. Lei (2015). "Effect of Electrolyte Concentration and Depth of Discharge for Zinc-Air Fuel Cell." International Journal of Electrochemical Science **10**(8): 12.

Ma, H., B. Wang, Y. Fan and W. Hong (2014). "Development and Characterization of an Electrically Rechargeable Zinc-Air Battery Stack." Energies **7**(10): 6549.

Mao, Z. and R. E. White (1992). "Mathematical Modeling of a Primary Zinc/Air Battery." Journal of The Electrochemical Society **139**(4): 1105-1113.

Marcus, Y. (2009). "The Standard Partial Molar Volumes of Ions in Solution. Part 4. Ionic Volumes in Water at 0−100 °C." The Journal of Physical Chemistry B **113**(30): 10285-10291.

Mathias, P. M. (2004). "Correlation for the density of multicomponent aqueous electrolytes." Industrial & Engineering Chemistry Research **43**(19): 6247-6252.

Newman, J. and K. E. Thomas (2004). Electrochemical Systems. Hoboken, Wiley-Interscience.

Pei, P., Z. Ma, K. Wang, X. Wang, M. Song and H. Xu (2014). "High performance zinc air fuel cell stack." Journal of Power Sources **249**: 13-20.

Pierson, H. O. (1993). 10 - Natural Graphite, Graphite Powders, Particles, and Compounds. Handbook of Carbon, Graphite, Diamonds and Fullerenes. Oxford, William Andrew Publishing**:** 226-243.

Puapattanakul, A., S. Therdthianwong, A. Therdthianwong and N. Wongyao (2013). "Improvement of Zinc-Air Fuel Cell Performance by Gelled KOH." Energy Procedia **34**: 173-180.

Saleh, M. M., J. W. Weidner and B. G. Ateya (1995). "Electrowinning of Non-Noble Metals with Simultaneous Hydrogen Evolution at Flow-Through Porous Electrodes: I . Theoretical." Journal of The Electrochemical Society **142**(12): 4113-4121.

Sapkota, P. and H. Kim (2009). "Zinc–air fuel cell, a potential candidate for alternative energy." Journal of Industrial and Engineering Chemistry **15**(4): 445-450.

Sapkota, P. and H. Kim (2010). "An experimental study on the performance of a zinc air fuel cell with inexpensive metal oxide catalysts and porous organic polymer separators." Journal of Industrial and Engineering Chemistry **16**(1): 39-44.

Savaskan, G., T. Huh and J. W. Evans (1992). "Further studies of a zinc-air cell employing a packed bed anode part I: Discharge." Journal of Applied Electrochemistry **22**(10): 909-915.

Schröder, D. (2016). Analysis of Reaction and Transport Processes in Zinc Air Batteries, Springer Fachmedien Wiesbaden.

Schröder, D. and U. Krewer (2014). "Model based quantification of air-composition impact on secondary zinc air batteries." Electrochimica Acta **117**: 541-553.

Schröder, D., V. Laue and U. Krewer (2016). "Numerical simulation of gas-diffusion-electrodes with moving gas–liquid interface: A study on pulse-current operation and electrode flooding." Computers & Chemical Engineering **84**: 217-225.

See, D. M. and R. E. White (1997). "Temperature and Concentration Dependence of the Specific Conductivity of Concentrated Solutions of Potassium Hydroxide." Journal of Chemical & Engineering Data **42**(6): 1266-1268.

Sharifi, B., M. Mojtahedi, M. Goodarzi and J. Vahdati Khaki (2009). "Effect of alkaline electrolysis conditions on current efficiency and morphology of zinc powder." Hydrometallurgy **99**(1–2): 72-76.

Simičić, M. V., K. I. Popov and N. V. Krstajić (2000). "An experimental study of zinc morphology in alkaline electrolyte at low direct and pulsating overpotentials." Journal of Electroanalytical Chemistry **484**(1): 18-23.

Smedley, S. I. and X. G. Zhang (2007). "A regenerative zinc–air fuel cell." Journal of Power Sources **165**(2): 897-904.

Song, C. and J. Zhang (2008). Electrocatalytic Oxygen Reduction Reaction. PEM Fuel Cell Electrocatalysts and Catalyst Layers: Fundamentals and Applications. J. Zhang. London, Springer London**:** 89-134.

Spiegel, C. (2008). Chapter 3 - Fuel Cell Electrochemistry. PEM Fuel Cell Modeling and Simulation Using Matlab. Burlington, Academic Press**:** 49-76.

Spiegel, C. (2008). Chapter 5 - Fuel Cell Mass Transport. PEM Fuel Cell Modeling and Simulation Using Matlab. Burlington, Academic Press**:** 97-125.

Stamm, J., A. Varzi, A. Latz and B. Horstmann (2017). "Modeling nucleation and growth of zinc oxide during discharge of primary zinc-air batteries." Journal of Power Sources **360**: 136-149.

Sunu, W. G. and D. N. Bennion (1980). "Transient and Failure Analyses of the Porous Zinc Electrode: I . Theoretical." Journal of The Electrochemical Society **127**(9): 2007-2016.

Tromans, D. (1998). "Oxygen solubility modeling in inorganic solutions: concentration, temperature and pressure effects." Hydrometallurgy **50**(3): 279-296.

Wang, K., P. Pei, Z. Ma, H. Chen, H. Xu, D. Chen and X. Wang (2015). "Dendrite growth in the recharging process of zinc–air batteries." Journal of Materials Chemistry A **3**: 8.

Wang, K., P. Pei, Z. Ma, H. Chen, H. Xu, D. Chen and H. Xing (2015). "Growth of oxygen bubbles during recharge process in zinc-air battery." Journal of Power Sources **296**: 40-45.

Wang, K., P. Pei, Z. Ma, H. Xu, P. Li and X. Wang (2014). "Morphology control of zinc regeneration for zinc–air fuel cell and battery." Journal of Power Sources **271**: 65-75.

Wen, Y.-H., J. Cheng, S.-Q. Ning and Y.-S. Yang (2009). "Preliminary study on zinc–air battery using zinc regeneration electrolysis with propanol oxidation as a counter electrode reaction." Journal of Power Sources **188**(1): 301-307.

Xu, M., D. G. Ivey, Z. Xie and W. Qu (2015). "Rechargeable Zn-air batteries: Progress in electrolyte development and cell configuration advancement." Journal of Power Sources **283**: 358-371.

Zabaleta, J. R. (2011). Zinc Air Fuel Cell Vehicles; Review of Different Technologies to Obtian Zinc from Zinc Oxide, Illinois Institute of Technology.

Zhu, A. L., D. Duch, G. A. Roberts, S. X. X. Li, H. Wang, K. Duch, E. Bae, K. S. Jung, D. Wilkinson and S. A. Kulinich (2015). "Increasing the Electrolyte Capacity of Alkaline Zn–Air Fuel Cells by Scavenging Zincate with Ca(OH)2." ChemElectroChem **2**(1): 134-142.

APPENDIX A

ADDITIONAL MODELLING

In following, additional information, equations and models for the simulations in this thesis are given.

A1 Knudsen Diffusion Model

The effective diffusivity for Oxygen in GDL with dm^2 / s is calculated with Knudsen diffusion model (Spiegel 2008). Knudsen diffusivity (D_{kn}) is calculated from equation (A.1) where $\bar{r}$ is average pore radius (~1×10^{-5}dm), Mw is molecular weight of oxygen.

$$D_{kn} = \frac{2}{3}\bar{r}\sqrt{\frac{8RT}{\pi Mw}} \quad \text{(A.1)}$$

$$D_{O_2 eff} = \varepsilon_{GDL}^{1.5} \cdot \left(\frac{1}{D_{O2,air}} + \frac{1}{D_{kn}}\right)^{-1} \quad \text{(A.2)}$$

A2 Diffusivity of Hydroxide Ion in Electrolyte

The diffusivity of hydroxide ion in KOH solution electrolyte with dm^2 / s is calculated with empirical expression fitted by Schröder (2016).

$$D_{OH-,KOH} = \frac{k_B \cdot T}{6\pi\mu_{KOH} R_{ion}} \times 10^2 \quad \text{(A.3)}$$

$$\mu_{KOH} = 0.799533504 \cdot \exp(0.155921614 \cdot c_{OH-}) \times 10^{-3} \quad \text{(A.4)}$$

Where k_B is the Boltzmann constant, which is equal to 1.3806×10^{-23} m2 / kg·s^2·K, μ_{KOH} is dynamic viscosity of KOH solution, R_{ion} is Stoke radius of hydroxide ion, which is equal to 4.642×10^{11} m.

A3 Ionic Conductivity of Electrolyte

The ionic conductivity of KOH solution with S/dm is calculated from correlation of KOH concentration and temperature proposed by See and White (1997).

$$\sigma_{electrolyte} = \left(K_9 \cdot T + K_{10} \cdot T^2 + K_{11} \cdot C_{KOH} + K_{12} \cdot C_{KOH}^2 + K_{13} \cdot T \cdot C_{KOH} + K_{14} \cdot \frac{C_{KOH}}{T} + K_{15} \cdot C_{KOH}^3 + K_{16} \cdot T^2 \cdot C_{KOH}^2\right) \times 10 \quad \text{(A.5)}$$

Where

K_9= -0.00342000614	S / cm K
K_{10}= 1.19699771×10^{-5}	S / cm K^2
K_{11}= -1.17298091	S L / cm mol
K_{12}= -0.00516794041	S L / cm^2 mol^2
K_{13}= 0.00328292638	S L / cm K mol
K_{14}= 119.604837	S L K / cm mol
K_{15}= 0.000624311676	S L^3 / cm mol^3
K_{16}= $-1.88320099 \times 10^{-7}$	S L^2 / cm mol^2 K^2

A4 Oxygen Dissolved in Electrolyte

The concentration of oxygen dissolved in KOH solution is calculated from correlation expressed by Tromans (1998). The oxygen solubility model is a function of KOH concentration, temperature and pressure of oxygen.

$$C_{O2,dissolved} = P_{O_2} \cdot \left(\frac{1}{1+0.102078\cdot(C_{KOH})^{1.00044}}\right)^{4.308933} \cdot \exp\left(\frac{0.046\cdot T^2+203.35\cdot T\cdot\log(T/298)-(299.378+0.092\cdot T)\cdot(T-298)-20591}{8.3144\cdot T}\right) \quad (A.6)$$

A5 Saturation concentration limit of zincate ion

The saturation concentration of zincate ion or ZnO solubility is calculated by the correlation fitted from the experiment data of Dyson, Schreier et al. (1968). The correlation expresses as:

$$C^{sat}_{Zn(OH)_4^{2-}} = 0.007239 \cdot {C_{KOH}}^2 + 0.056151 \cdot C_{KOH} - 0.03267 \quad (A.7)$$

A6 Current Efficiency

The current efficiency (C.E.) for zinc electrolyzer is defined as the ratio of the equivalent current for zinc regeneration to the total applied current. C.E. can be calculated following this:

$$C.E. = \frac{i_{Zn}}{i_{Cell}} \quad (A.8)$$

A7 Estimated Parameters of ZAFC modelling

The estimated parameters of ZAFC modelling in section 5.1 were listed in table A.1.

Table A.1 Estimated parameters of ZAFC model

Experiment data	R_{comp} (Ω)	δ_{active} (μm)	ε_{active}
This work	1.25	1	0.2191
Sapkota and Kim (2010)	0.005	420	0.25

A8 Resistance Comparison

The resistance involved with the ZAFC simulation was comparison in table A.2. The R_{comp} (1.25 Ω) was used to calculated the percentage ratio of R_{comp} to R_{tot}.

Table A.2 Comparison of total resistance, anode resistance, electrolyte resistance and the percentage ratio of component resistance to total resistance between various simulation case of ZAFC.

Simulation case	R_{tot} (Ω)	R_{anode} (Ω)	$R_{electrolyte}$ (Ω)	$\%\ R_{comp}/R_{tot}$
4 M KOH, 0% ZnO, 0% Carbon	1.7754	5.46e-5	0.178	70.4
6 M KOH, 0% ZnO, 0% Carbon	1.7540	5.4626e-5	0.1581	71.3
8 M KOH, 0% ZnO, 0% Carbon	1.7581	5.4627e-5	0.1619	71.1
10 M KOH, 0% ZnO, 0% Carbon	1.7803	5.4629e-5	0.1826	70.2
12 M KOH, 0% ZnO, 0% Carbon	1.8218	5.4631e-5	0.2212	68.6
14 M KOH, 0% ZnO, 0% Carbon	1.8817	5.4634e-5	0.2769	66.4
8 M KOH, 33% ZnO, 0% Carbon	1.7581	6.8339e-5	0.1619	71.1
8 M KOH, 50% ZnO, 0% Carbon	1.7581	8.4523e-5	0.1619	71.1
8 M KOH, 66% ZnO, 0% Carbon	1.7581	1.1589e-4	0.1619	71.1
8 M KOH, 90% ZnO, 0% Carbon	1.7584	3.5726e-4	0.1619	71.1
8 M KOH, 0% ZnO, 10% Carbon	1.7581	6.1219e-5	0.1619	71.1
8 M KOH, 0% ZnO, 20% Carbon	1.7581	6.3477e-5	0.1619	71.1
8 M KOH, 0% ZnO, 30% Carbon	1.7581	6.2779e-5	0.1619	71.1
8 M KOH, 90%ZnO, 10%Carbon	1.7581	2.7917e-4	0.1619	71.1
8 M KOH, 90%ZnO, 20%Carbon	1.7582	2.1926e-4	0.1619	71.1
8 M KOH, 90%ZnO, 30%Carbon	1.7582	1.7184e-4	0.1619	71.1

APPENDIX B

EXPERIMENTAL DATA

In following, more details of experimental data for this thesis are given.

B1 Zinc-Air Fuel Cell

The following ZAFC experimental data were plotted as polarization curve which was used to compare with simulation result in section 5.1 (figure 5.1).

Table B.1 Experimental Cell Performance data for ZAFC

Current density (mA/cm^2)	Cell voltage (Volt)	Power density (mW/cm^2)	Current density (mA/cm^2)	Cell voltage (Volt)	Power density (mW/cm^2)
0	1.33	0	15	0.819	12.285
1	1.259	1.259	16	0.79	12.64
2	1.22	2.44	17	0.761	12.937
3	1.183	3.549	18	0.728	13.104
4	1.152	4.608	19	0.696	13.224
5	1.118	5.59	20	0.662	13.24
6	1.086	6.516	21	0.623	13.083
7	1.058	7.406	22	0.584	12.848
8	1.027	8.216	23	0.552	12.696
9	0.998	8.982	24	0.513	12.312
10	0.969	9.69	25	0.474	11.85
11	0.94	10.34	27	0.405	10.935
13	0.879	11.427	27.7	0.373	10.3321
14	0.848	11.872			

B2 Alkaline Zinc Electrolyzer

The following zinc electrolyzer experimental data were plotted as polarization curve which was used to compare with simulation result in section 5.2 (figure 5.17).

Table B.2 Experimental Cell Performance data for zinc electrolyzer

Current density (mA/cm^2)	Cell voltage (Volt)	Power density (mW/cm^2)	Current density (mA/cm^2)	Cell voltage (Volt)	Power density (mW/cm^2)
0	1.775	0.000	31.25	2.222	69.449
0.625	1.902	1.189	37.5	2.256	84.603
1.25	1.849	2.311	43.75	2.298	100.545
2.5	1.959	4.896	50	2.342	117.078
3.75	1.975	7.404	56.25	2.383	134.059
5	1.990	9.950	62.5	2.466	154.137
6.25	1.997	12.482	75	2.534	190.085
7.5	2.025	15.186	87.5	2.585	226.153
8.75	2.035	17.809	100	2.647	264.663
10	2.045	20.452	112.5	2.758	310.250
11.25	2.058	23.157	125	2.816	352.060
12.5	2.062	25.777	137.5	2.874	395.169
18.75	2.110	39.557	150	2.967	445.031
25	2.160	53.992			

VITA

Mr.Woranunt Lao-atiman was born in Chiang Mai, Thailand on June 18, 1991. He graduated high school from Montfort College Secondary School, Chiang Mai in 2008. He finished Bachelor's Degree in Chemical Engineering from Mahidol University in 2012. He continued to study Master's Degree Program in Chemical Engineering of Department of Chemical Engineering, Chulalongkorn University, Thailand since January 2015.